U.S. Department of Transportation

Federal Railroad Administration

Next-Generation Foundations for Special Trackwork Phase III

Office of Research,
Development,
and Technology
Washington, DC 20590

DOT/FRA/ORD-16/14

Final Report
May 2016

NOTICE

This document is disseminated under the sponsorship of the Department of Transportation in the interest of information exchange. The United States Government assumes no liability for its contents or use thereof. Any opinions, findings and conclusions, or recommendations expressed in this material do not necessarily reflect the views or policies of the United States Government, nor does mention of trade names, commercial products, or organizations imply endorsement by the United States Government. The United States Government assumes no liability for the content or use of the material contained in this document.

NOTICE

The United States Government does not endorse products or manufacturers. Trade or manufacturers' names appear herein solely because they are considered essential to the objective of this report.

REPORT DOCUMENTATION PAGE

Form Approved
OMB No. 0704-0188

1. AGENCY USE ONLY (Leave blank)	2. REPORT DATE	3. REPORT TYPE AND DATES COVERED
	May 2016	Technical Report – December 2015

4. TITLE AND SUBTITLE
Next Generation Foundations for Special Trackwork - Phase III

5. FUNDING NUMBERS
DTFR53-11-00008
Task Order 308

6. AUTHOR(S)
David Davis and Rafael Jimenez

7. PERFORMING ORGANIZATION NAME(S) AND ADDRESS(ES)
Transportation Technology Center, Inc.
55500 DOT Road
Pueblo, CO 81001

8. PERFORMING ORGANIZATION REPORT NUMBER

9. SPONSORING/MONITORING AGENCY NAME(S) AND ADDRESS(ES)
U.S. Department of Transportation
Federal Railroad Administration
Office of Railroad Policy and Development
Office of Research, Development, and Technology
Washington, DC 20590

10. SPONSORING/MONITORING AGENCY REPORT NUMBER
DOT/FRA/ORD-16/14

11. SUPPLEMENTARY NOTES
COR: Luis Maal

12a. DISTRIBUTION/AVAILABILITY STATEMENT
This document is available to the public through the FRA Web site at http://www.fra.dot.gov.

12b. DISTRIBUTION CODE

13. ABSTRACT (Maximum 200 words)

Transportation Technology Center, Inc. (TTCI) conducted a series of tests, funded by the Federal Railroad Administration, which evaluated the potential beneficial effects of various configurations of high angle frogs and frog foundations on wheel-rail vertical forces and frog performance. The tests were conducted under 315,000-pound cars with nominal 39-ton axle loads at the High Tonnage Loop of the Facility for Accelerated Service Testing at the Transportation Technology Center in Pueblo, CO.

Results from previous phases of this project were used to develop this testing plan, and the project had previously determined that track stiffness, track damping and frog flexibility (i.e., the capability for differential vertical movement between opposite sides of the frog across the flangeway) affects wheel-rail vertical forces. A prototype crossing diamond was built using an existing design that offered the potential for increasing frog flexibility, while the commercially available straight rail reversible design was modified to add rail seat pads of various configurations above the frog platework. Additionally, the team developed options for joining the four castings that make up each frog. These options allowed assessment of frog flexibility on wheel-rail forces and frog performance. A total of 14 frog configurations were evaluated over about 70 MGT.

14. SUBJECT TERM
Dynamic load environment, special trackwork frog foundations, wheel-rail impact

15. NUMBER OF PAGES
98

16. PRICE CODE

17. SECURITY CLASSIFICATION OF REPORT	18. SECURITY CLASSIFICATION OF THIS PAGE	19. SECURITY CLASSIFICATION OF ABSTRACT	20. LIMITATION OF ABSTRACT
Unclassified	Unclassified	Unclassified	

METRIC/ENGLISH CONVERSION FACTORS

ENGLISH TO METRIC	METRIC TO ENGLISH
LENGTH (APPROXIMATE)	**LENGTH (APPROXIMATE)**
1 inch (in) = 2.5 centimeters (cm)	1 millimeter (mm) = 0.04 inch (in)
1 foot (ft) = 30 centimeters (cm)	1 centimeter (cm) = 0.4 inch (in)
1 yard (yd) = 0.9 meter (m)	1 meter (m) = 3.3 feet (ft)
1 mile (mi) = 1.6 kilometers (km)	1 meter (m) = 1.1 yards (yd)
	1 kilometer (km) = 0.6 mile (mi)
AREA (APPROXIMATE)	**AREA (APPROXIMATE)**
1 square inch (sq in, in^2) = 6.5 square centimeters (cm^2)	1 square centimeter (cm^2) = 0.16 square inch (sq in, in^2)
1 square foot (sq ft, ft^2) = 0.09 square meter (m^2)	1 square meter (m^2) = 1.2 square yards (sq yd, yd^2)
1 square yard (sq yd, yd^2) = 0.8 square meter (m^2)	1 square kilometer (km^2) = 0.4 square mile (sq mi, mi^2)
1 square mile (sq mi, mi^2) = 2.6 square kilometers (km^2)	10,000 square meters (m^2) = 1 hectare (ha) = 2.5 acres
1 acre = 0.4 hectare (he) = 4,000 square meters (m^2)	
MASS - WEIGHT (APPROXIMATE)	**MASS - WEIGHT (APPROXIMATE)**
1 ounce (oz) = 28 grams (gm)	1 gram (gm) = 0.036 ounce (oz)
1 pound (lb) = 0.45 kilogram (kg)	1 kilogram (kg) = 2.2 pounds (lb)
1 short ton = 2,000 pounds (lb) = 0.9 tonne (t)	1 tonne (t) = 1,000 kilograms (kg)
	= 1.1 short tons
VOLUME (APPROXIMATE)	**VOLUME (APPROXIMATE)**
1 teaspoon (tsp) = 5 milliliters (ml)	1 milliliter (ml) = 0.03 fluid ounce (fl oz)
1 tablespoon (tbsp) = 15 milliliters (ml)	1 liter (l) = 2.1 pints (pt)
1 fluid ounce (fl oz) = 30 milliliters (ml)	1 liter (l) = 1.06 quarts (qt)
1 cup (c) = 0.24 liter (l)	1 liter (l) = 0.26 gallon (gal)
1 pint (pt) = 0.47 liter (l)	
1 quart (qt) = 0.96 liter (l)	
1 gallon (gal) = 3.8 liters (l)	
1 cubic foot (cu ft, ft^3) = 0.03 cubic meter (m^3)	1 cubic meter (m^3) = 36 cubic feet (cu ft, ft^3)
1 cubic yard (cu yd, yd^3) = 0.76 cubic meter (m^3)	1 cubic meter (m^3) = 1.3 cubic yards (cu yd, yd^3)
TEMPERATURE (EXACT)	**TEMPERATURE (EXACT)**
[(x-32)(5/9)] °F = y °C	[(9/5) y + 32] °C = x °F

QUICK INCH - CENTIMETER LENGTH CONVERSION

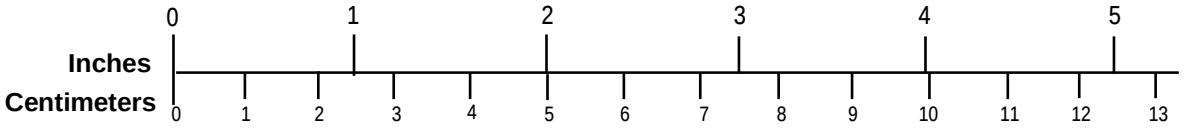

QUICK FAHRENHEIT - CELSIUS TEMPERATURE CONVERSIO

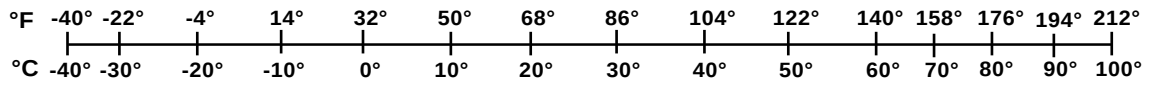

For more exact and or other conversion factors, see NIST Miscellaneous Publication 286, Units of Weights and Measures. Price $2.50 SD Catalog No. C13 10286

Updated 6/17/98

Acknowledgements

Transportation Technology Center, Inc. (TTCI) would like to acknowledge Getzner, USA, Inc. for its technical support in designing the pad tested and for donating materials.

Likewise, TTCI thanks voestalpine Nortrak for designing and donating its pad material.

Contents

Illustrations

Tables

Executive Summary

Transportation Technology Center, Inc. (TTCI) performed a series of tests, under Federal Railroad Administration (FRA) funding, that evaluated the potential beneficial effects of various configurations of high angle frogs and frog foundations on wheel-rail vertical forces and frog performance. The tests were conducted under 315,000-pound cars with nominal 39-ton axle loads at the High Tonnage Loop (HTL) of the Facility for Accelerated Service Testing (FAST) at the Transportation Technology Center (TTC) in Pueblo, CO.

The testing plan was developed using results from the previous phases of this project, and this project has determined that track stiffness, track damping, and frog flexibility (i.e., the capability for differential vertical movement between opposite sides of the frog across the flangeway) affect wheel-rail vertical forces. A prototype crossing diamond was built using an existing design that offered the potential for increasing frog flexibility, while the commercially available Straight Rail Reversible (SRR) design was modified to add rail seat pads of various configurations above the frog platework. Additionally, options for joining the four castings that make up each frog were developed. These options allowed the team to assess frog flexibility on wheel-rail forces and frog performance. A total of 14 frog configurations were evaluated over approximately 70 MGT of 315,000-pound car traffic.

Conclusions from the project include:

- Rail seat pads contribute significantly to wheel-rail force reduction. Reductions of 20 to 30 percent were measured for maximum and 99th percentile vertical dynamic wheel loads.
    - A range of rail seat pads were tested. A relatively soft pad intended to produce optimal stiffness, based on the theoretical results, disintegrated under the first 100 trains.
    - Two supplier recommended pads were tested with good success. The softer of the two pads tested produced lower track stiffness and lower dynamic vertical loads.
- Adding more flexibility to the SRR design provided little dynamic performance improvement when rail seat pads were in place.
    - The flexible frog design, with no direct connections between the four castings that make up a frog, did not significantly affect dynamic vertical loads.
        - The additional degrees of freedom did contribute to maintenance issues involving the inner guard position and related component breakage.
        - From previous phases of the project, a jointed frog (one with the ability for the two sides of the flangeway to move vertically with respect to one another) had lower dynamic vertical loads than a traditional solid (one-piece) frog.

The results of the project can serve as a guide for frog designers to the potential ranges of track stiffness and frog flexibility that can improve high angle frog performance. This may spur development of additional concepts that will improve frog performance.

One conclusion that can be drawn from the tests is that a flexible frog is useful in lowering dynamic forces. But the addition of a simple mechanical joint, as was done in three rail crossing

diamonds, is probably near optimal in terms of flexibility. Additional flexibility, such as split flangeway spacers in the SRR design, adds little to dynamic performance. However, it does increase related component maintenance and add to the alignment degradation of the frog.

Rail seat pads were very effective at lowering dynamic vertical loads. In the FAST test situation, the pads were able to reduce vertical dynamic wheel loads at 40 mph to a level similar to that at 20 mph without pads. The, prototype's long-term durability and dynamic performance, as well as its design features should be determined.

1. Introduction

A series of experiments were conducted on a prototype crossing diamond to evaluate the effects of design elements which may improve a diamond's performance. These tests were conducted at the HTL of FAST at TTC under (HAL) freight train operations. The results will help guide frog designers and maintainers toward improved performance designs and maintenance practices.

1.1 Background

Special trackwork components—particularly switches, turnout frogs, and crossing diamonds—are prone to rapid degradation, due to the combination of high dynamic loading (resulting from running surface discontinuities) and the use of conventional open track foundation designs. The rapid degradation of the foundation results in loss of track surface and ride quality, and increases maintenance needs. According to accident statistics, track surface defects are one of the leading causes of track-caused accidents. Special trackwork foundations are designed using static or quasi-static design techniques, and these procedures often ignore the dynamic stiffness and damping characteristics of the materials being used. Further, there are few published results of service environment measurements, such as typical stiffness and deflections for crossing diamonds (whole or components).

The first phase of this project consisted of a one year effort to (1) measure the service environment of a typical diamond crossing, (2) model the diamond with dynamic simulations, and (3) determine the scope of benefits to be gained by changes in design and materials. [1] The initial results suggested that optimizing foundation performance can generate significant benefits. After the team conducted the dynamic simulations using measured track parameters, wheel-rail dynamic forces were shown to be reduced by about 30 percent with optimized frog foundations.

The first phase report also suggested that the ballast layer is a major source of the variability in the frog's performance. While it is a relatively inexpensive way to provide damping and adjustability to the frogs and crossing diamond, the relatively rapid settlement, stiffening, and loss of damping result in increased dynamic loads and component degradation.

The second phase of this project continued to explore the relationships between track foundation parameters and vehicle-track performance at frogs. [2] Modeling and calibration with a limited range of field cases has shown some interesting results. For example, the effect of track stiffness is relatively important. Previous studies suggested that stiffness was unimportant over the likely range of values seen in the field, but this is true only when sufficient damping is present. Currently, damping is far less than optimal for turnout and crossing diamond frogs. The Phase I work showed there might be an optimal stiffness level that minimizes wheel-rail forces for frogs. Further, the field measurements have shown that the relative movement of components within the frog may contribute significantly to the performance of the frog in service. This was shown in foundation tests where use of a cut rail and spacer to simulate a flangeway produced much lower wheel-rail forces than use of a milled flangeway of the same dimensions in a continuous rail. [2]

Thus, the findings from Phase II led to the development of a prototype crossing diamond to further evaluate the following design elements:

- Use of impact attenuation and damping elements in the rail seats of the frogs
- Adding flexibility to the frogs in terms of allowing relative movement between castings in a four-casting frog design.

The focus of this phase was to evaluate the performance of a prototype frog specially designed for maximum flexibility between the superstructure components using split spacers and elastomeric materials.

Two types of crossing diamond structures are currently used in revenue service:

- The cast crossing with running rails and the flangeway cast in one piece with the crossing connected to the running rails through bolts, as Figure 1 shows, or through the leg rail and bolts as Figure 2 shows. This type of diamond is generally stiffer and has fewer parts.
- The three-rail crossing where the running rails in two lines are cut through and connected with leg rails, as Figure 3 shows. This type of diamond is easier to fabricate and does not require a casting pattern (mold). It can be made to any angle using the same basic pieces. There is a definite mainline route for this design. As Figure 3 shows, the running surfaces do not conform to the wheels on the crossing route.

Figure 1. An Intermediate Angle Cast Crossing in Revenue Service

Figure 2. Cast Diamond Crossing Tested at FAST

Figure 3. Three-Rail Crossing Diamond

Cast crossings are currently more popular than three-rail crossings in North American railroads, because it is widely believed that a cast frog crossing has the longest service life. The common wisdom asserts that a cast frog crossing is stronger than a three-rail frog crossing. More importantly, frogs cast with austenitic manganese steel (AMS) in the preferred railbound configuration, as shown in Figures 1 and 2, are robust designs. The AMS castings have good impact resistance, which leads to relatively slow deterioration rates as compared to rail steel, and it takes much longer for fatigue cracking to progress through the cross section of the frog before fracture occurs. Repairs to the casting, while not easy, generally can be done without disassembling the frog.

However, both testing at FAST and practice in revenue service showed that the cast flangeway wore faster than expected, and the crossing performance deteriorated quickly because of the impact. The stronger, stiffer frogs cause higher dynamic loading at the same speeds as the three-rail design crossing diamond. At FAST, the high wheel-rail impacts broke not only the fastening components and the leg rail, but also the arm of the casting itself, as Figure 4 shows.

Figure 4. Components Failures in Cast Crossing

1.2 Objectives

The research is intended to improve safety by enhancing the dynamic performance of frogs in revenue service. Direct benefits include lower forces and reduced derailment risk at frogs, and indirect benefits include lower vehicle component dynamic loading, which results in longer fatigue lives and fewer service failures for wheels, axles, and other truck components.

2. FAST Prototype Testing

The test prototype, shown in Figures 5 and 6, is a modified version of the voestalpine Nortrak (Nortrak) Straight Rail Reversible (SRR) crossing diamond design [3]. This design was selected because the frog configuration has four separate castings bolted together through flangeway spacers for each frog. The SRR design was modified to allow more vertical relative movement between the four castings in a frog. The design modifications include:

- Two-part flangeway spacers (split spacers) between the running rails and the guardrails
- "Tile" type flangeway spacers at the intersection of the four casting corners of each frog (Figure 7)
- Milled seat platework
- ½-in rubber pads between the rails/castings and the platework (Figure 8). The tile spacer keeps the flangeways open, but does not provide any capability to carry tensile, longitudinal load.

The prototype crossing diamond was designed to evaluate the benefits that were achieved in previous short-term, as well as scaled panel tests, where flexibility in the superstructure resulted in the reduction of the wheel-rail impacts.

Figure 5. The test prototype crossing diamond as installed is a modified version of the basic SRR crossing diamond design

Figure 6. The crossing diamond was installed in typical HTL test configuration, where traffic runs over a single route

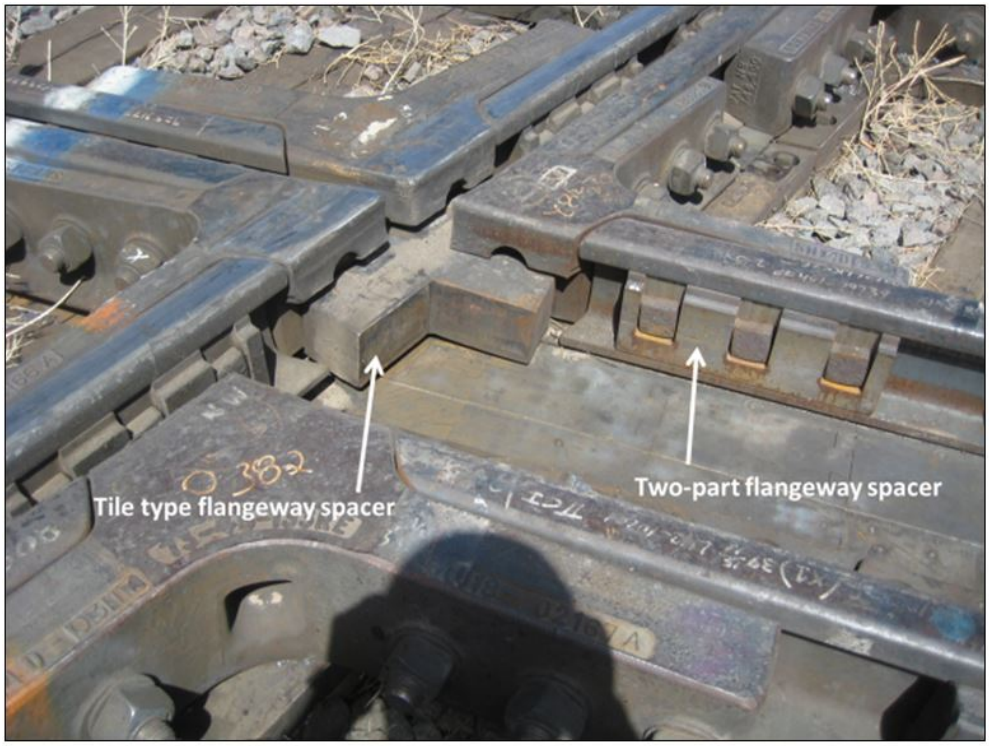

Figure 7. Tile type flangeway spacer at the casting corners and two-part (split) running rail/guardrail flangeway spacer

Figure 8. Milled platework and 0.5-in rubber pads

On June 3, 2014, the prototype 73-degree, 45-minute, 0-second crossing diamond, made by Nortrak, was installed on the HTL at FAST on a section of straight track in 12 in (nominal) of AREMA 4A ballast over an existing 8-in hot-mix asphalt underlayment, as shown in Figure 9.

Figure 9. Test prototype crossing diamond installation

2.1 Methodology

The crossing diamond was tested in the load environment of the HTL, where it was subjected to the FAST train's 39-ton axle load (315,000-pound gross rail load (GRL)) high sided gondola cars traveling at 40 mph. The direction of traffic over the single track on which the crossing diamond was tested was about 50 percent clockwise (CW) and 50 percent counterclockwise (CCW).

As initially installed and tested, the configuration of the crossing diamond provided maximum flexibility between adjacent running surface rails and between running surface rails and guardrails. The split spacers allowed movement between these components. The rail seat pad, which was between the rails/castings and the platework, was made of rubber.

The performance of the crossing diamond was evaluated in 13 test cases with respect to wheel impact forces, running surface degradation, track stiffness, track surface, component failure, and vertical/lateral/longitudinal displacement of castings and vertical displacement of the track structure under traffic. The team also measured the effective wheel gap and wheel drop, the longitudinal profile of the running surface across the casting corners, and the running surface hardness.

Initially, the test plan had two variables: (1) track stiffness/damping and (2) frog flexibility. As the testing progressed and more information was gained about the performance of the crossing diamond, additional variables were added. These variables included the location of the damping elements in the structure and ways to limit lateral and longitudinal movement of components.

The flexibility of the crossing diamond superstructure was incrementally reduced by replacing the split spacers with solid spacers and through bolts. Different pad types and materials were installed and tested in place of the original rubber between the milled platework and the castings/rails as well as at different levels under the casting corners to evaluate the effect of these changes on the performance parameters. The pad materials are described below and Table 1 shows the test cases and the variable(s) in red text that were introduced for each case.

- Nortrak Full Coverage Pad - Nortrak describes the material as a thermoplastic polyurethane (TPU) elastomer with a Shore hardness of 52D. Intrinsically, this material acts as both a spring and dampener in compression, allowing the crossing castings to move independently while absorbing a portion of the energy imparted during each compression. Shape factoring geometry (cylindrical depressions in the case of this pad) works in concert with the base material properties to yield a pad that can withstand repeated loading without suffering compression set or, in the worst case, thermal degradation.
- Getzner Pad Type A – The type A pad is intended for under-tie use.
- Getzner Pad Type B, Full Coverage Pad – Getzner describes its Sylodyn pad as specially selected for the geometry of the crossing diamond under investigation at FAST. Sylodyn is a closed cell polyurethane with combined elastic and shock-absorbing properties. Getzner selected a Sylodyn within its "high resilient" range of materials to withstand the extreme loading predicted at the crossing diamond. Getzner's High Resilient Sylodyn materials can withstand long-term static loads in the range of 430 psi and 870 psi, and short-term loads as high as 1,300 psi.

- Getzner Pad Type C – Under Tile & Layered Tile Pad: This pad is a variation of the Getzner Type B pad.

Table 1. Crossing Diamond Test Cases
(Test variables are shown in red/italic text)

<table>
<tr><th>Test Case</th><th>Pads:
Full-Coverage Between Rails/ Castings & Platework</th><th>Pads:
Under Spacer Tile or Solid Rubber</th><th>Pads:
Layered in the Spacer Tile</th><th>Flangeway Gap Spacers between Running Rails & Guardrails</th></tr>
<tr><td>Test Case 1</td><td>Basic Rubber</td><td colspan="2" rowspan="3">None</td><td rowspan="2">All Split Spacers</td></tr>
<tr><td>Test Cases 2a & 2b</td><td>Nortrak</td></tr>
<tr><td>Test Case 3</td><td>Nortrak</td><td rowspan="5">None</td><td rowspan="10">Solid Through-Bolt Spacers: 4 on the crossing track and 2 on the running track (inside rail)
Split Spacers: 2 on the running track (outside rail)</td></tr>
<tr><td>Test Case 4</td><td>Nortrak</td><td>Nortrak Under-Tile</td></tr>
<tr><td>Test Case 5</td><td>Getzner (Type A)</td><td>Getzner (Type C) Under-Tile</td></tr>
<tr><td>Test Case 6</td><td>Getzner (Type B)</td><td>None</td></tr>
<tr><td>Test Case 7</td><td>Getzner (Type B)</td><td>Getzner (Type C) Under-Tile</td></tr>
<tr><td>Test Case 8</td><td>Nortrak</td><td rowspan="2">None</td><td>Nortrak Layered Tile</td></tr>
<tr><td>Test Case 9</td><td>Getzner (Type B)</td><td>Getzner (Type C) Layered Tile</td></tr>
<tr><td>Test Case 10</td><td>Getzner (Type B) No pad under rubber tile</td><td>Solid Rubber Tile & ½ in steel top plate</td><td rowspan="4">None</td></tr>
<tr><td>Test Case 11</td><td>Getzner (Type B) No pad under rubber tile</td><td>Solid Rubber Tile & ½ in steel top plate</td><td>All Solid Through-bolts Spacers</td></tr>
<tr><td>Test Case 12 Baseline</td><td>None, steel plates</td><td>None, steel plates</td></tr>
<tr><td>Test Case 13</td><td>Getzner (Type B)</td><td>None</td></tr>
</table>

2.1.1 Test Case 1

The Test Case 1 configuration is described and illustrated at the beginning of Section 2. It included the basic rubber pads and all split spacers. This is the case in which the crossing diamond had maximum flexibility.

2.1.2 Test Case 2a and 2b

Figures 10 and 11 display the Nortrak-designed pad in Test Case 2a and 2b that was used in place of the basic rubber pad from Test Case 1. Test Case 2a was measured when the pads were

initially installed; Test Case 2b was measured after the pads had been in service 32.8 MGT and the results were used to evaluate the long-term performance of the pads.

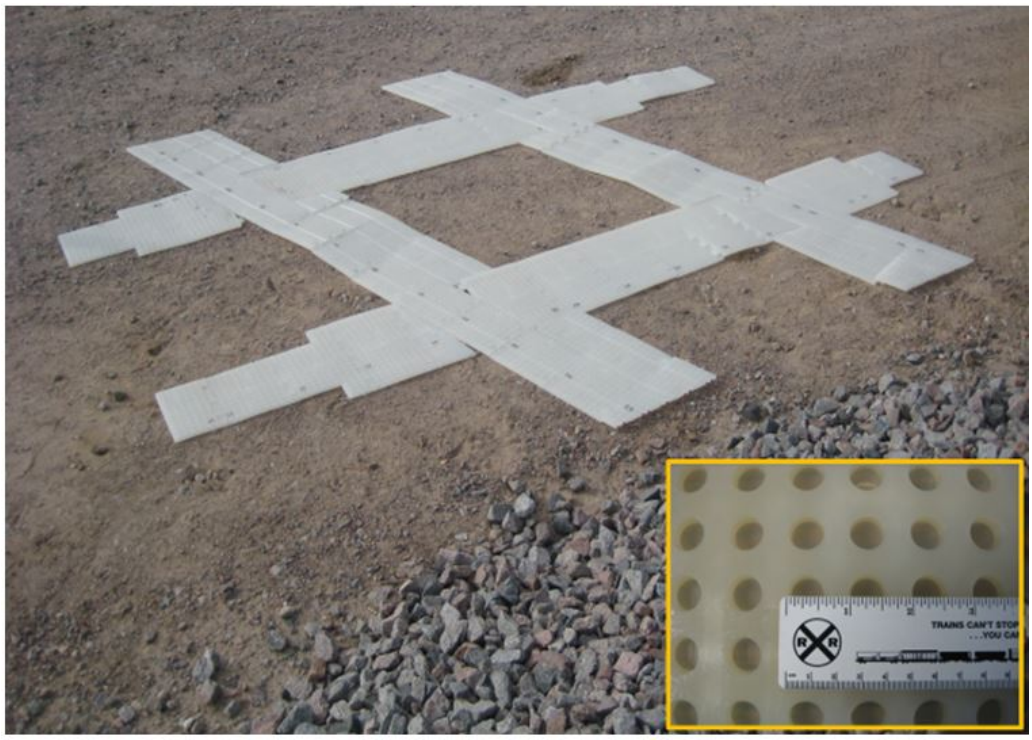

Figure 10. Nortrak-designed pad

Figure 11. Nortrak-designed pad in place between the milled platework and the castings. View with the center guardrail piece removed.

2.1.3 Test Case 3

For Test Case 3, selected split spacers were replaced with solid spacers and through bolts to evaluate the effect of reduced freedom of movement between components and reduced design flexibility on the performance of the crossing diamond. In this configuration, the common corner of the frog was isolated from the other three corners. This still allowed relative movement of the two sides of the frog on each route. But, it limited lateral and longitudinal relative movement of the frog castings. Figure 12 shows a split spacer and a solid spacer. Figure 13 shows the locations where each type of spacer was installed for Test Case 3 and kept the same through Test Case 10.

Figure 12. Split flangeway spacer on the left. Solid spacer for use with through bolts on the right (upside down in the photo)

Figure 13. The black dashed lines show the running surfaces on which the train traveled. Green ovals indicate where the solid spacers and through-castings bolts were installed. Gold ovals indicate the split spacers.

2.1.4 Test Case 4

Test Case 4 was designed to evaluate the effect of doubling the Nortrak pad material directly under the flangeway spacer tile. A piece of the Nortrak pad material was cut to the shape of the tile (Figure 14) and placed above the existing full-coverage rail seat pad to evaluate the effect of double padding directly under the flangeway spacer tile.

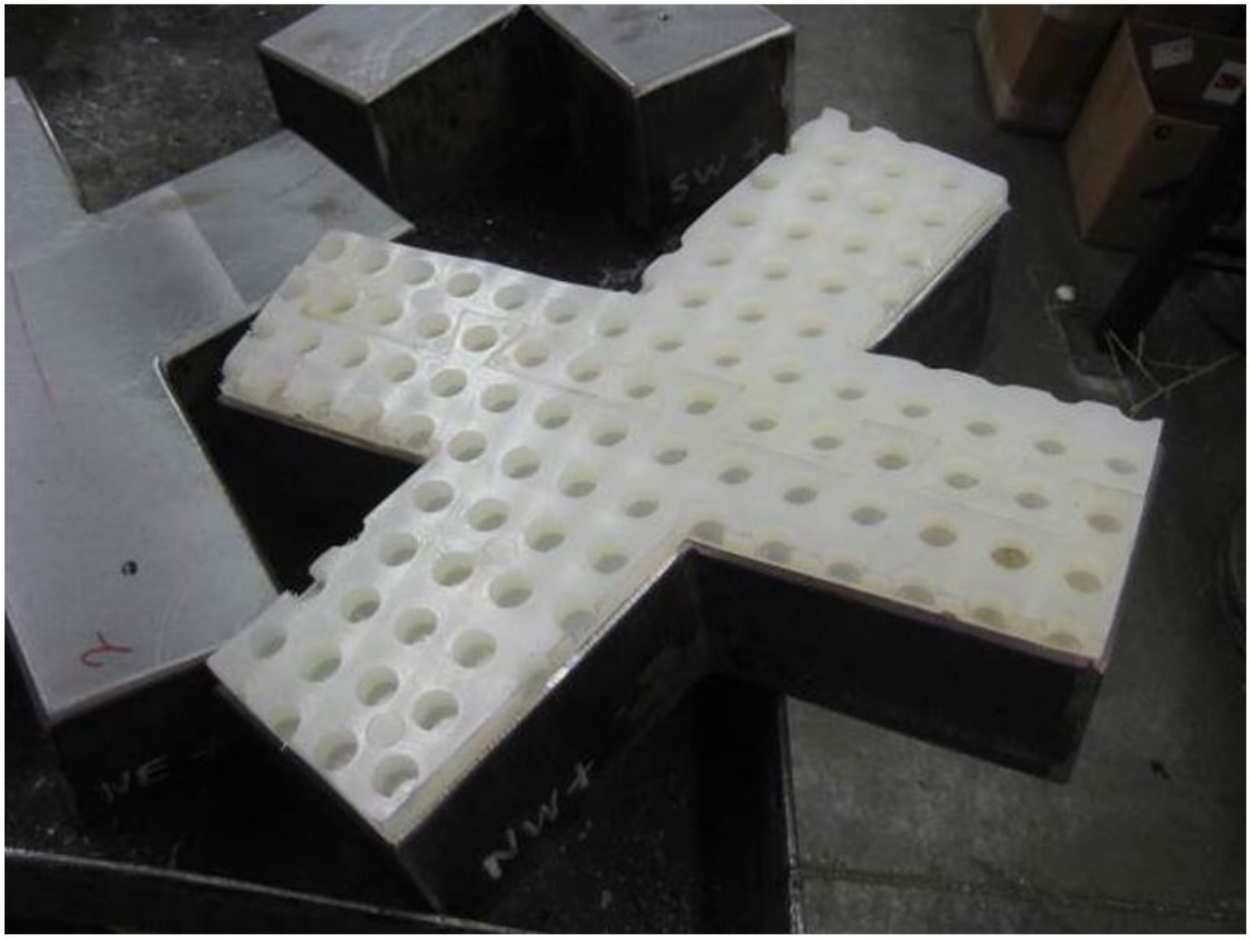

Figure 14. Nortrak pad material was cut and placed under the flangeway spacer tile to evaluate the effect of double padding

2.1.5 Test Case 5

For Test Case 5, the Getzner Type A pad material is intended for under-tie use. In this case, it was used as the full-coverage rail seat pad between the platework and the castings (Figure 15). As in Test Case 4, a piece of the Getzner Type C material (Figure 16) intended for the layered tile configuration of Test Case 9 was placed above the full-coverage rail seat pad to evaluate the effect of double padding directly under the flangeway spacer tile.

Figure 15. Getzner Type A pad intended for under-tie use was tested as a full-coverage rail seat pad

Figure 16. The Getzner Type C pad designed for the layered configuration of Test Case 9 was used to evaluate the effect of double padding under the flangeway spacer tile

2.1.6 Test Case 6

In Test Case 6, the pad intended for the full-coverage rail seat application (Getzner pad Type B) , was installed as shown in Figures 17 and 18.

Figure 17. Getzner pad Type B cut to size. This is the Getzner pad type intended for use in the full-coverage rail seat configuration

Figure 18. Getzner Type B full-coverage rail seat pad in place

2.1.7 Test Case 7

In Test Case 7, the Getzner Type B full-coverage rail seat pad was left in place and the under-tile pad was installed for a second combination of double pads.

2.1.8 Test Case 8

For Test Case 8, the full-coverage rail seat Nortrak pad tested in Test Case 4 was reinstalled and the Nortrak layered-tile configuration was introduced as a variable to determine if raising the pad material higher in the superstructure and closer to the source of impact affected the pad's performance (Figure 19).

Figure 19. The steel flangeway spacer tile was cut in half and ¼ in of material was milled from each half to accommodate a layer of the ½-in Nortrak pad material

2.1.9 Test Case 9

For Test Case 9, the full-coverage rail seat Getzner type B pad from Test Case 7 was reinstalled and the Getzner Type C material layered-tile configuration was introduced as a variable to determine if raising the pad material higher in the superstructure and closer to the source of impact affected its performance (Figure 20).

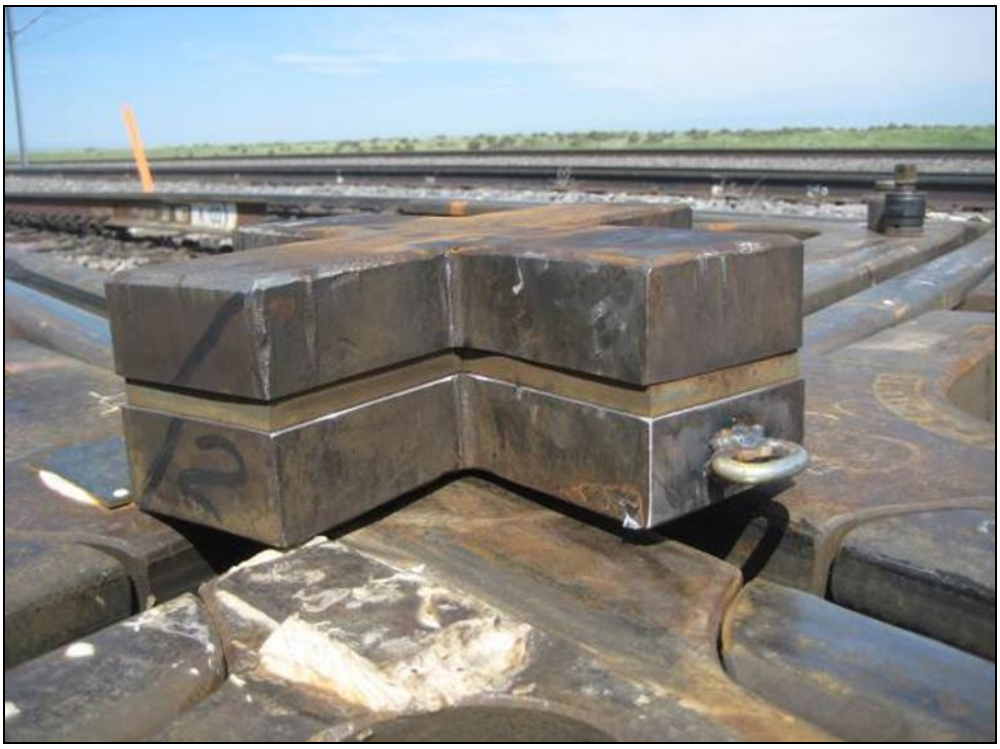

Figure 20. The steel flangeway spacer tile was cut in half and ¼ in of material was milled from each half to accommodate a layer of the ½-in Getzner Type C pad material

2.1.10 Test Case 10

For Test Case 10, the steel spacer tile was replaced with a solid rubber flangeway gap spacer tile that was cut at TTCI's machine shop. The test's goal was to significantly increase the thickness of the resilient material onto which the casting corners bear and measure the results. A ½-in strike plate was placed between the top of the rubber tile and the bottom of the casting corners.

The rest of the crossing diamond remained on the full-coverage rail seat Getzner Type B pad, but the shape of the tile was cut out in order to place the rubber tile directly on the platework, as Figures 21, 22, and 23 show.

Figure 21. The solid rubber flangeway spacer tile and its shape cut out of the full-coverage rail seat section of Getzner Type B pad that fits directly under the tile

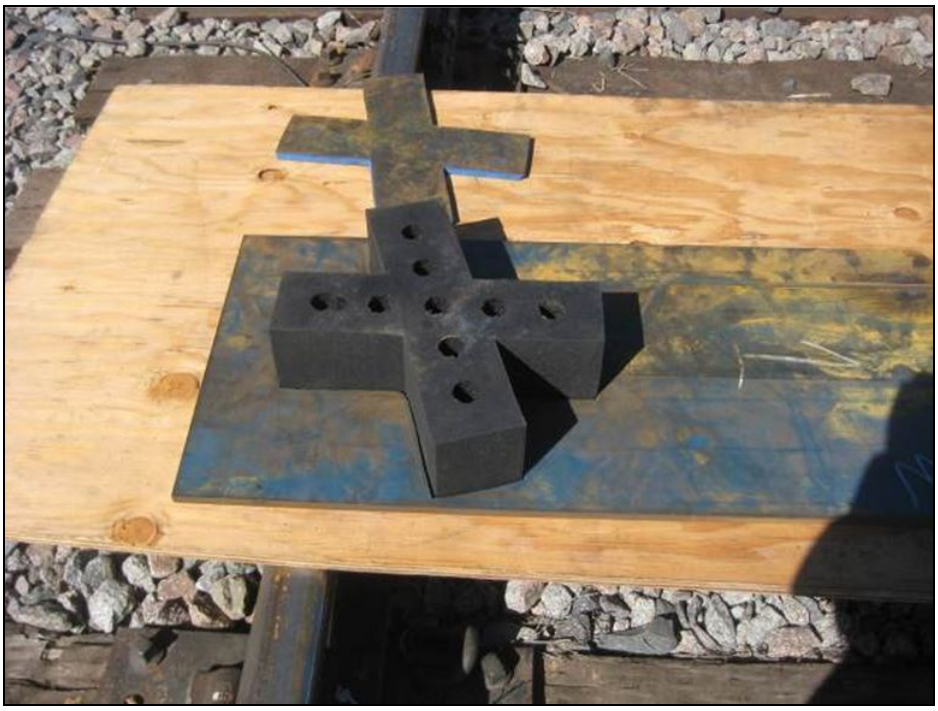

Figure 22. The solid rubber flangeway spacer tile embedded in the full-coverage rail seat Getzner Type B pad

Figure 23. The solid rubber flangeway spacer tile embedded in the Getzner Type B full-coverage rail seat pad resting directly on the platework. The strike plate between the rubber tile and the bottom of the casting corners was designed to protect the rubber.

2.1.11 Test Case 11

The resilient material configuration from Test Case 10 was left in place for Test Case 11. In this test case, the team replaced the remaining split spacers with solid spacers and through bolts. All of the connections were fitted with solid spacers and through bolts, which helped the team to evaluate the crossing diamond in its least flexible configuration.

2.1.12 Test Case 12

Test Case 12 provided the baseline performance of a typical crossing diamond of this type with no impact attenuation/damping materials. The steel flangeway spacer tile was reinstalled and the full-coverage rail seat pads were replaced with steel plate.

2.1.13 Test Case 13

For Test Case 13, the crossing diamond was fitted with the Getzner Type B pad in the full-coverage rail seat configuration, to evaluate this pad material over a longer-term period of service. No wheel force or displacement measurements were taken, because this configuration was measured during Test Case 6.

2.2 Performance Measurements

The performance measurements, which were described in Sections 2.2.1 through 2.2.8, were taken so the team could characterize the conditions at the crossing diamond and quantify the dynamic response as the HAL train passed over it at 40 mph. A set of measurements was taken for each of the back-to-back test cases.

2.2.1 Wheel Forces

TTCI's two instrumented wheelsets (IWS) were installed on the leading truck of a loaded (315,000-pound GRL) high sided gondola car. This car was one of four loaded cars, along with the data collection caboose and locomotive, that made up the test train shown in Figure 24. The IWS data provided the vertical and lateral load conditions over the crossing diamond. This data was used to determine the effect that the changing variables of each test case had on the load environment.

Figure 24. IWS test consist on the HTL approaching the crossing diamond in a CCW run

2.2.2 Running Surface Degradation

The running surface profiles at each casting corner and its approaching rails were measured at tonnage intervals using a rail profilometer, as shown in Figure 25. Profiles were taken at 2, 4, 6, 12, and 18 in from the center of its respective flangeway gap, where the 2-, 4-, and 6-in profiles were on the casting and the 12- and 18-in profiles were on the approaching rails. The initial and final profiles were overlaid to calculate the total vertical height loss resulting from wear, degradation, and maintenance grinding.

The series of profiles taken during the test at the 2-in location were overlaid to calculate the rate at which the height loss occurred.

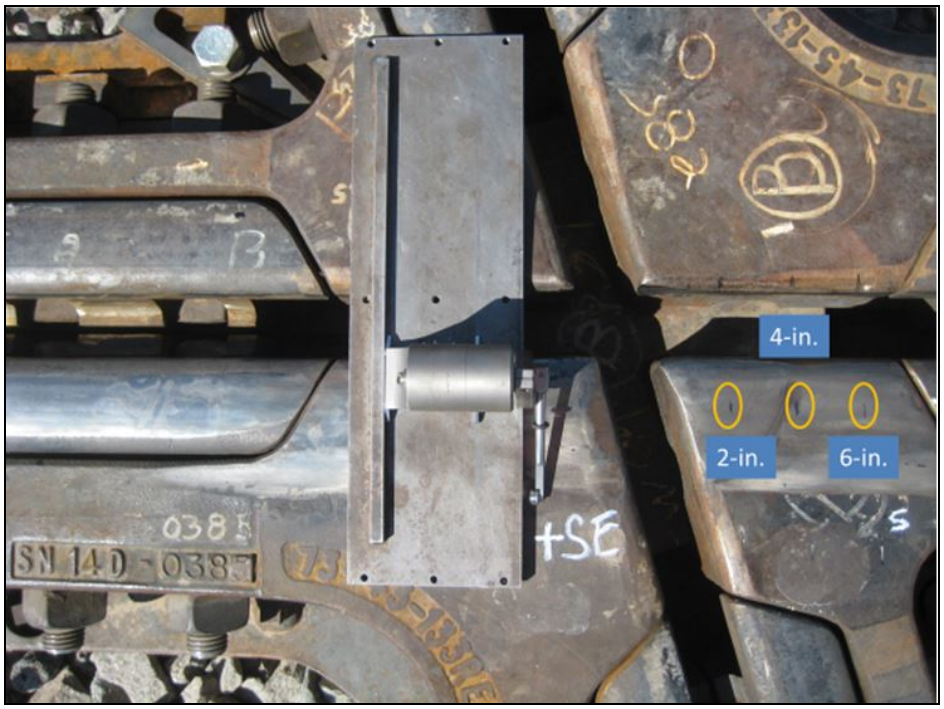

Figure 25. Profilometer in place to measure the 2-in profile of one of the casting corners at the southeast frog

2.2.3 Vertical Track Stiffness

The vertical track stiffness over the crossing diamond and its approaches was calculated with the light and heavy car method, where the difference in the known weight of the two cars and the difference in the resulting deflection measured under each of the two cars are used to calculate the stiffness. Figure 26 shows the test train and automatic level used to measure track deflection.

Figure 26. Vertical stiffness: light and heavy cars used to load the track vertically. The survey equipment is used to measure the resulting track deflection.

2.2.4 Track Surface

The vertical profile of the crossing diamond and its approaches were measured by taking top of rail elevation readings every other tie using survey equipment. These measurements were taken to quantify the vertical settlement.

2.2.5 Longitudinal, Lateral, and Vertical Displacement

The southwest frog was selected to measure displacement as the train passed over the crossing diamond. Two castings on the HTL inside rail were instrumented and identified as the inside and outside corners, where the inside corner is between the gage of the crossing track and the outside corner is directly opposite. The measurements were taken relative to the ground using bending beams fitted with a strain gage, and fastened to a 4-foot steel rod driven into the ballast section as shown in Figures 27 and 28.

These measurements were taken to do the following:

1. Understand how the frog components move under traffic.
2. Determine whether changes in the way the castings and guardrails were fastened (i.e., split spacers versus solid spacers with through bolts) affects the relative displacement of these components.
3. Determine if those fastening changes affect the wheel impact load environment
4. To understand the overall vertical displacement of the track structure, i.e., the crossing diamond and its ties, under HAL traffic.

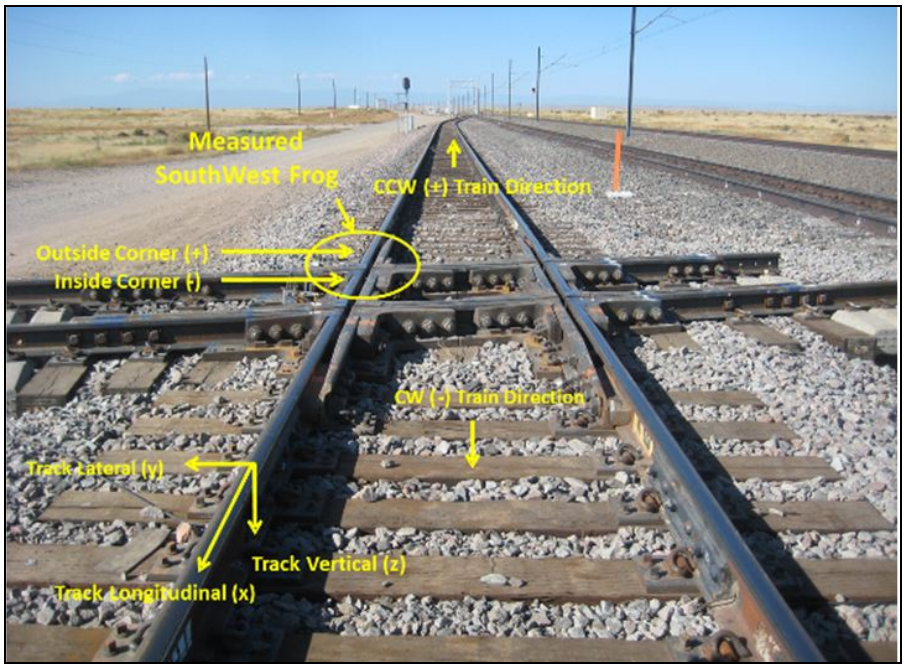

Figure 27. Sketch of the sign convention used to measure the movement of the crossing diamond and its components under HAL traffic

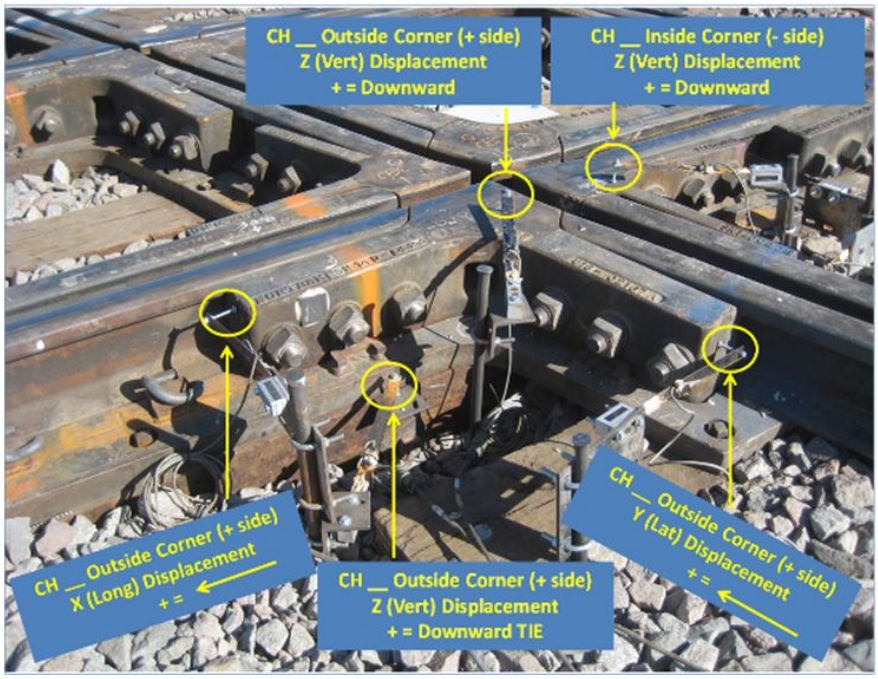

Figure 28. Sketch showing the location of bending beams used to measure the longitudinal, vertical and lateral displacement of the frog components and the track structure.

2.2.6 Effective Flangeway Gap and Wheel Drop

The effective flangeway gap is the distance from the point of the last wheel contact at one casting corner to the point of the first wheel contact beyond the flangeway gap on the next corner along the wheel's path. TTCI's prototype Effective Flangeway Gap and Wheel Drop gage (Figure 29) was used to measure the effective gap so the team could evaluate the relationship between the effective gap that the wheels negotiate over a crossing diamond, the connections used (i.e., split spacers versus solid spacers and through bolts), and the vertical wheel impact forces measured. It was also used to see the effect of rail temperature, and thereby thermal expansion and contraction, on the effective wheel gap in this particular crossing diamond design.

The effective wheel drop was measured in order to evaluate the relationship between the distance the wheel drops as it crosses the effective gap (relative to the approaching track) and vertical wheel impact forces.

In the wheel drop measurement mode, a baseline running surface measurement is taken at the end of the leveling rod, with the gage set up at the approach to the crossing diamond. To measure the effective wheel drop, the plastic 8-in chord section of a 36-in wheel, shown circled in Figure 29, is moved to span the flangeway gap, where another measurement is taken with the digital depth gage. The effective gap is the difference between the two measurements.

Figure 29. TTCI's prototype Effective Flangeway Gap and Wheel Drop gage in wheel drop measurement mode

In the flangeway gap measurement mode, the leveling rod is removed. A two-layer piece of carbonless paper is clipped to the wheel section; the wheel section is placed to span the flangeway gap; the gage is rocked over the gap with downward force (Figure 30) to create an imprint of the effective gap that is then measured (Figure 31).

Figure 30. TTCI's prototype Effective Flangeway Gap and Wheel Drop gage in wheel gap measurement mode at a revenue service crossing diamond

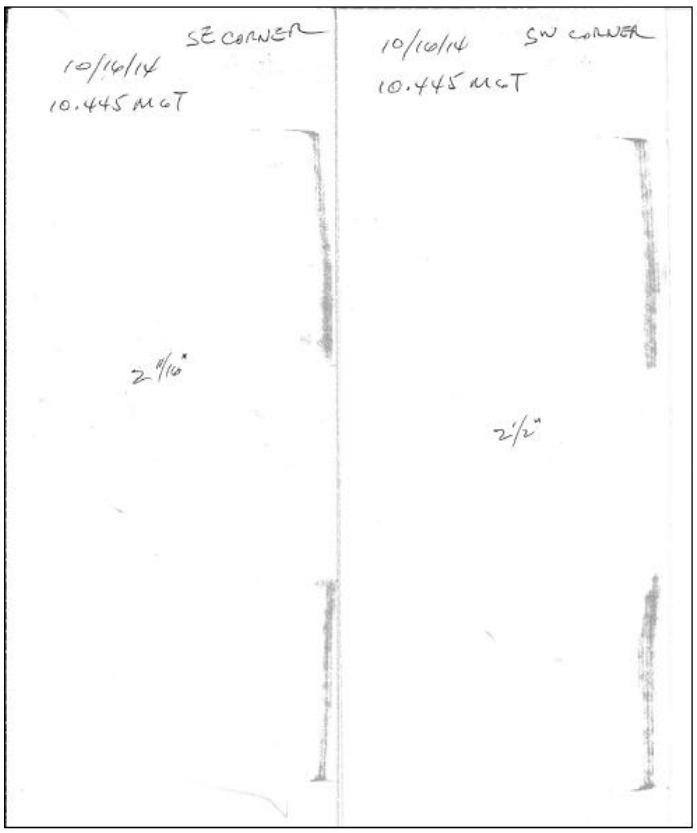

Figure 31. Imprint of the effective gap on the southeast and southwest frogs of the prototype crossing diamond after 10 MGT

2.2.7 Longitudinal Profile across the Casting Corners

The longitudinal profile along the running surface, across the casting corners, was measured at 1-in intervals to document changes early in the test. These static, unloaded measurements were taken with a straightedge to span the flangeway gap and a digital depth gage to measure down to the running surface (Figure 32).

Figure 32. Longitudinal profile measurements at 1-in intervals across the casting corners using a steel straightedge and digital depth gage

2.2.8 Running Surface Hardness

The initial change in running surface hardness was measured with a portable Leeb rebound hardness tester. Measurements were taken at 2, 4, 6, 12, and 18 in. from the center of each flangeway gap.

3. Results

3.1 Wheel Forces

3.1.1 Effect of Rail Seat Pads

Wheel-rail forces were measured for each of the 12 cases at speeds of 20, 30, and 40 mph. The standard deviation of the maximum vertical wheel forces measured after the initial deformation of the castings (Test Case 2b through Test Case 11) varied between 4.31 kips and 6.09 kips for all three train speeds. Similarly, the standard deviation of the 99th percentile vertical forces measured varied between 2.78 kips and 4.63 kips for all three train speeds.

Given the relatively small variation in the measured wheel forces during Test Cases 2b through Test Case 11, these cases were grouped to compare the padded crossing diamond cases with baseline Test Case 12 without pads. Figure 33 shows maximum rail forces measured over the crossing diamond with and without pads in place during CW and CCW train operation. Figure 34 shows the 99th percentile vertical wheel forces measured over the crossing diamond with and without pads in place during CW and CCW train operation.

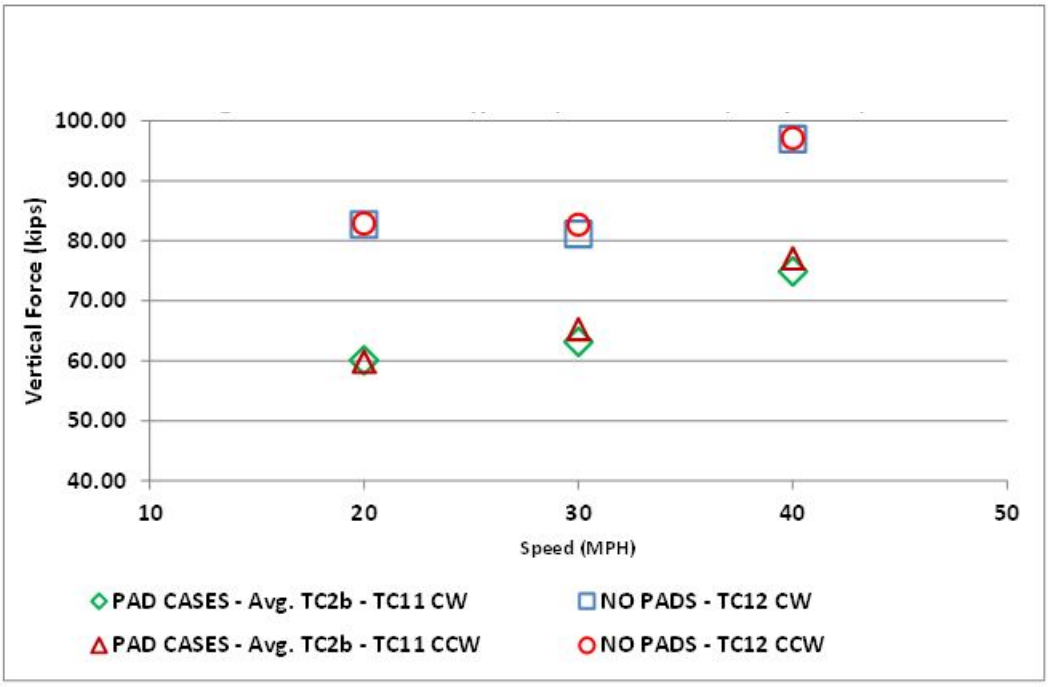

Figure 33. Maximum vertical wheel forces measured over the crossing diamond with and without pads in place during CW and CCW train operation

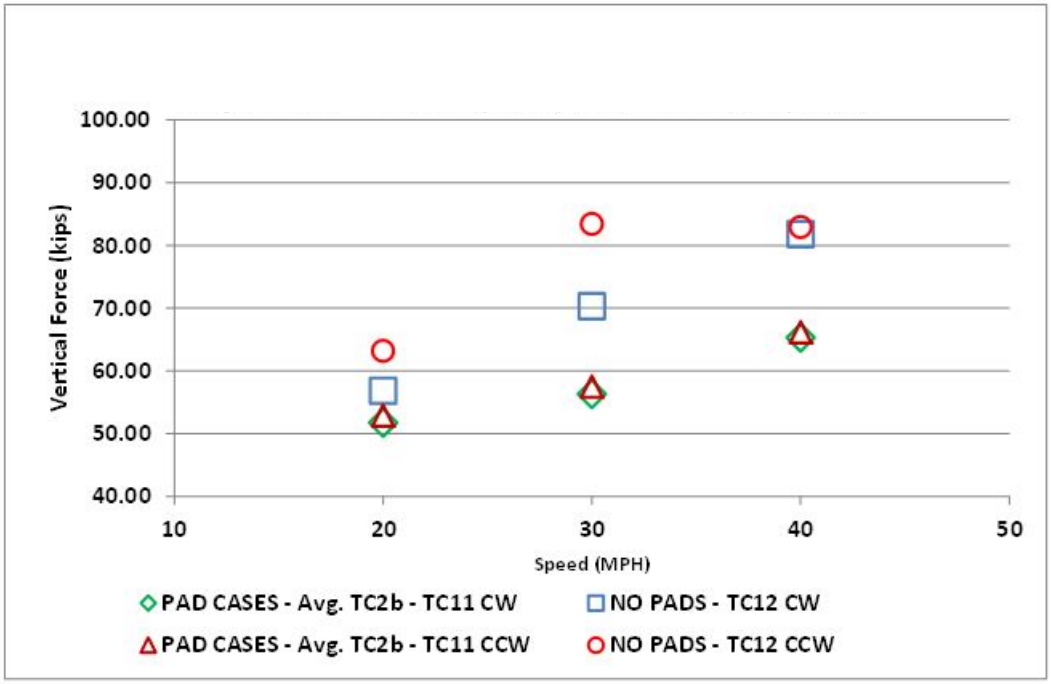

Figure 34. Ninety-ninth percentile vertical wheel forces measured over the crossing diamond with and without pads in place during CW and CCW train operation

The impact attenuation pads provided significant reduction in the vertical wheel forces measured over the crossing diamond in the ranges of 21 to 28 percent (maximum loads) and 9 to 31 percent (99th percentile). See Tables 2 and 3.

Table 2. Maximum vertical wheel forces and percent reduction when the impact attenuation pads were in place as compared to no pads

	CW	**CW**	
	Avg. Pad Cases	TC 12 - No Pads	
	TC 2b - TC11		
Speed (MPH)	Force (kips)	Force (kips)	%change
20	60.06	82.72	-27%
30	63.11	81.13	-22%
40	74.87	96.97	-23%
	CCW	**CCW**	
	Avg. Pad Cases	TC 12 - No Pads	
	TC 2b - TC11		
Speed (MPH)	Force (kips)	Force (kips)	%change
20	59.89	82.88	-28%
30	65.29	82.68	-21%
40	77.09	97.13	-21%

Table 3. Ninety-ninth percentile vertical wheel forces and percent reduction when the impact attenuation pads were in place as compared to no pads

	CW	CW	
	Avg. Pad Cases	TC 12 - No Pads	
	TC 2b - TC11		
Speed (MPH)	Force (kips)	Force (kips)	%change
20	51.76	56.84	-9%
30	56.32	70.30	-20%
40	65.29	81.80	-20%
	CCW	CCW	
	Avg. Pad Cases	TC 12 - No Pads	
	TC 2b - TC11		
Speed (MPH)	Force (kips)	Force (kips)	%change
20	52.90	63.18	-16%
30	57.50	83.41	-31%
40	66.17	82.94	-20%

The practical significance of the rail seat pads is that they have the potential to either reduce wheel-rail forces by 20 to 30 percent at a given operating speed or increase the operating speed by up to 20 mph for the same vertical forces. The former case should result in a significant increase in fatigue life for the frogs. One study done by TTCI under the Association of American Railroads' Strategic Research Initiative Program suggests that this life increase will be 50 to 100 percent. [4] The latter case should result in a significant decrease in train delay costs for locations that have speed restrictions. For heavily used mainlines, train delay costs can dominate life cycle costs for the crossing diamonds. [5]

3.1.2 Effect of Flangeway Spacers

Inside Rail

The test began with split-type flangeway spacers throughout the prototype crossing diamond, as originally designed, for the maximum flexibility evaluations. As the test progressed (Test Case 3), split spacers were replaced with solid spacers and through bolts at selected locations. And finally, all solid spacers were installed in place of the split spacers throughout the crossing diamond for the minimum design-flexibility evaluation. This was done to determine how much relative movement of frog castings was needed to provide a wheel-rail force reduction. Freedom of vertical movement comes with freedom of lateral and longitudinal movement as well, and they are largely detrimental, with resulting alignment and component maintenance issues. For Test Cases 3 through 10, the inside rail frog castings still had mostly split connections. The inner guard was fixed to the crossing track castings, while the outside rail was configured so that only the casting common to both routes was free to move relative to the other castings in a frog.

Figures 35 through 38 show the vertical wheel force response measurements as the freedom of movement between components was incrementally reduced. The data is presented in three test configuration categories and in both directions of traffic:

- Test Case 2b, in which the entire crossing diamond was fitted with split spacers
- Test Cases 3 through 10, in which selected locations were retrofitted with solid spacers and through bolts in place of the split spacers
- Test Case 11, in which all solid spacers were in place. (See Figure 13 to review the spacer configuration during Test Cases 3 through 10.)

While the maximum force data suggests a benefit in lowering forces by using split spacers, the benefit may not be of much practical significance. This may be the case for both magnitude and distribution of the vertical force data recorded at 40 mph in the CW direction shown in Figure 35. Given the relatively small difference in the 99th percentile data between the three test configuration categories at 40 mph in both the CW and CCW directions, shown in Figure 36, it appears the spacers had minimum effect.

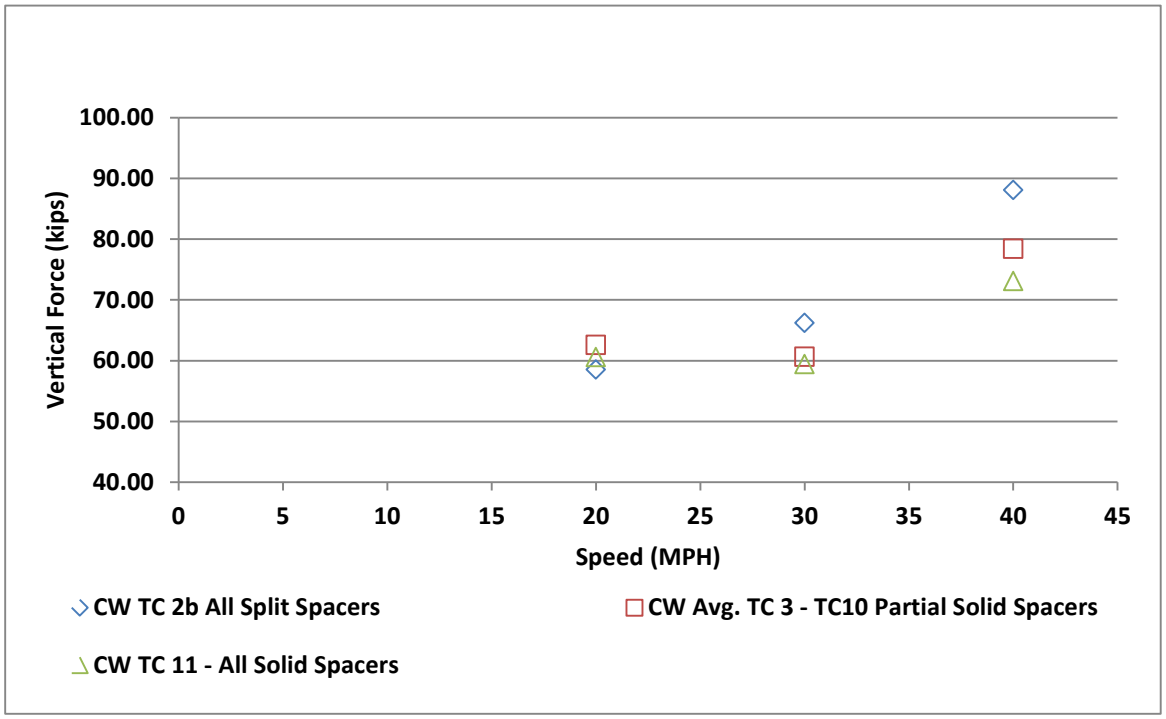

Figure 35. Maximum vertical wheel force during test cases of different design flexibility, CW traffic

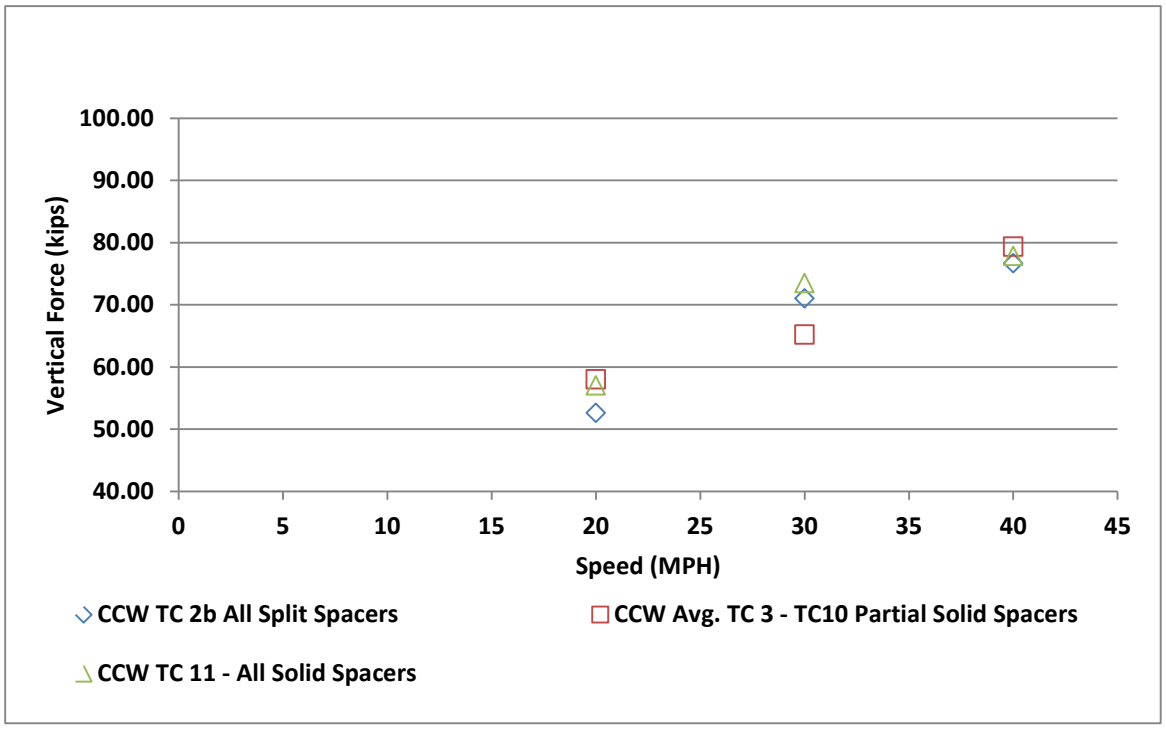

Figure 36. Maximum vertical wheel force during test cases of different design flexibility, CCW traffic

Table 4. Maximum vertical wheel load – Inside rail

Inside Rail Only	**CW**	**CW**	**CW**
	TC 2b All Split Spacers	Avg. TC 3 - TC10 Partial Solid Spacers	TC 11 - All Solid Spacers
Speed (MPH)	Force (kips)	Force (kips)	Force (kips)
20	58.55	62.59	60.58
30	66.19	60.65	59.42
40	88.05	78.40	73.11
	CCW	**CCW**	**CCW**
	TC 2b All Split Spacers	Avg. TC 3 - TC10 Partial Solid Spacers	TC 11 - All Solid Spacers
Speed (MPH)	Force (kips)	Force (kips)	Force (kips)
20	52.59	58.03	57.01
30	71.02	65.23	73.48
40	76.67	79.32	77.83

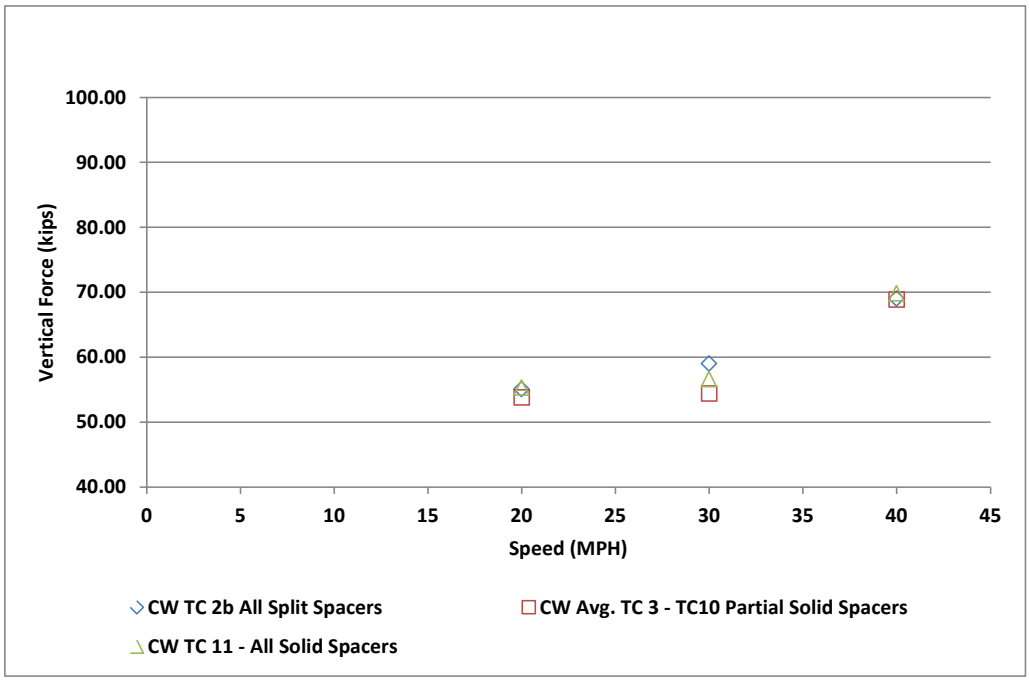

Figure 37. Ninety-ninth percentile vertical wheel force during test cases of different design flexibility, CW traffic

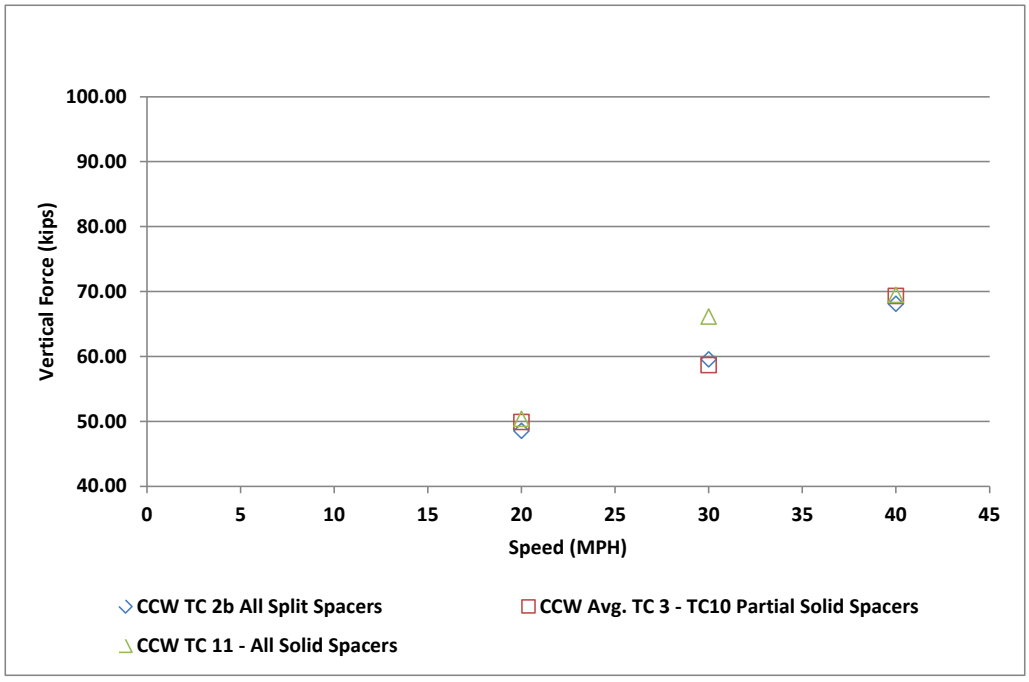

Figure 38. Ninety-ninth percentile vertical wheel force during test cases of different design flexibility, CCW traffic

Table 5. Ninety-ninth percentile vertical wheel load – Inside rail

Inside Rail Only	CW	CW	CW
	TC 2b All Split Spacers	Avg. TC 3 - TC10 Partial Solid Spacers	TC 11 - All Solid Spacers
Speed (MPH)	Force (kips)	Force (kips)	Force (kips)
20	55.07	53.79	55.32
30	59.00	54.39	56.60
40	69.01	68.88	69.84
	CCW	**CCW**	**CCW**
	TC 2b All Split Spacers	Avg. TC 3 - TC10 Partial Solid Spacers	TC 11 - All Solid Spacers
Speed (MPH)	Force (kips)	Force (kips)	Force (kips)
20	48.54	49.88	50.38
30	59.54	58.67	66.14
40	68.11	69.30	69.46

Outside Rail

The vertical wheel-rail force response at the outside rail is similar to that of the inside rail in that the 99th percentile data shows minimum effect resulting from the different flangeway spacer configurations as shown in Figures 39–42.

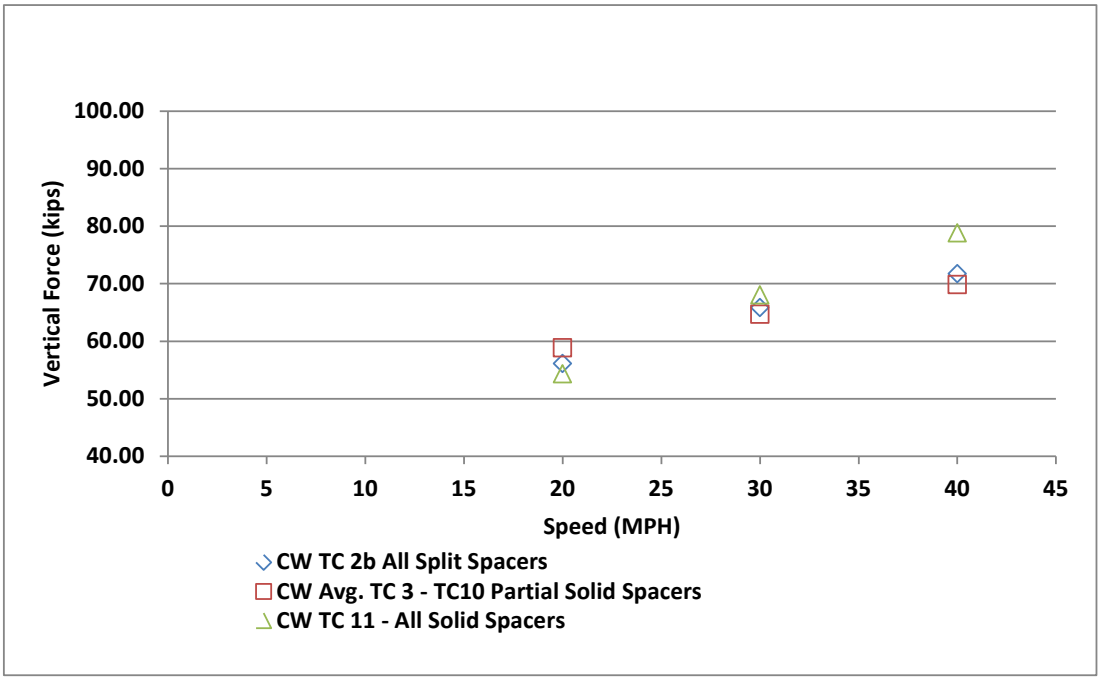

Figure 39. Maximum vertical wheel force during test cases of different design flexibility, CW traffic

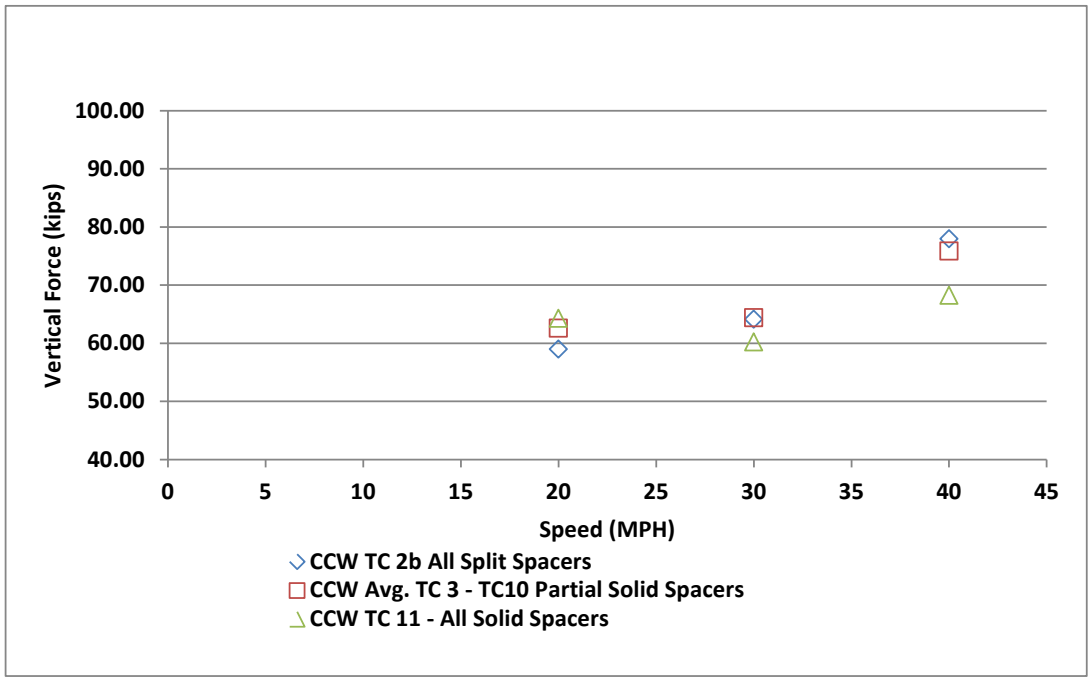

Figure 40. Maximum vertical wheel force during test cases of different design flexibility, CCW traffic

Table 6. Maximum vertical wheel load – Outside rail

Outside Rail Only	**CW**	**CW**	**CW**
	TC 2b All Split Spacers	Avg. TC 3 - TC10 Partial Solid Spacers	TC 11 - All Solid Spacers
Speed (MPH)	Force (kips)	Force (kips)	Force (kips)
20	56.13	58.86	54.34
30	65.82	64.70	68.03
40	71.75	69.82	78.84
	CCW	**CCW**	**CCW**
	TC 2b All Split Spacers	Avg. TC 3 - TC10 Partial Solid Spacers	TC 11 - All Solid Spacers
Speed (MPH)	Force (kips)	Force (kips)	Force (kips)
20	58.99	62.57	64.28
30	64.11	64.40	60.20
40	77.98	75.83	68.24

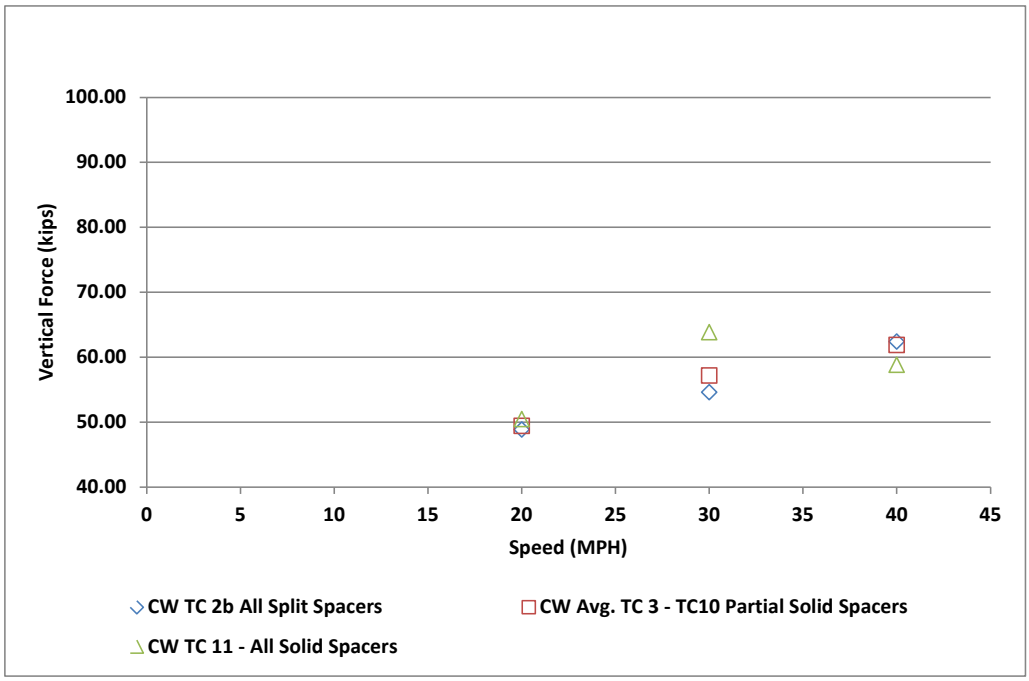

Figure 41. Ninety-ninth percentile vertical wheel force during test cases of different design flexibility, CW traffic

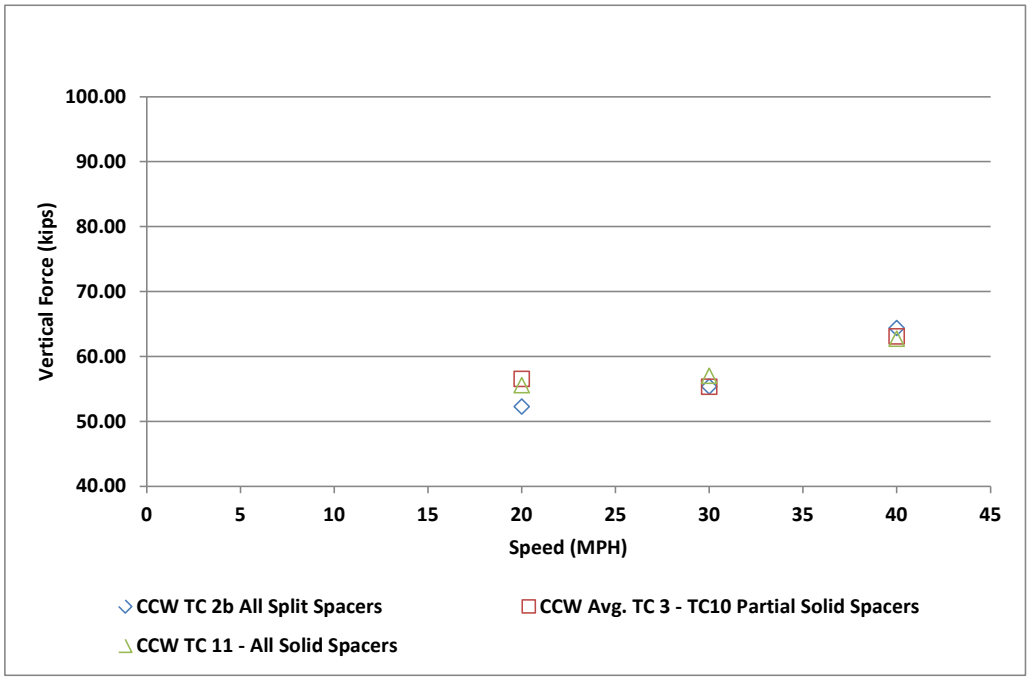

Figure 42. Ninety-ninth percentile vertical wheel force during test cases of different design flexibility, CCW traffic

Table 7. Ninety-ninth percentile vertical wheel load – Outside rail

Outside Rail Only	CW	CW	CW
	TC 2b All Split Spacers	Avg.	TC 11 - All Solid Spacers
		TC 3 - TC10 Partial Solid Spacers	
Speed (MPH)	Force (kips)	Force (kips)	Force (kips)
20	48.82	49.42	50.41
30	54.56	57.15	63.80
40	62.36	61.86	58.76
	CCW	**CCW**	**CCW**
	TC 2b All Split Spacers	Avg.	TC 11 - All Solid Spacers
		TC 3 - TC10 Partial Solid Spacers	
Speed (MPH)	Force (kips)	Force (kips)	Force (kips)
20	52.24	56.53	55.57
30	55.37	55.32	56.99
40	64.35	63.06	62.71

3.1.3 Summary of Rail Seat Pads and Flangeway Spacers

This section provides a global view and comparison of the vertical wheel load environment over various existing crossing diamond types and the Phase III prototype evaluated during this test. Figure 43 shows the maximum vertical wheel load versus speed for three currently used designs. The most flexible designs (the 3-rail and the flexible frog) had the lowest maximum vertical wheel loads. A confounding factor is the angle of the frogs in each crossing diamond. The higher angle frogs are known to produce higher forces. A better comparison can be made between the solid design 76-degree crossing diamond and the flexible design 78-degree crossing diamond. In this comparison, the flexible design produced 32 to 17 percent lower maximum forces at speeds of 20 to 40 mph. While a 76-degree vs 78-degree crossing diamond comparison was better, it was still not adequate to determine the relative effects of rail seat pads and flexible frog design.

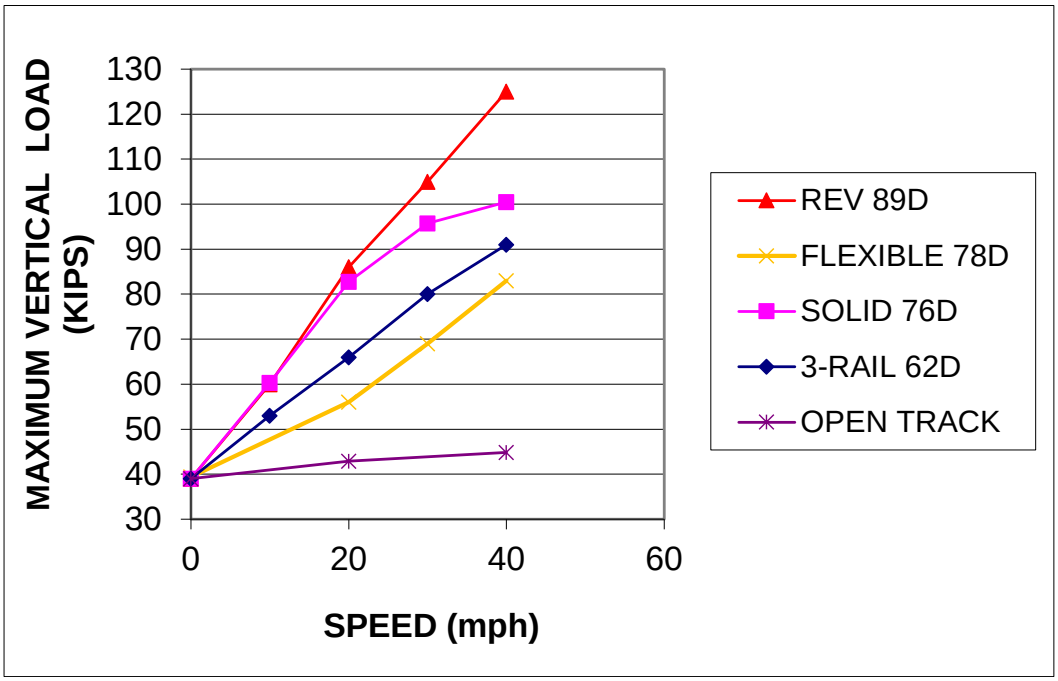

Figure 43. Maximum vertical wheel load vs. speed for various crossing diamonds evaluated at FAST

Using the Phase III prototype, the effects of rail seat pads and frog configuration were determined independently. Figure 44 shows how the addition of rail seat pads to the SRR crossing diamond decreased maximum vertical forces by 20-30 percent. The figure also shows that split flangeway spacers did not significantly affect maximum vertical forces (the SRR 78 with pads and Flexible 78 with pads comparison). Also note that the more flexible SRR design without pads had maximum vertical forces similar to a 76-degree solid design frog crossing diamond.

Additional tests evaluated two configurations of flexible frog by using four or two split flangeway spacers per frog (i.e., all four frog corners can move vertically relative to the others versus only the common corner can move relative to the other three). Figure 45 shows 99th percentile vertical forces over the crossing diamond. A better comparison can be made using 99th percentile forces instead of maximum forces. The reduced freedom between the four frog castings resulted in less alignment degradation and maintenance. Figure 45 shows there was some small benefit of either flexible frog configuration at 20 and 30 mph, but no reduction in vertical forces at 40 mph. Also note that there was almost no performance difference between the full flexible frog and the easier-to-maintain partial split spacer flexible frog.

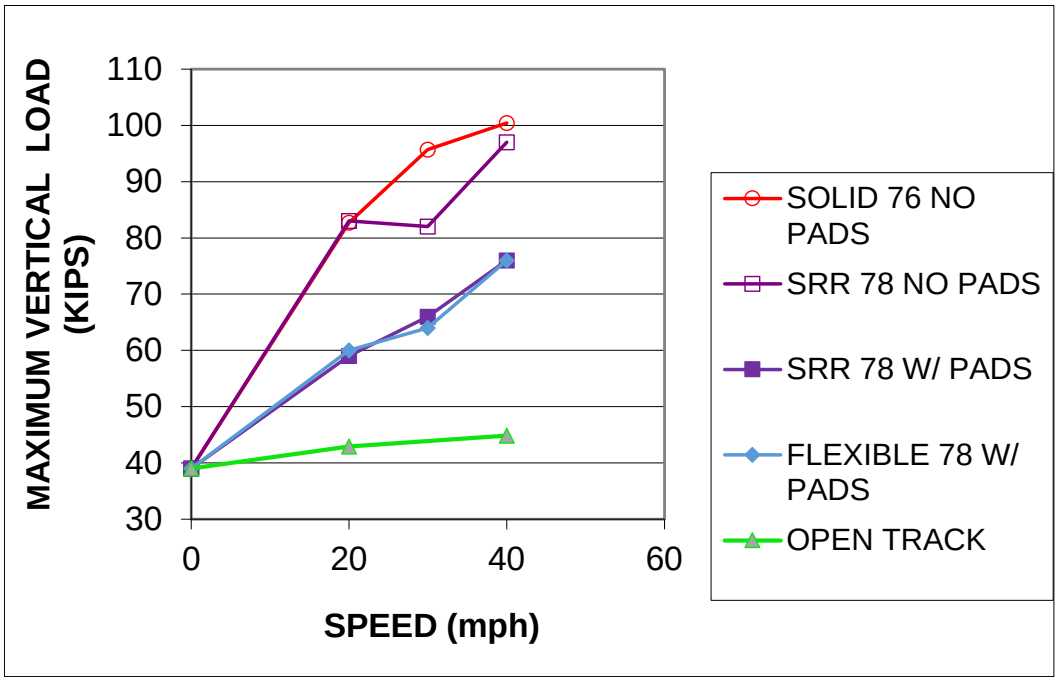

Figure 44. Maximum vertical wheel load vs. speed for various crossing diamonds foundations evaluated at FAST

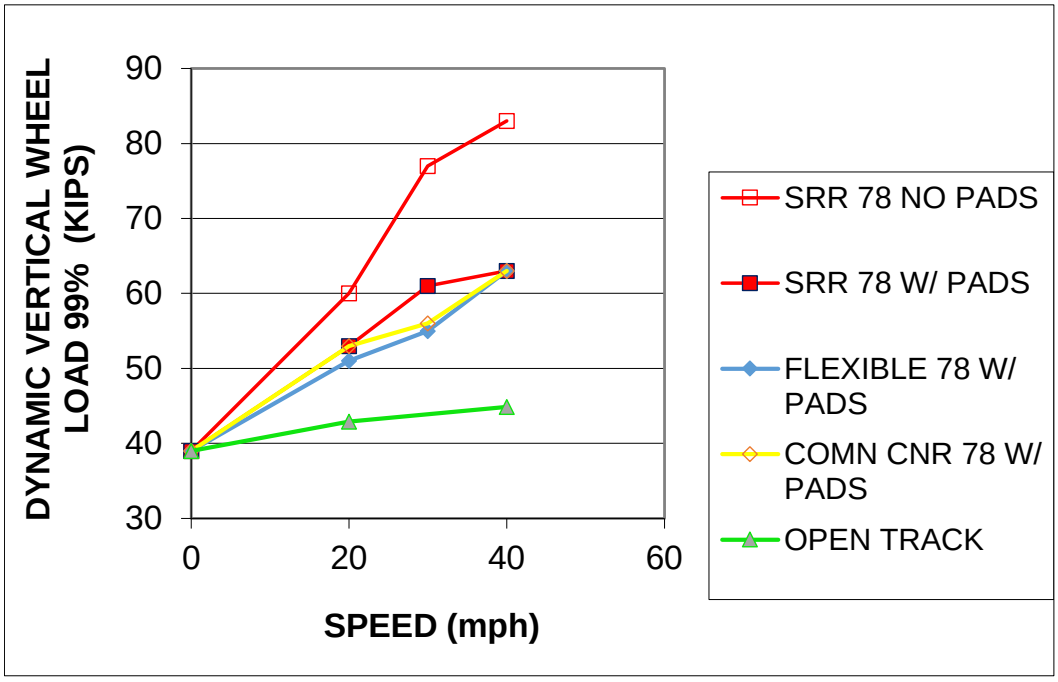

Figure 45. Maximum vertical wheel load vs. speed for various rail seat pad and flangeway spacers evaluated at FAST

3.1.4 Effect of Vertical Track Stiffness

The vertical stiffness of the crossing diamond structure was measured each time vertical wheel-rail forces were measured over the crossing. The stiffness measurements were taken at five locations over each of the two running rails as shown in Section 2.2.3 Vertical Track Stiffness of this report.

Figure 46 indicates that during most test cases, the vertical stiffness of the inside rail was higher than that of the outside rail.

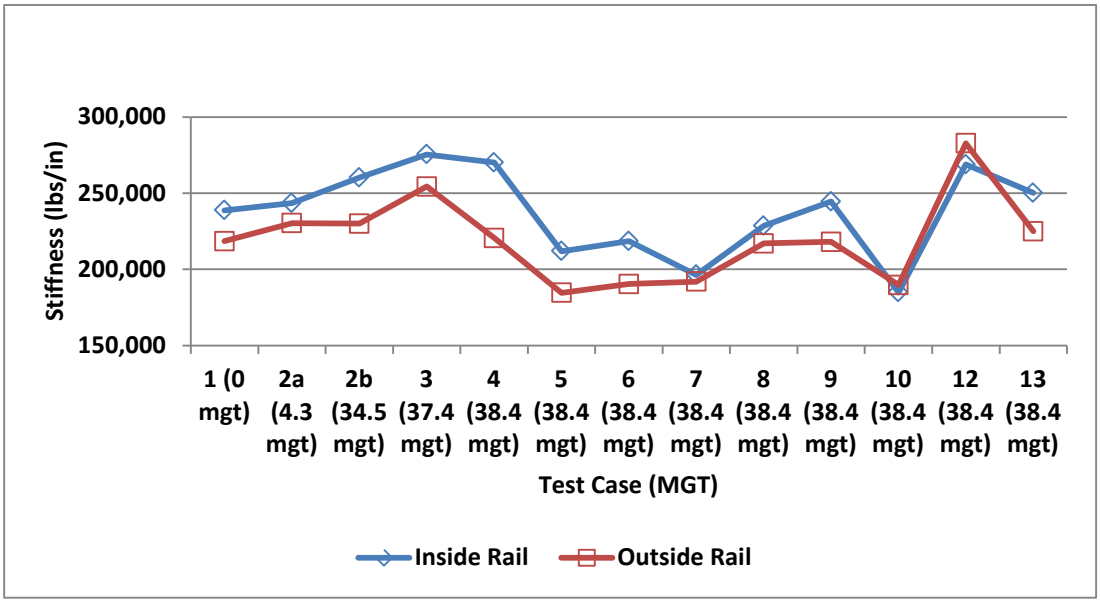

Figure 46. Vertical track stiffness over the core of the crossing diamond

General Relationship

The general relationship between the 40 mph vertical wheel forces measured during each test case versus the vertical stiffness of the crossing diamond is plotted in Figures 47–50. Tables 8-11 contain the measured wheel force and stiffness data.

Each graph pairs the separate vertical track stiffness of the inside and outside rail with the corresponding maximum and 99th percentile vertical force measured during CW and CCW train operation. Each graph also displays the separate average stiffness/force of all the inside-rail data points and all the outside-rail data points. In Figure 47, the results indicate that the average wheel-rail force measured was about 13 percent higher on the inside rail, which was about 8 percent stiffer than the outside rail. Over the range of stiffness measured, the vertical forces generally trend higher as stiffness increases.

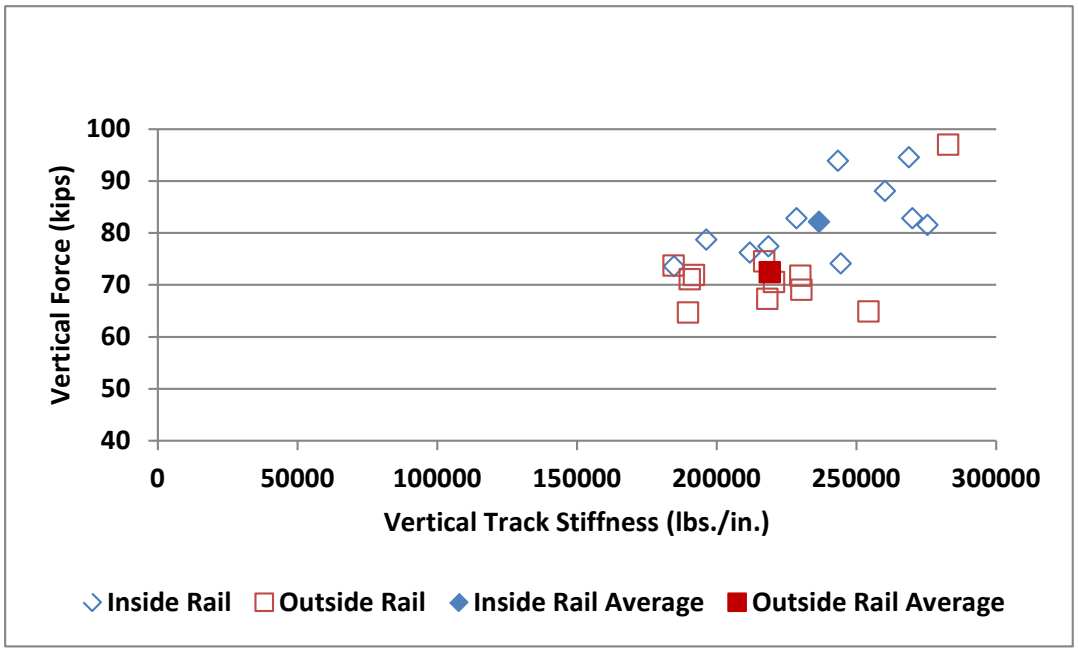

Figure 47. Maximum vertical wheel force vs. vertical crossing diamond stiffness (CW traffic), where the inside rail was about 8% stiffer than the outside rail and the wheel force was about 13% higher on the same rail (averages, shown as solid data points)

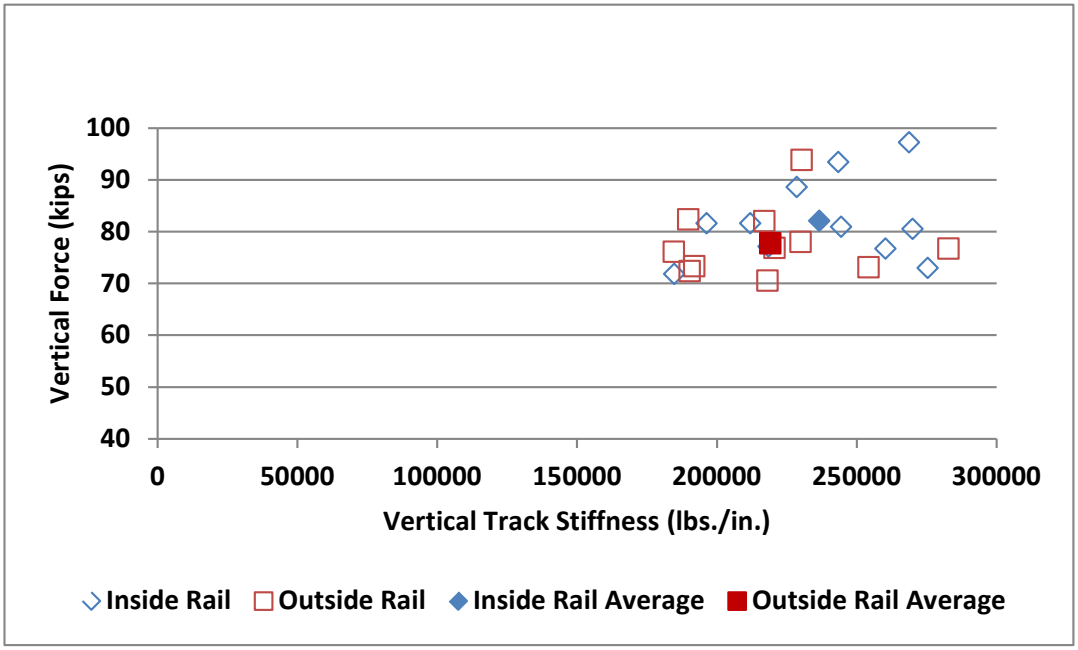

Figure 48. Maximum vertical wheel force vs. vertical crossing diamond stiffness (CW traffic), where the inside rail was about 8% stiffer than the outside rail and the wheel force was about 5% higher on the same rail (averages, shown as solid data points)

Table 8. Crossing diamond vertical stiffness and maximum CW vertical force

Test Case	Vertical Stiffness (lbs./in.) Inside Rail	Vertical Force (kips) Inside Rail	Vertical Stiffness (lbs./in.) Outside Rail	Vertical Force (kips) Outside Rail
2a (4.3 mgt)	243439	93.84	230372	69.08
2b (34.5 mgt)	260256	88.05	229994	71.75
3 (37.4 mgt)	275397	81.53	254307	64.86
4 (38.4 mgt)	270028	82.83	220574	70.57
5 (38.4 mgt)	211894	76.19	184617	73.70
6 (38.4 mgt)	218471	77.40	190332	71.09
7 (38.4 mgt)	196337	78.71	191929	71.90
8 (38.4 mgt)	228542	82.82	216981	74.51
9 (38.4 mgt)	244438	74.13	218094	67.28
10 (38.4 mgt)	184768	73.58	189736	64.64
12 (38.4 mgt)	268784	94.54	282789	96.97

Table 9. Crossing diamond vertical stiffness and maximum CCW vertical force

Test Case	Vertical Stiffness (lbs./in.) Inside Rail	Vertical Force (kips) Inside Rail	Vertical Stiffness (lbs./in.) Outside Rail	Vertical Force (kips) Outside Rail
2a (4.3 mgt)	243439	93.38	230372	93.83
2b (34.5 mgt)	260256	76.67	229994	77.98
3 (37.4 mgt)	275397	72.94	254307	73.12
4 (38.4 mgt)	270028	80.42	220574	76.83
5 (38.4 mgt)	211894	81.50	184617	76.13
6 (38.4 mgt)	218471	77.04	190332	72.38
7 (38.4 mgt)	196337	81.52	191929	73.30
8 (38.4 mgt)	228542	88.54	216981	81.99
9 (38.4 mgt)	244438	80.85	218094	70.54
10 (38.4 mgt)	184768	71.73	189736	82.36
12 (38.4 mgt)	268784	97.13	282789	76.70

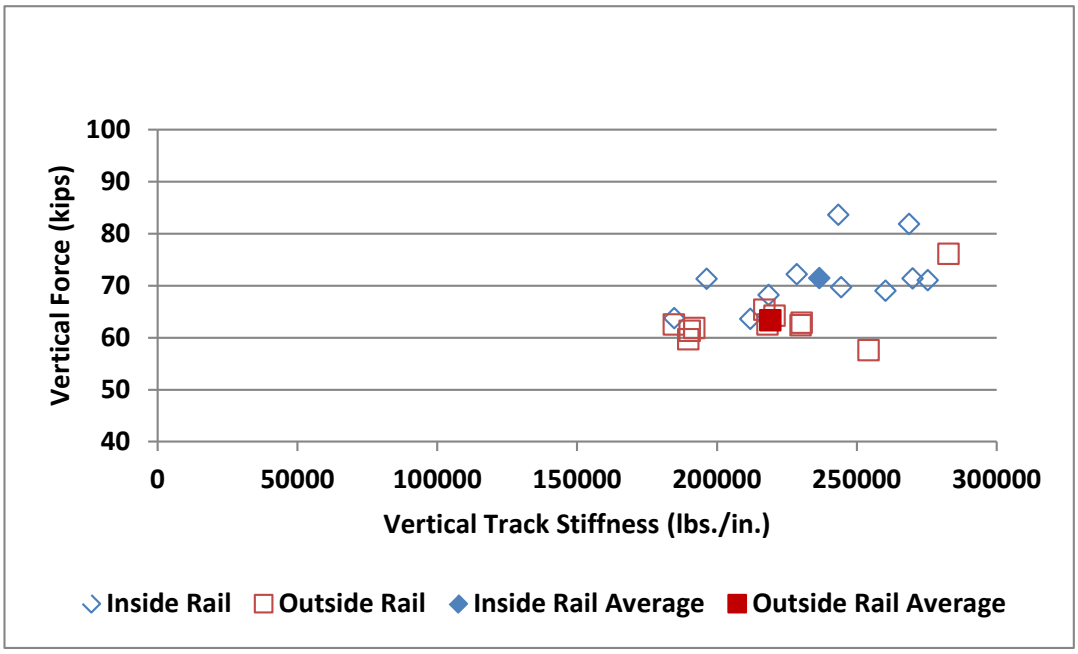

Figure 49. Ninety-ninth vertical wheel force vs. vertical crossing diamond stiffness (CW traffic), where the inside rail was about 8% stiffer than the outside rail and the wheel force was about 13% higher on the same rail (averages, shown as solid data points)

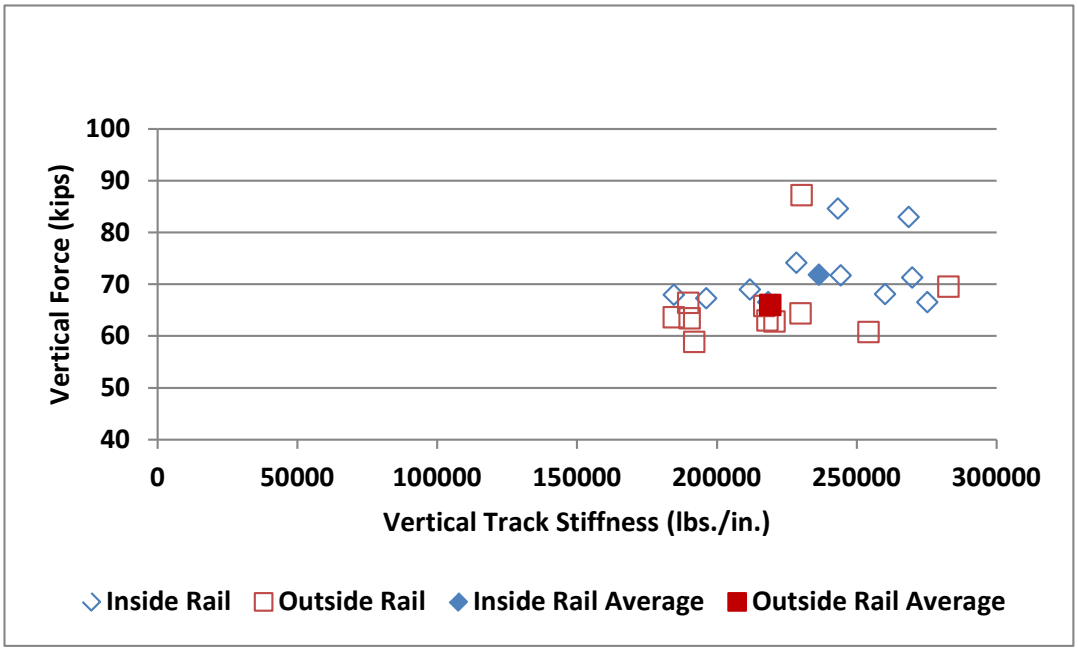

Figure 50. Ninety-ninth vertical wheel force vs. vertical crossing diamond stiffness (CCW traffic), where the inside rail was about 8% stiffer than the outside rail and the wheel force was about 9% higher on the same rail (averages, shown as solid data points)

Table 10. Crossing diamond vertical stiffness and 99th CW vertical force

Test Case	Vertical Stiffness (lbs./in.) Inside Rail	Vertical Force (kips) Inside Rail	Vertical Stiffness (lbs./in.) Outside Rail	Vertical Force (kips) Outside Rail
2a (4.3 mgt)	243439	83.56	230372	62.84
2b (34.5 mgt)	260256	69.01	229994	62.36
3 (37.4 mgt)	275397	71.02	254307	57.57
4 (38.4 mgt)	270028	71.37	220574	64.18
5 (38.4 mgt)	211894	63.59	184617	62.50
6 (38.4 mgt)	218471	68.21	190332	61.27
7 (38.4 mgt)	196337	71.30	191929	61.84
8 (38.4 mgt)	228542	72.15	216981	65.35
9 (38.4 mgt)	244438	69.65	218094	62.50
10 (38.4 mgt)	184768	63.71	189736	59.65
12 (38.4 mgt)	268784	81.80	282789	76.08

Table 11. Crossing diamond vertical stiffness and 99th CCW vertical force

Test Case	Vertical Stiffness (lbs./in.) Inside Rail	Vertical Force (kips) Inside Rail	Vertical Stiffness (lbs./in.)	Vertical Force (kips) Outside Rail
2a (4.3 mgt)	243439	84.60	230372	87.16
2b (34.5 mgt)	260256	68.11	229994	64.35
3 (37.4 mgt)	275397	66.54	254307	60.74
4 (38.4 mgt)	270028	71.25	220574	62.78
5 (38.4 mgt)	211894	68.99	184617	63.57
6 (38.4 mgt)	218471	66.54	190332	63.41
7 (38.4 mgt)	196337	67.28	191929	58.82
8 (38.4 mgt)	228542	74.13	216981	65.77
9 (38.4 mgt)	244438	71.71	218094	63.01
10 (38.4 mgt)	184768	67.94	189736	66.37
12 (38.4 mgt)	268784	82.94	282789	69.52

Detailed Relationship

The detailed relationship between vertical stiffness and vertical force for each test case is shown in Figure 51. This is a plot of the average track stiffness (both rails, five measurements per rail) of the crossing diamond structure and the corresponding vertical wheel force at 40 mph. The vertical force in each case is the highest 99th percentile value of the inside rail, outside rail, CW and CCW runs).

The following observations were made for each test case:

- Test Case 2a at 4.3 MGT was measured during the break-in period, when the ramped casting corners were relatively new, probably resulting in the high vertical wheel force.
- Test Case 2b saw a 21 percent reduction in force after 34.5 MGT
- The partial solid flangeway configuration was installed for Test Case 3 and a slight (3 percent) increase in force was recorded

- There was no significant change in the vertical wheel force environment between Test Cases 3 and 4, when the Nortrak pad was doubled under the flangeway spacer tile.
- The lowest stiffness recorded occurred under the conditions of Test Cases 5, 6, 7, and 10, when Getzner pads were in place for full coverage in the rail seat area. During Test Cases 5 and 7, Getzner pads were inserted under the flangeway spacer tile for the double-deep pad evaluation. During Test Case 10, a solid rubber spacer tile replaced the steel tile.
- Test Cases 8 (Nortrak) and 9 (Getzner) tested the layered-tile configuration, and pad material was sandwiched between two layers of steel tile.
- Test Case 12 saw a 47 percent increase in vertical stiffness accompanied by a 22 percent increase in vertical wheel force over Test Case 10. Test Case 12 was the baseline, where no pads were used and all solid spacers and through bolts were installed.
- To evaluate this pad material over a longer-term period of service in Test Case 13, the crossing diamond was fitted with the Getzner Type B pad in the full-coverage rail seat configuration.

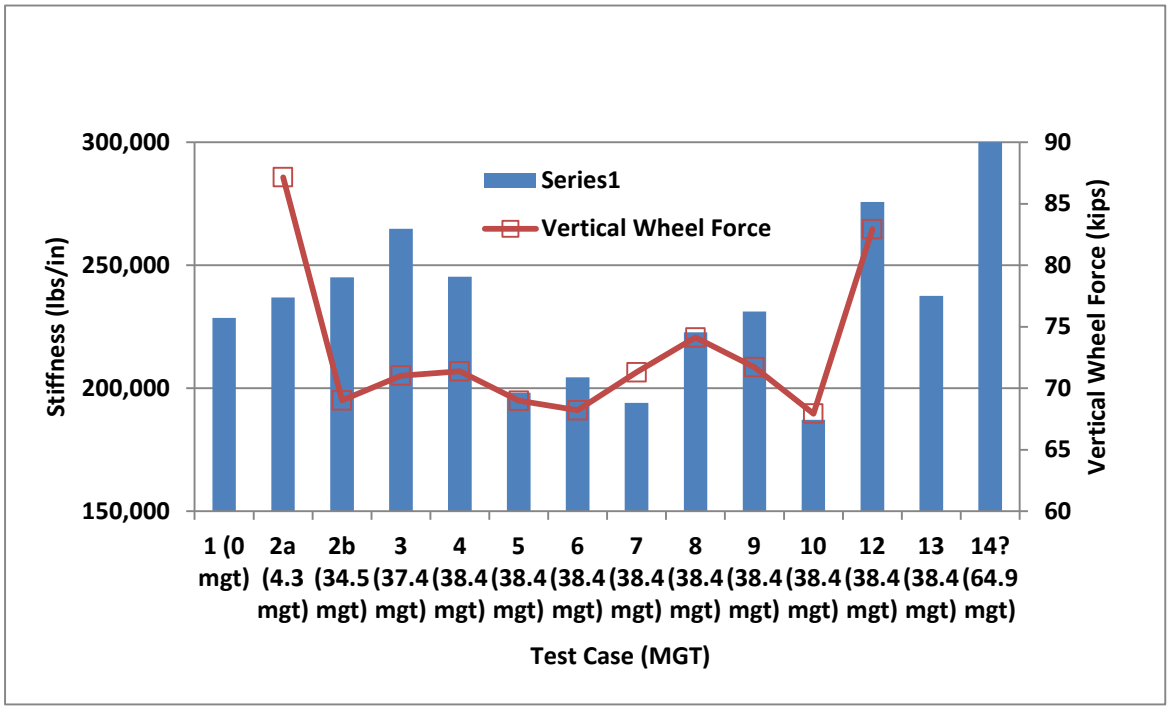

Figure 51. Relationship between vertical stiffness (bars) and vertical force for each test case

3.1.5 Summary of Vertical Wheel Force Data

Figures 52 and 53 are graphs of the maximum vertical wheel forces measured over the crossing diamond during all of the test cases for CW and CCW train operation.

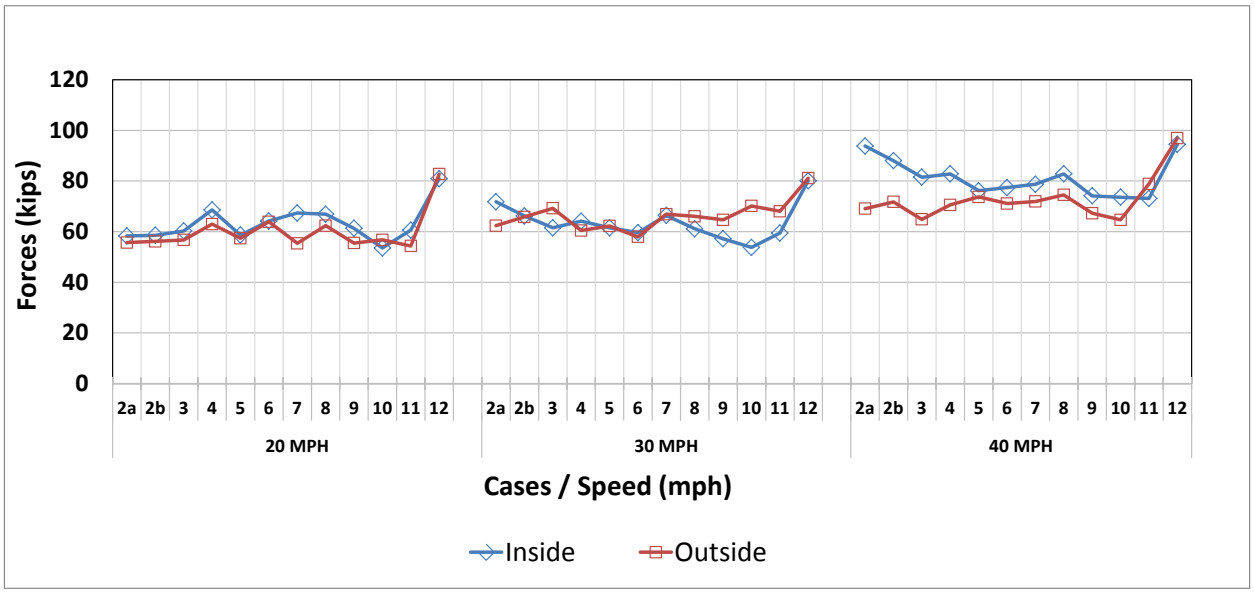

Figure 52. Maximum vertical wheel forces during all the test cases for CW train operation

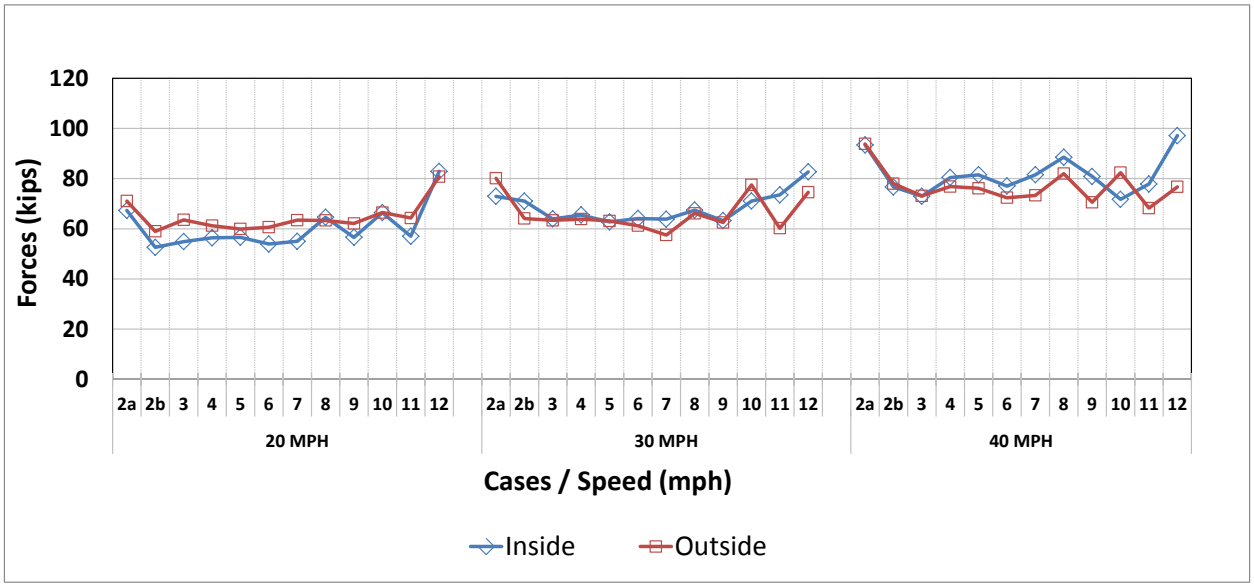

Figure 53. Maximum vertical wheel forces during all the test cases for CCW train operation

Figures 54 and 55 are graphs of the 99th percentile vertical wheel forces measured over the crossing diamond during all of the test cases for CW and CCW train operation.

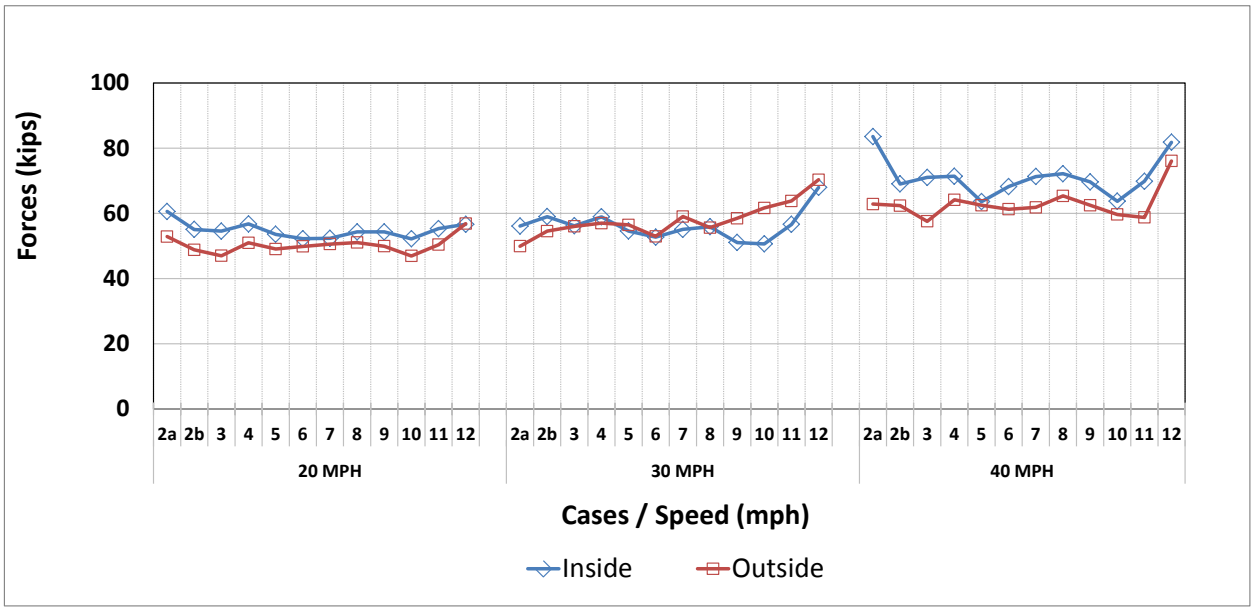

Figure 54. Ninety-ninth percentile vertical wheel forces during all the test cases for CW train operation

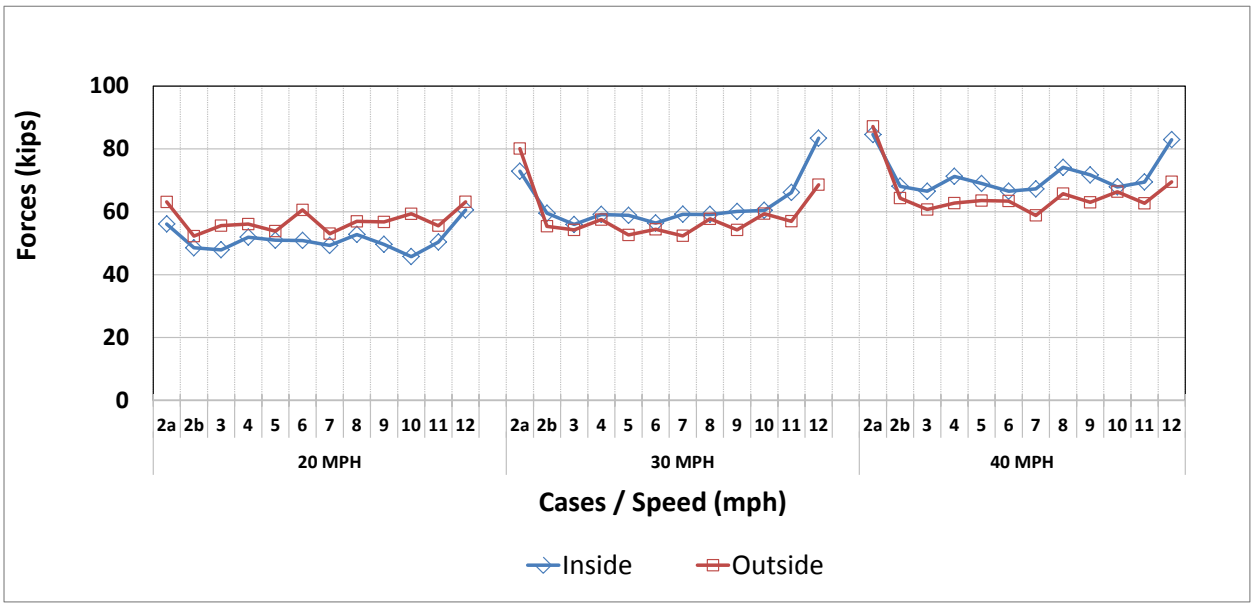

Figure 55. Ninety-ninth percentile vertical wheel forces during all the test cases for CCW train operation

The maximum lateral force data shows significantly more variation in both the CW and CCW train direction. The highest maximum lateral wheel force recorded was about 51.5 kips at 40 mph on the inside HTL rail in the CCW direction. Figures 56 and 57 are graphs of the maximum lateral forces in both train directions.

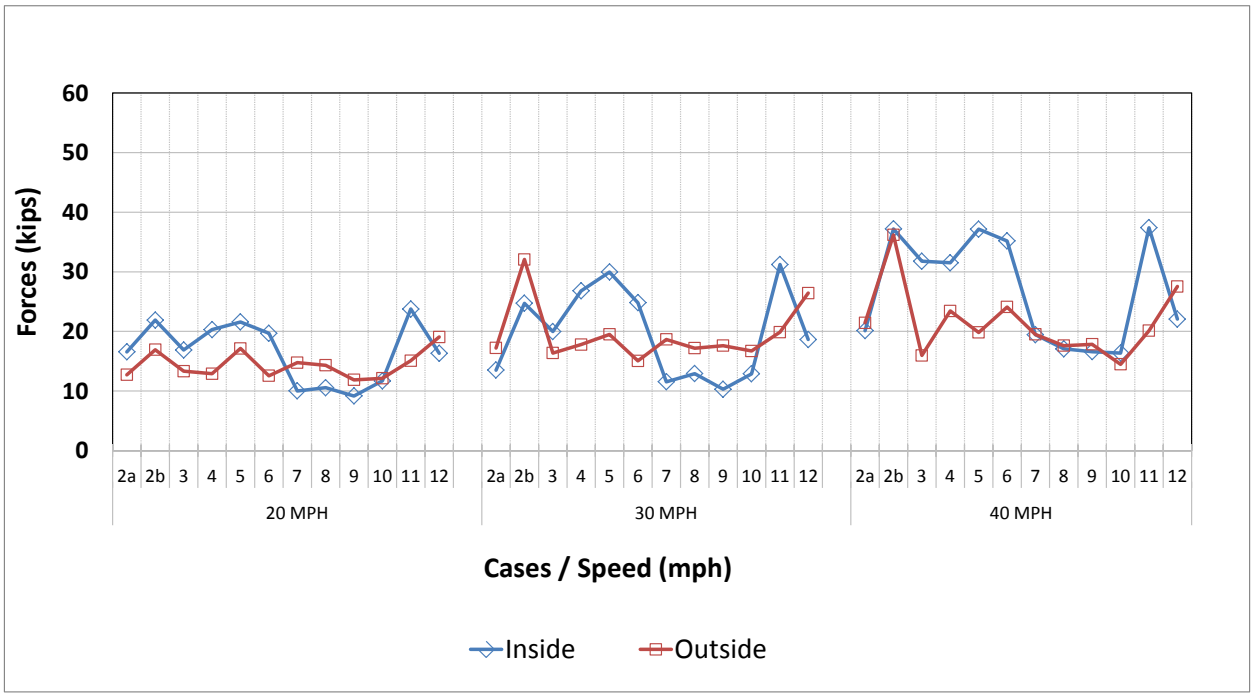

Figure 56. Maximum lateral wheel forces during all test cases for CW train operation

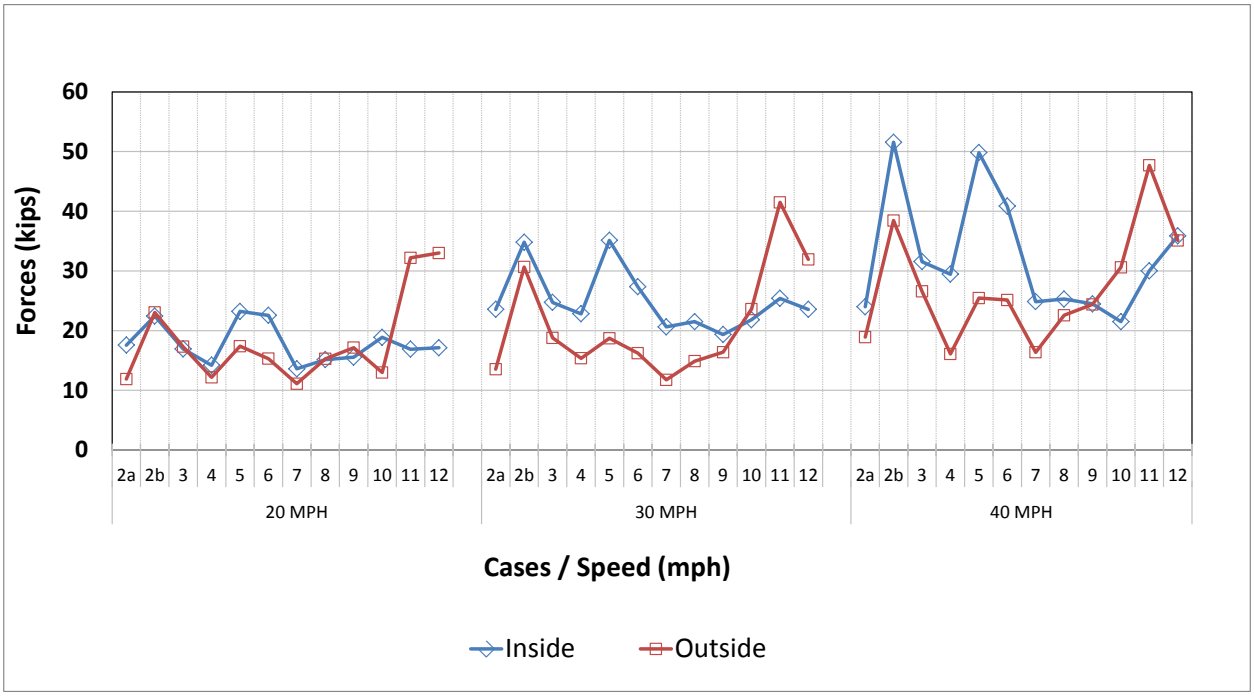

Figure 57. Maximum lateral wheel forces during all test cases for CCW train operation

With the maximum force peaks excluded in the 99th percentile lateral wheel force data, the largest spike at each speed occurs during Test Case 11. This is the first case tested with all the solid spacers and through bolts in place. In the CW direction, the high force occurs on the inside rail. In that direction and due to the angle of the crossing, it is the second frog that is loaded with

a given wheelset. In the CCW train direction the opposite occurs, where the high force was measured on the outside rail, the second frog loaded with a given wheelset. Figure 58 shows the direction of train travel, the inside and outside rails and the frog that is loaded first as the wheelset passes over the crossing, while Figures 59 and 60 graph the 99th percentile lateral wheel forces.

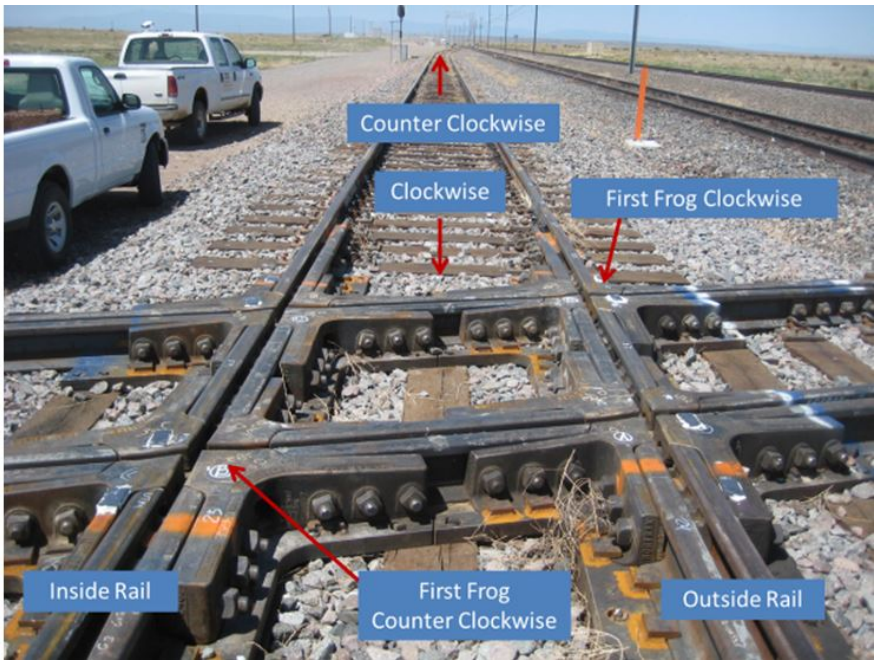

Figure 58. Shown is the direction of train travel, the inside/outside rails and the frog that is loaded first as the wheelset passes over the crossing

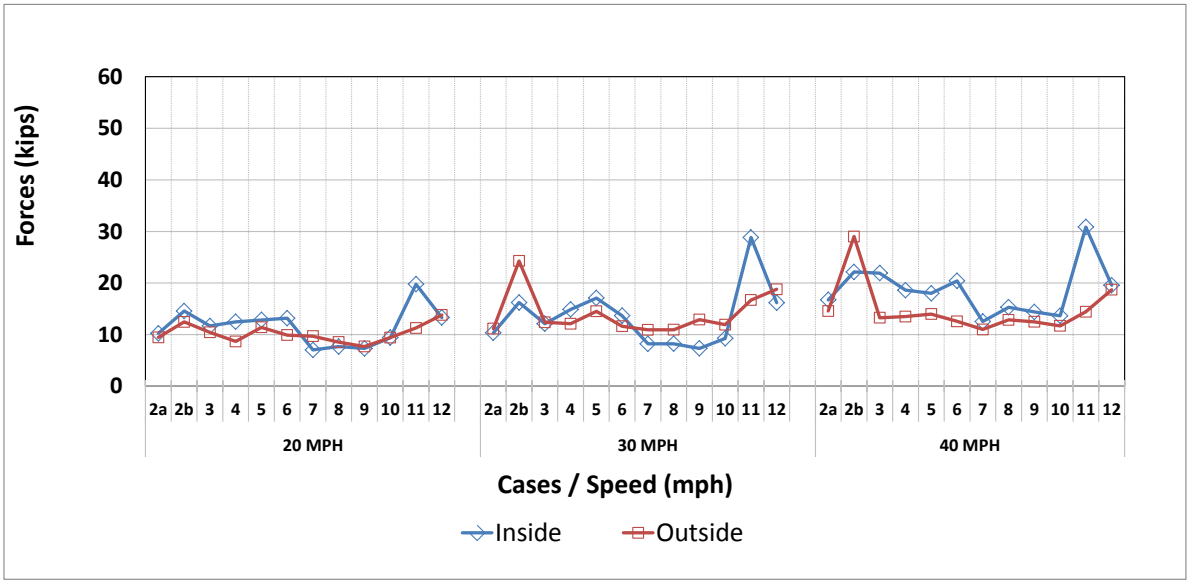

Figure 59. The highest 99th percentile lateral wheel force for each speed occurs on the inside rail in the CW train direction during Test Case 11 (all solid spacers and through bolts)

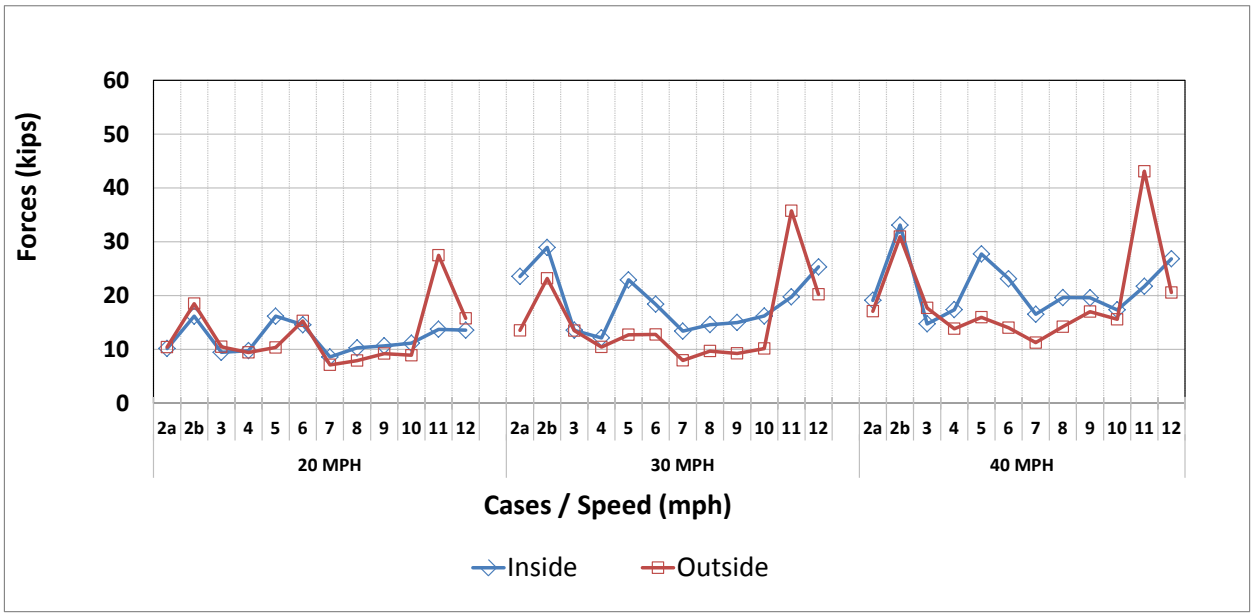

Figure 60. In the CCW train direction, the opposite occurs, the highest 99th percentile lateral wheel force for each speed is measured on the outside rail during Test Case 11 (all solid spacers and through bolts)

3.2 Running Surface Degradation

Figure 61 shows the total height loss at each of the casting corners and its respective approach rails based on profiles measured with a rail profilometer. The wear shown at 2-, 4-, and 6-in locations (relative to the center of the flangeway gap) occurred on the castings, and the wear shown at the 12- and 18-in locations occurred on the approaching rails. In every case, the highest loss of height occurred at the 2-in location, where the wheels impacted the casting corners.

The two northeast frog castings were in service for 39.97 MGT and the two northwest castings for 62.53 MGT, because they were swapped with the unused castings of the southeast and southwest frogs when spalling developed at the respective tonnages. In Figure 61, the height loss data for these pairs of castings are illustrated.

The maximum height loss of a casting in track for 64.87 MGT was about 0.15 in at the southwest frog. The average height loss on a railhead was about 0.025 in.

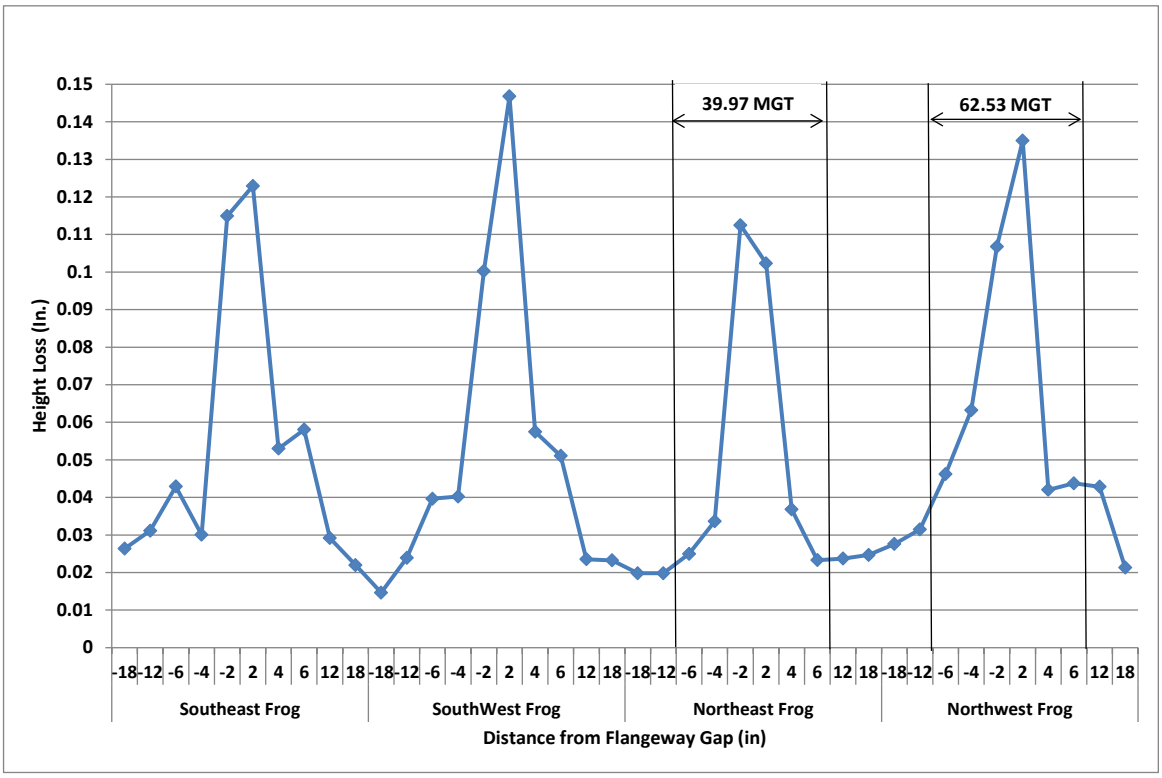

Figure 61. Total height loss at each of the casting corners and its respective approach rails based on transverse running surface profiles measured using a rail profilometer

Figures 62 through 65 indicate the rate at which the height of each of the casting corners was reduced due to wear/deformation at 2 in from the center its flangeway gap. The 2-in location experienced the most overall height loss. The results indicate steady state was achieved at all four frogs after the initial break-in period at 10 MGT.

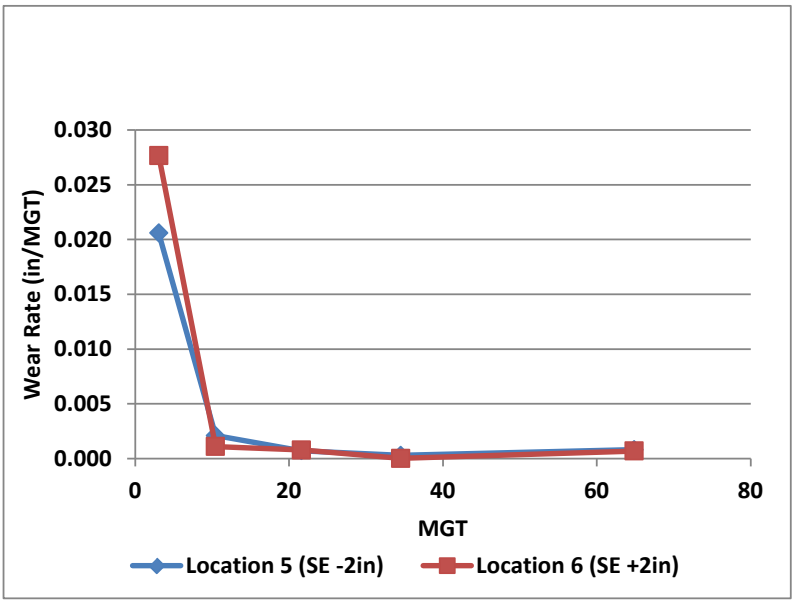

Figure 62. Southeast frog, 64.87 MGT: Height loss rate at both casting corners

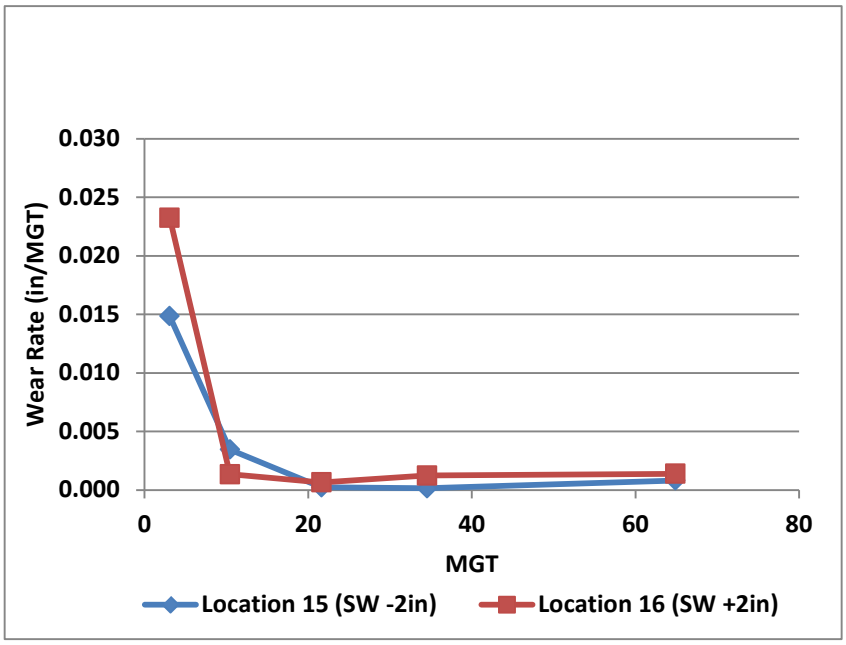

Figure 63. Southwest frog, 64.87 MGT: Height loss rate at both casting corners

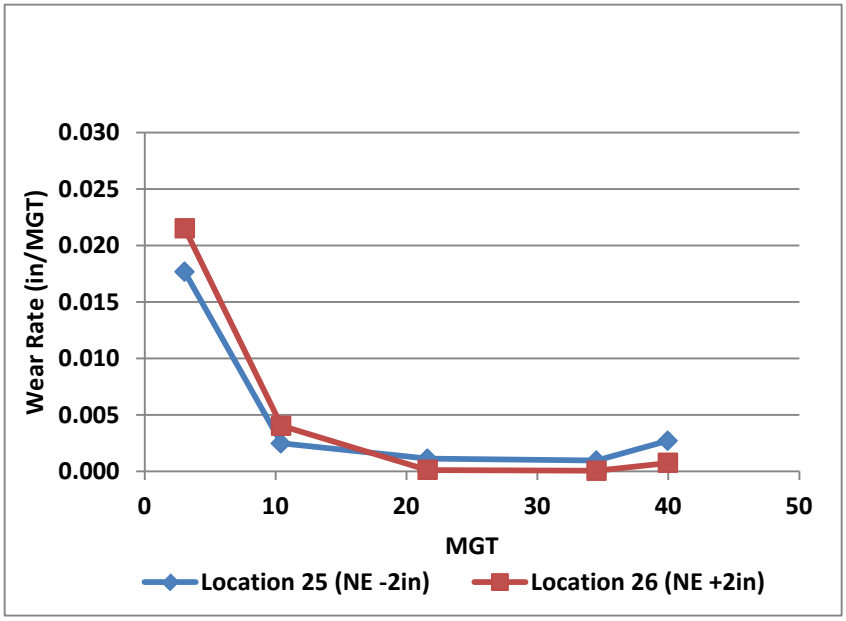

Figure 64. Northeast frog, 39.97 MGT: Height loss rate at both casting corners

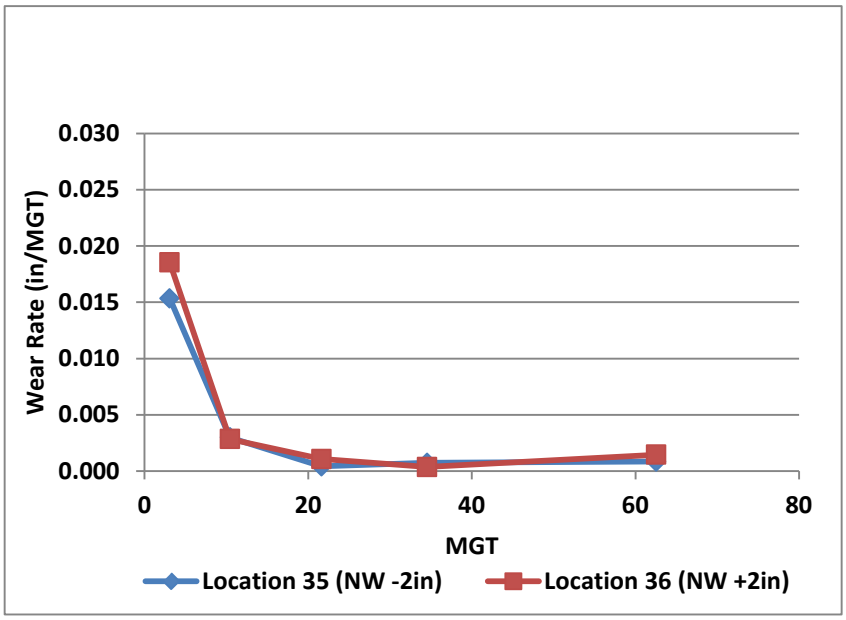

Figure 65. Northwest frog, 62.53 MGT. Height loss rate at both casting corners

The overlay shown in Figure 66 shows the changes in the shape of the casting corner profile due to wear, deformation, and maintenance grinding after 64.87 MGT.

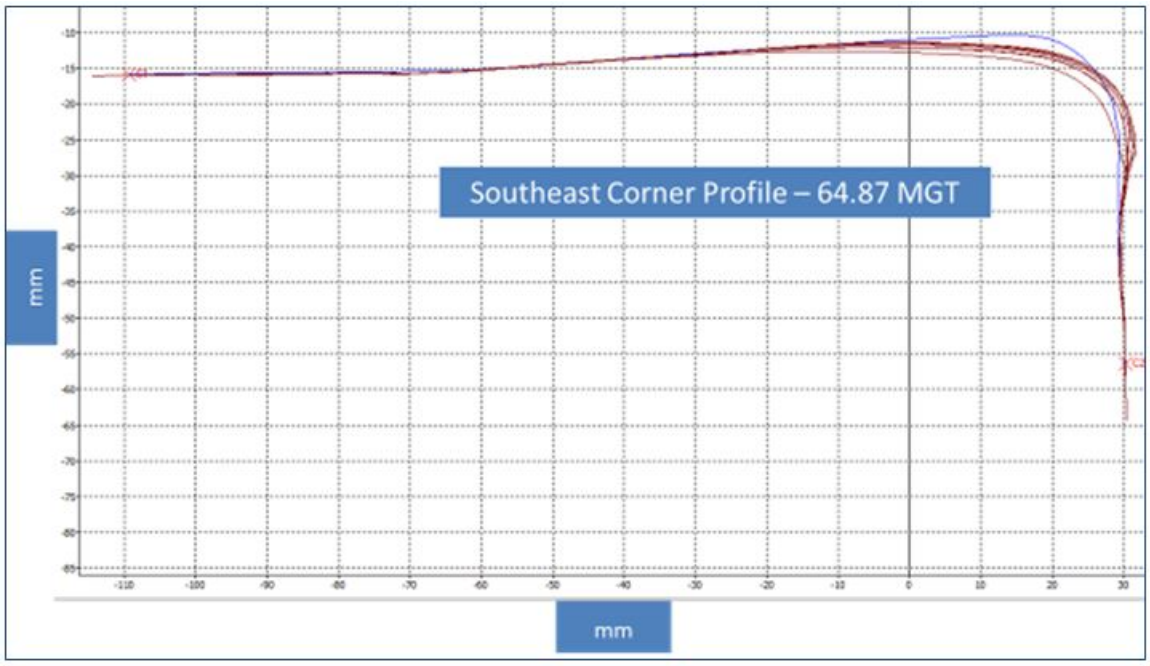

Figure 66. Changes in the shape of the casting corner 2 in from the center of the flangeway gap due to wear, deformation, and grinding after 64.87 MGT

3.3 Running Surface Hardness

The running surface hardness was measured at the same locations on the casting corners where the profile measurements were taken, that is, at 2, 4, and 6 in from the center of the flangeway gap. The average hardness of all the casting corners before traffic was about 422 BHN. Within 5 MGT, the average hardness increased to about 503 BHN. After 64 MGT, as shown in Figure 67, the running surface hardness reached about 540 BHN.

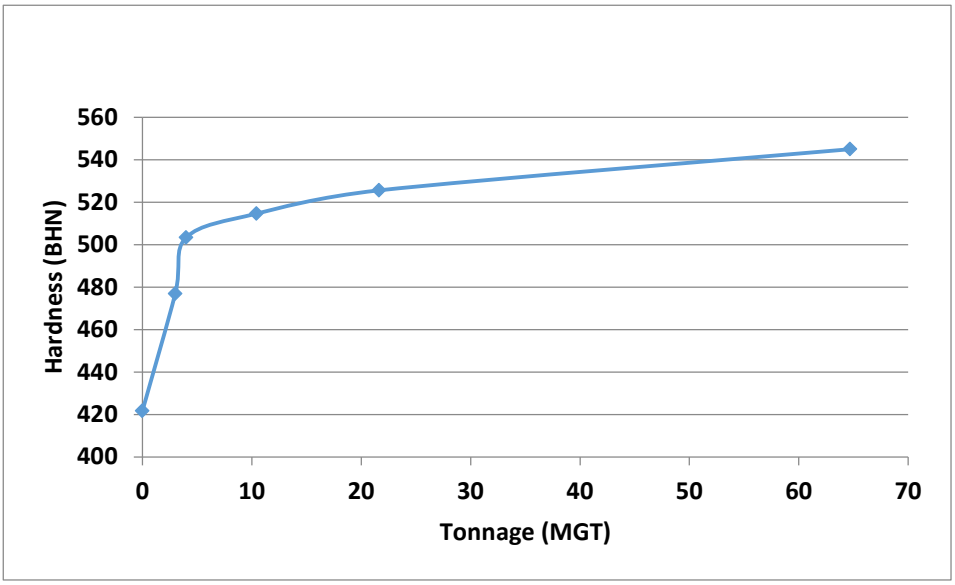

Figure 67. Average running surface hardness measured at 2, 4, and 6 in from the center of the flangeway gap at all 8 casting corners

3.4 Effective Flangeway Gap and Wheel Drop

The effective flangeway gap varied during the course of the test, as is shown in Figure 68. The first six measurements were taken during summer and early fall when the ambient temperature was primarily between 70° F and 80° F (rail temperature was only taken during one of the six measurements; at 12.48 MGT the rail temperature was 87° F.). During this period, the average effective gap was about 2.6 in.

The 7th, 8th, and 9th measurements were taken when the rail temperature was, 19°F, 15°F, and 22° F, respectively. During this time in February and March, the average effective gap was about 3.27 in; an increase in the size of the gap was likely due to cold weather rail contraction.

The remaining measurements were taken when the rail temperature was between 61°F and 109° F, which led to various flangeway gaps.

Figure 69 shows flangeway effective gap versus rail temperature. This comparison indicates that when the rail temperature was around 20° F, the gap opened as much as 3.5 in with the split spacers in place. Conversely, it appears that even at the highest rail temperature recorded (109° F), the gap did not close more than about 2.7 in. This is likely due to the flangeway spacer tile at the center of each frog.

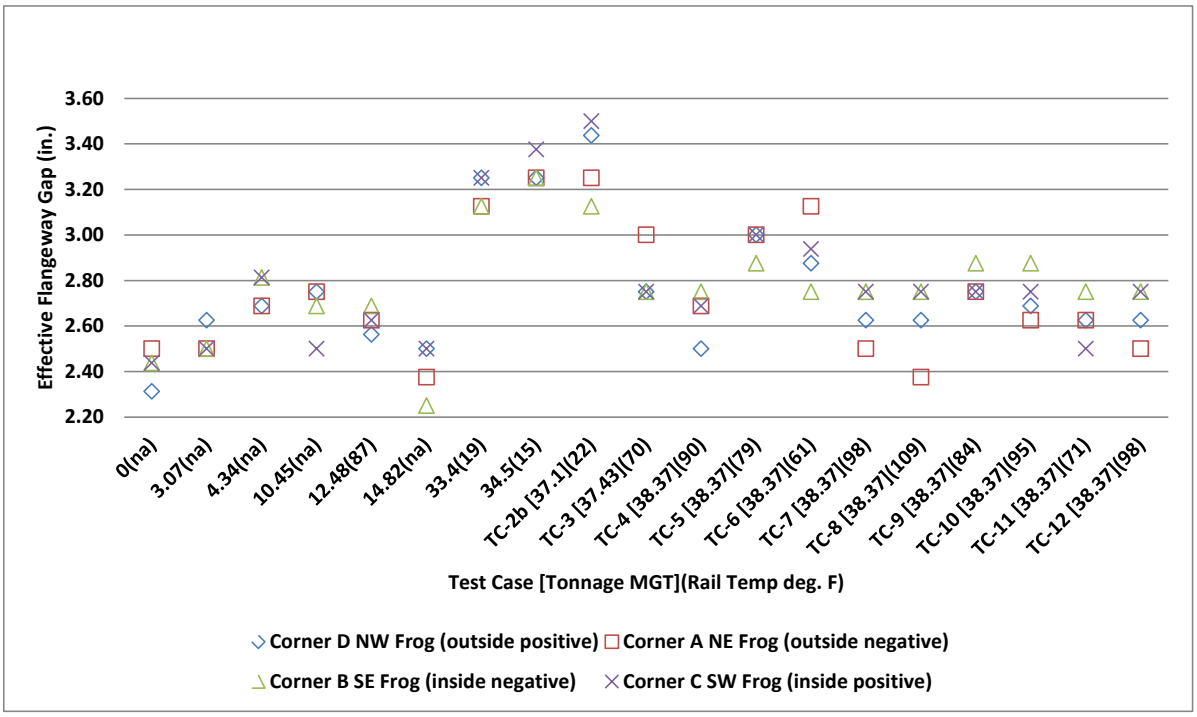

Figure 68. Effective Flangeway Gap measured over a wide range of rail temperatures

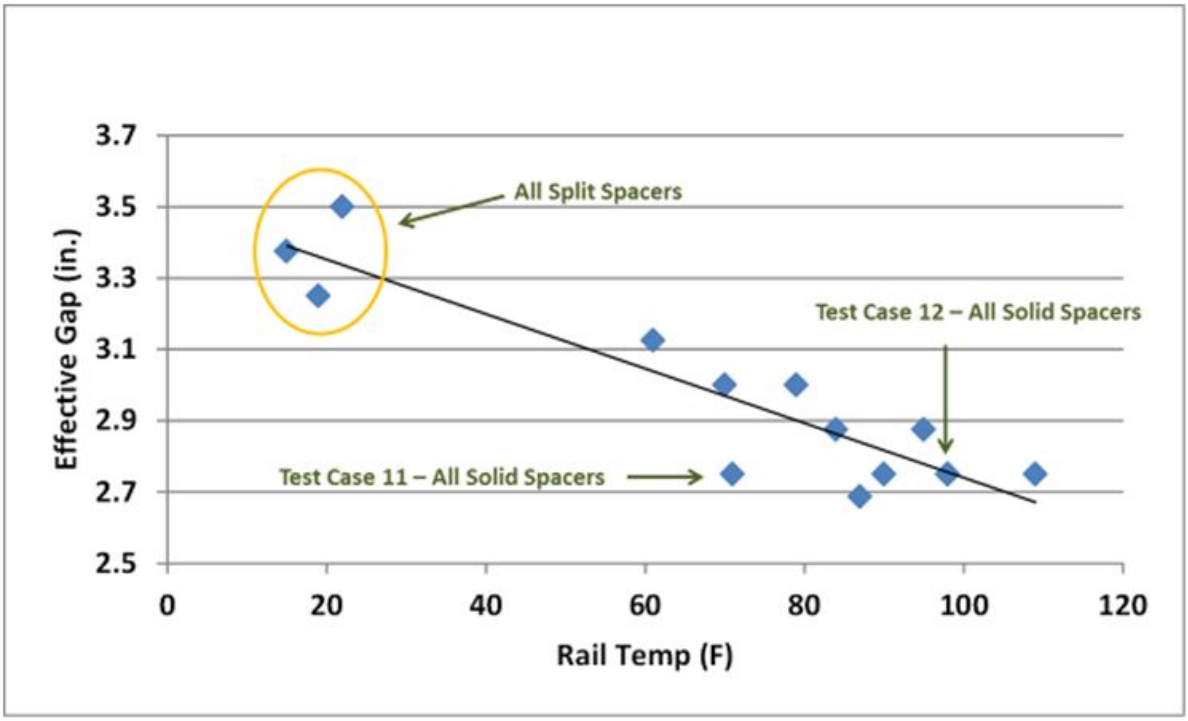

Figure 69. The effective gap widened to as much as 3.5 in as a result of the coldest rail temperature; however, it did not close to less than about 2.7 in during the warmest temperatures (likely due to the flangeway spacer tile at frog centers)

The flangeway gap measurements, which were taken with TTCI's prototype Flangeway Gap & Wheel Drop gage, indicate that this combination of instrument and methodology is appropriate for quantifying this parameter. However, the wheel drop measurements did not produce data of the same level of quality and usefulness. TTCI will evaluate this method and make the instrument design changes that are needed to quantify this parameter.

3.5 Vertical Track Stiffness

Figure 70 shows a typical example of the 10 vertical stiffness measurements taken at the core of the crossing diamond (this one after 38.4 MGT). Figure 71 shows the location of these measurements on the crossing; on each rail, one was taken at the center, one at the each frog, and one at each leg.

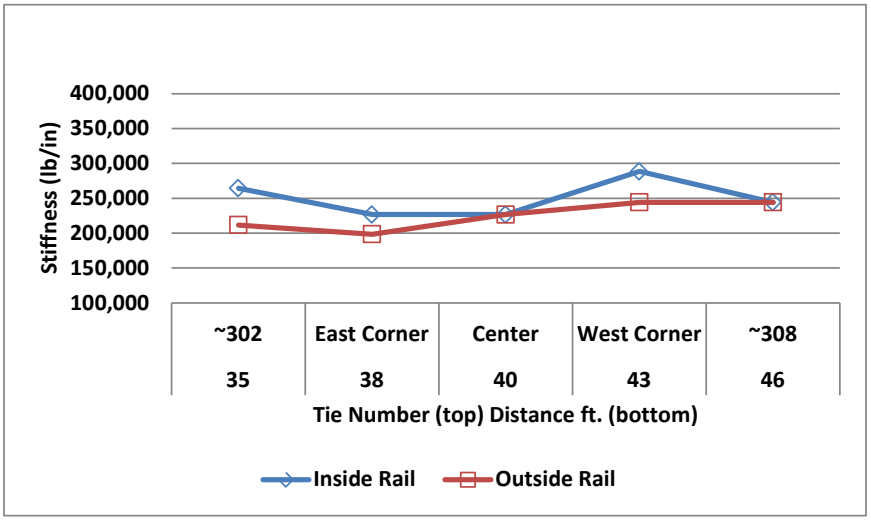

Figure 70. Typical vertical track stiffness measurements taken at the core of the crossing diamond

Figure 71. Locations of the 10 (5 on each rail) vertical track stiffness measurements taken at the core of the crossing diamond for each test case

Figure 72 shows the average vertical stiffness (both rails) that was measured for each test case. The stiffness appears to have increased in Test Cases 3 and 12. Although these cases coincide with the installation of three pairs of solid spacers and through bolts (Case 3) and the installation of all remaining solid spacers (Case 12), the stiffness measured afterward, in both cases, diminishes. The temporary changes in stiffness shown in the data is probably the effect of temperature and rail stress, not changes in pad material or the increased restraint of the solid spacers.

The average stiffness of the crossing diamond core for all cases was about 228,000 lb/in. By comparison, the core stiffness of a solid casting crossing diamond without pads after 17 MGT was about 225,000 lb/in.

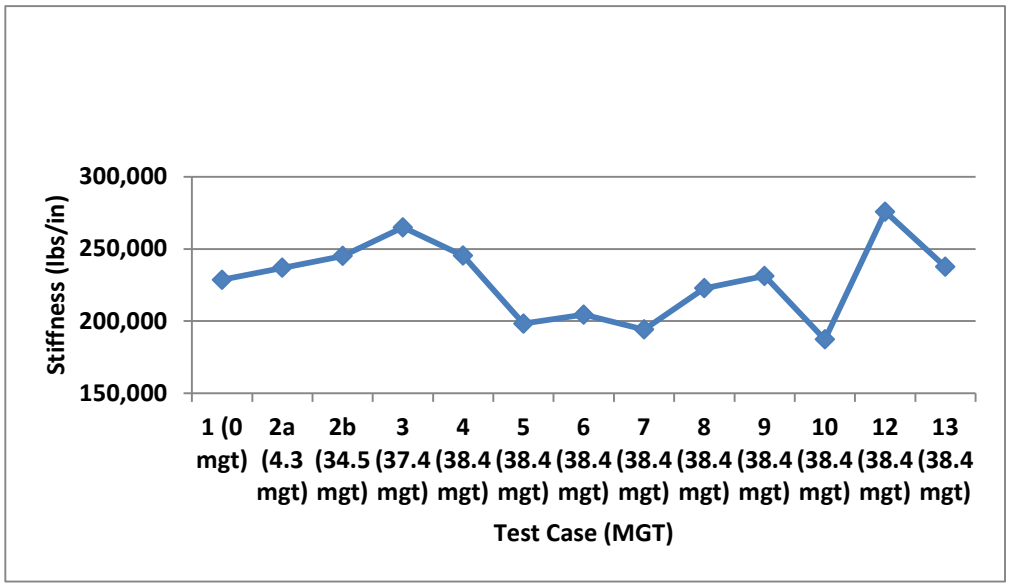

Figure 72. Average vertical track stiffness measured at the core of the diamond for each test case

Figure 73 shows the vertical track stiffness measured during the test at the core of the crossing diamond and at its approaches. There was less variation in stiffness at the core than at the approaches.

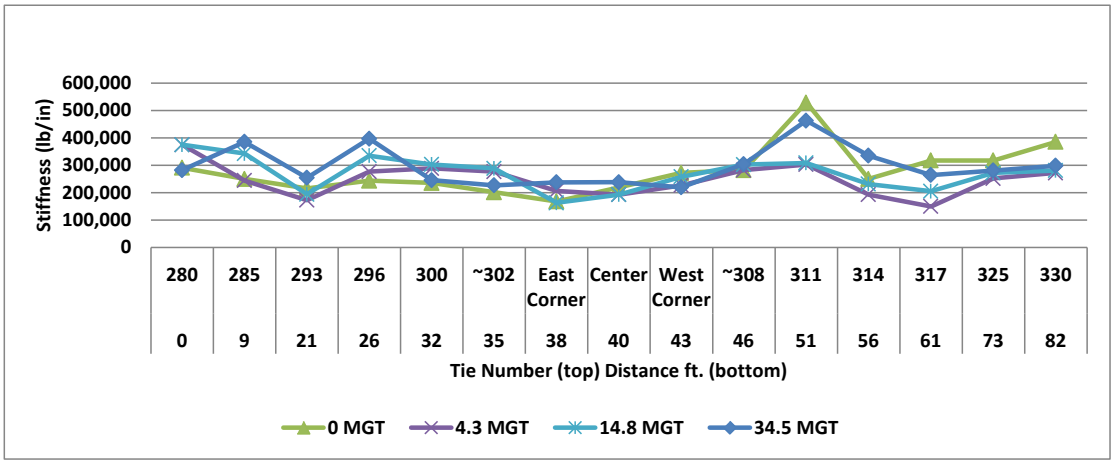

Figure 73. Vertical track stiffness at the core of the crossing diamond and its approaches at tonnage intervals

3.6 Longitudinal Profile across the Casting Corners

Figures 74 through 77 show the changes that occurred in the longitudinal profile between measurements taken at 4.34 and 12.48 MGT, when the entire crossing diamond was fitted with split spacers. Measurements were not taken at 0 MGT. The graphs indicate the location of the castings along the data curve, and beyond the castings are the leg rails.

The changes in the longitudinal profile of these adjacent casting corners are probably due to a combination of deformation caused by wheel impacts, relative movement at the bolted connection between the leg rails and the castings, and relative movement between the adjacent castings. These static, unloaded measurements were taken with a straightedge to span the flangeway gap and a digital depth gage to measure all the way down to the running surface.

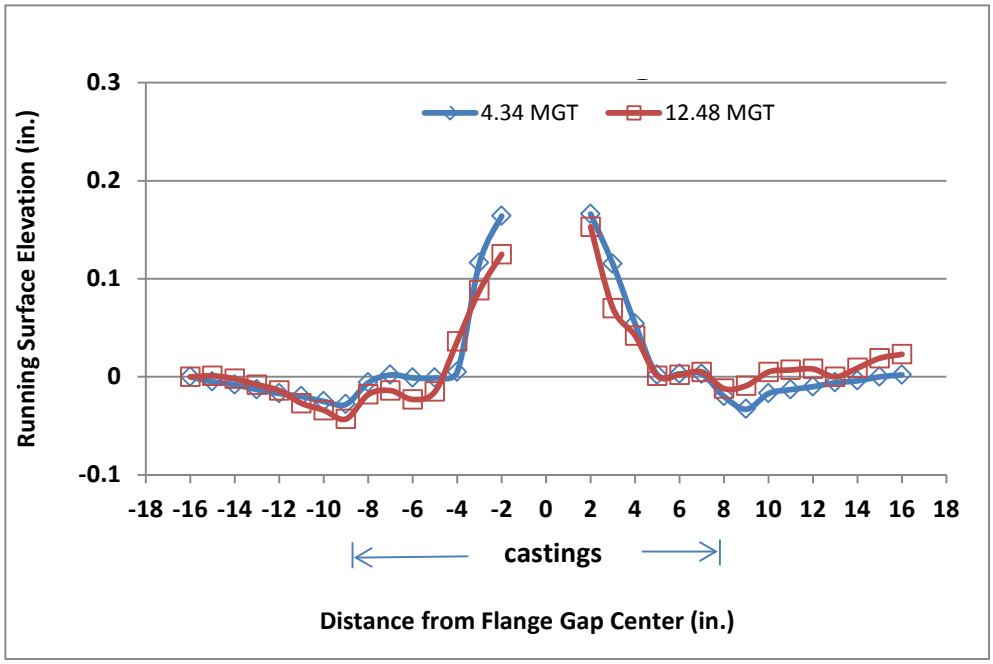

Figure 74. Longitudinal profile over the northwest frog

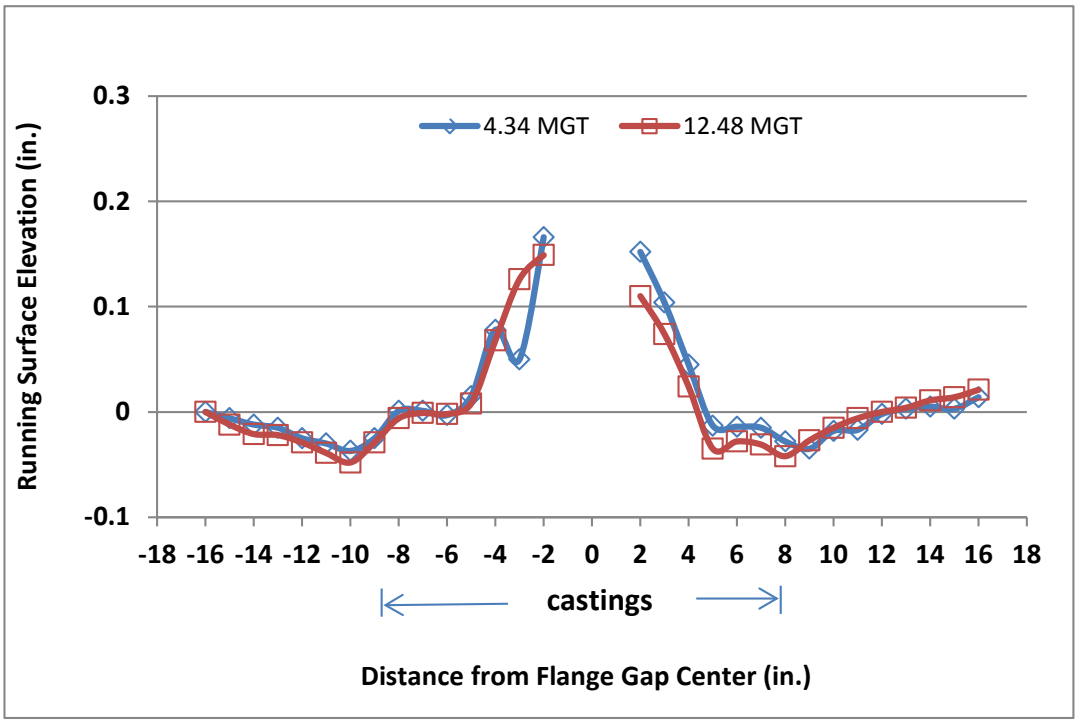

Figure 75. Longitudinal profile over the northeast frog

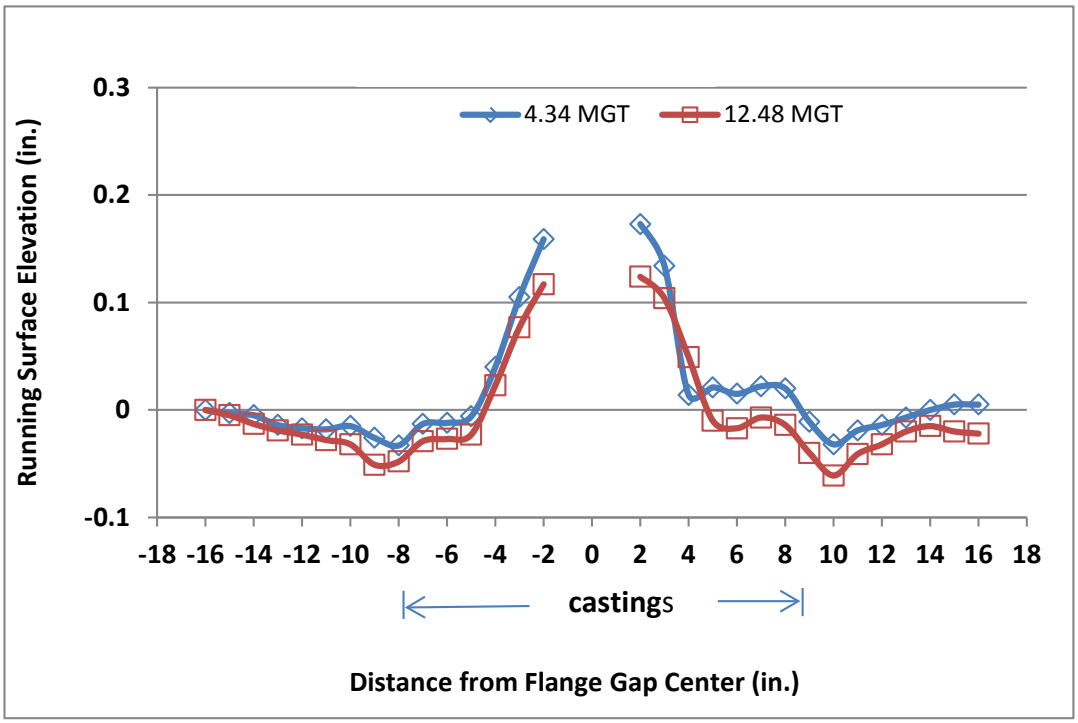

Figure 76. Longitudinal profile over the southwest frog

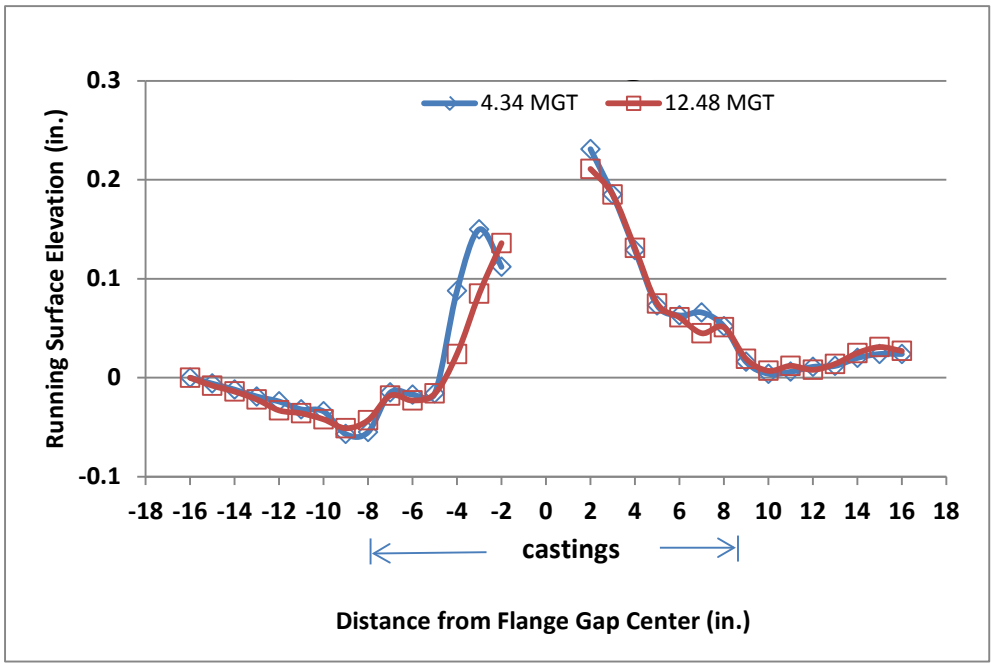

Figure 77. Longitudinal profile over the southeast frog

3.7 Track Surface

The track surface over the crossing diamond has held quite well. Figure 78 indicates that the core of the crossing was not raised to the ideal elevation at initial installation. After 1.7 MGT, the crossing settled about 1 in, as shown in Figure 79. At this point, the core of the diamond was raised and tamped with an overlift, as shown by the curve labeled 1.7 MGT (post tamp) in Figure 78. The crossing then settled about 1 in after a further 1.3 MGT, when top of rail elevation measurements were taken before the original rubber pads were replaced with the Nortrak pads. During the next 7 MGT (at 10 MGT total), the crossing settled another inch. No additional surfacing has been required. The overlift allowed for about 2.68 in of settlement during 63.2 MGT without exceeding the track surface degradation limit.

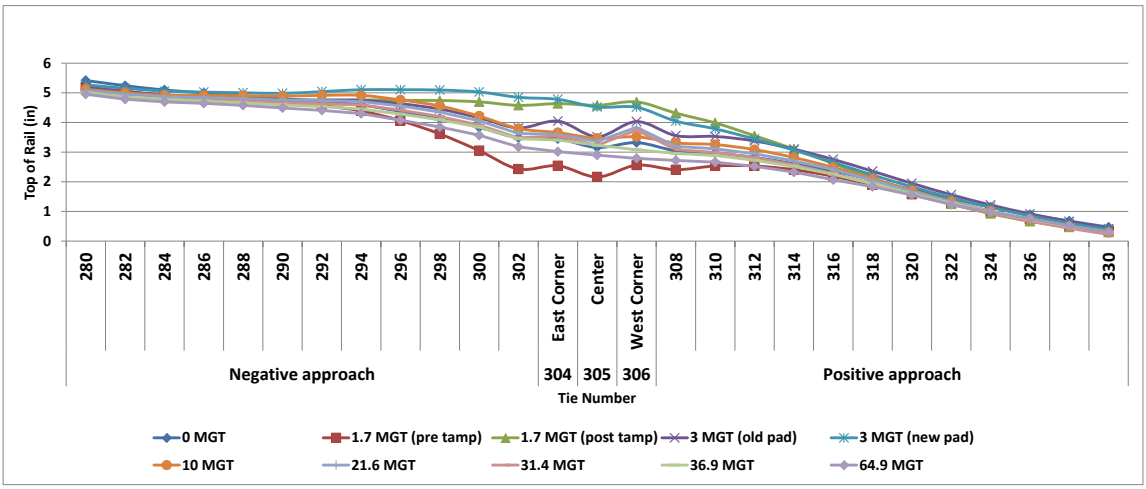

Figure 78. Top of rail elevation at each of the measurement cycles over the crossing diamond and its open-track approaches

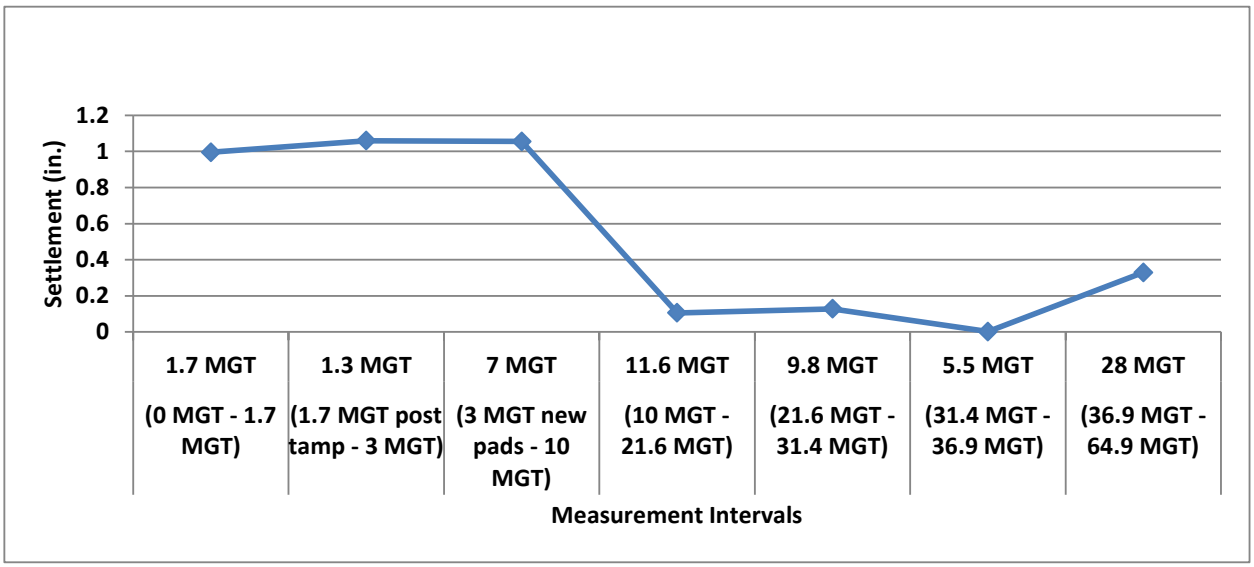

Figure 79. Settlement of the crossing diamond center between measurement intervals

Figure 80 shows the actual change in elevation at the center of the crossing diamond during the 64.9 MGT period of performance, where zero elevation is the initial surface. The three 1-in settlements that occurred within the first 10 MGT correspond to the first three events described in the x axis of Figure 79.

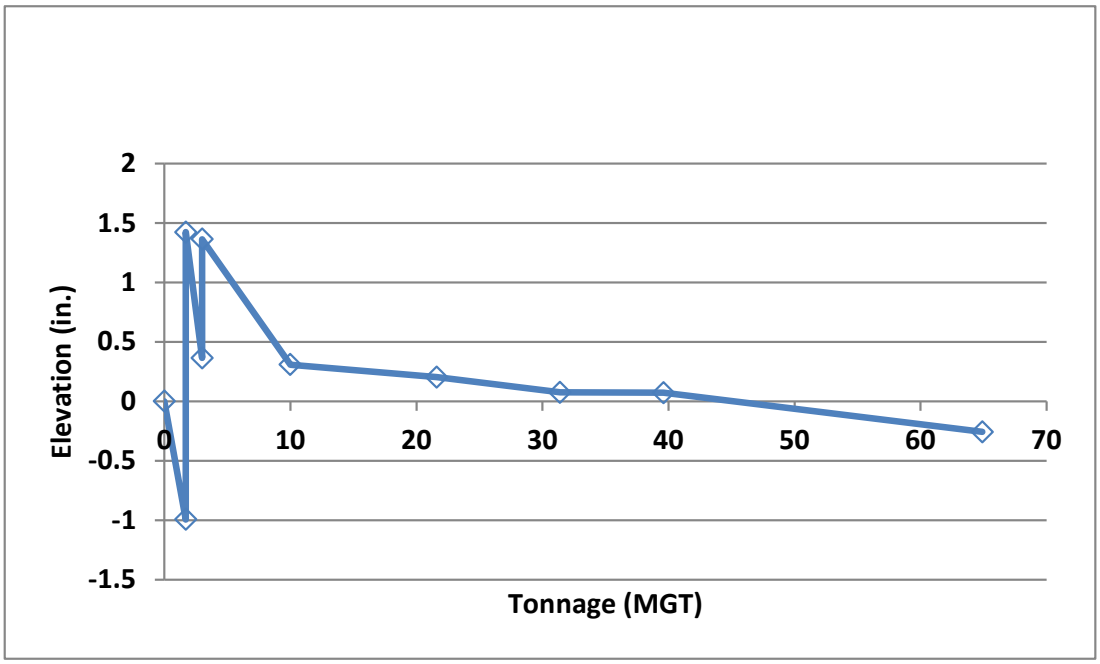

Figure 80. Changes in elevation due to surfacing and settlement during 64.9 MGT

3.8 Longitudinal, Lateral, and Vertical Displacement

Test Cases 2a and 2b tested the crossing diamond with all split flangeway spacers; Test Cases 3 through 10 tested the crossing with partial solid spacers; and Test Cases 11 through 13 were used to test the effect of all solid spacers.

As the train passes over the crossing diamond, the castings move cyclically forward and aft and side to side relative to the direction the train is traveling. Similarly, the castings and the entire track structure move vertically downward and upward as the train's wheels pass.

Figures 82 through 84 are graphs of the maximum x (longitudinal), y (lateral), and z (vertical) displacement measured at the outside casting corner of the southwest frog during Test Case 3 with the train traveling CCW. (Figure 58 has the order in which the wheels negotiate the frogs, given the crossing angle.) Figure 81 has details regarding the casting corners that were measured in the southwest frog, the direction of components movement, the location of split and solid flangeway spacers during Test Cases 3 through 10, and the wheel path across the frog.

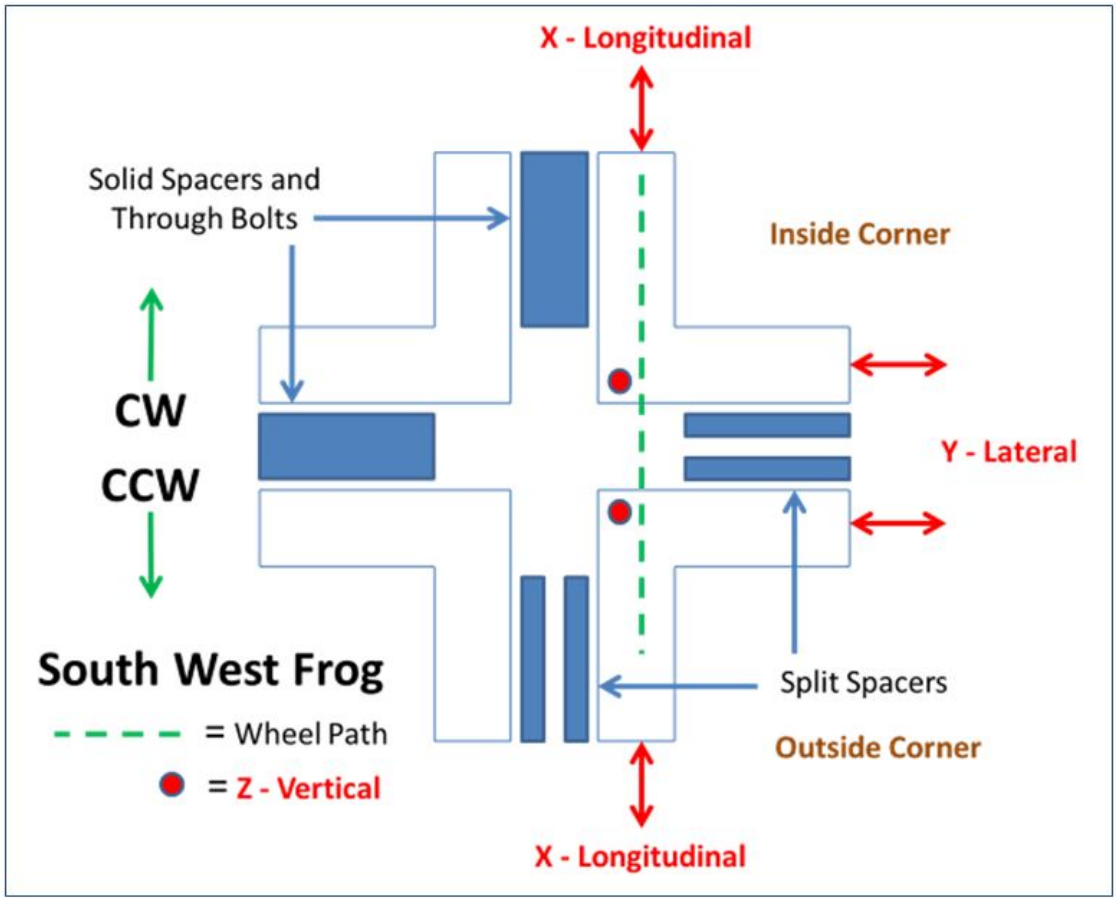

Figure 81. The inside and outside casting corners of the southwest frog were measured for longitudinal, lateral, and vertical displacement under traffic during each test case. The hybrid split spacer/solid spacer configuration shown was in place during Test Cases 3–10. All split spacers were in place during Test Cases 2a and 2b and all solid spacers were installed for Test Cases 11–13.

Figure 82 indicates that at 20 mph, the maximum longitudinal displacement of this casting corner (toward the train, negative values), for the entire train, was about 0.05 in and the maximum longitudinal displacement (away from the train, positive values), for the entire train, was about 0.07 in.

The graph also indicates an increase in longitudinal displacement at 40 mph, where the maximum displacement toward the train was about 0.1 in and away from the train about 0.11 in.

Figures 83 illustrates the lateral displacement of the same casting, where the positive values indicate gage widening direction (0.11 in at 40 mph) and negative values indicate gage tightening direction (0.19 in at 40 mph). And finally, Figure 84 indicates about 0.34 in upward displacement and about 0.49 in downward displacement at 40 mph.

One should keep in mind when considering the magnitude of displacement measured during this test that the crossing diamond is tied in to only one track. Displacement in revenue service, therefore, may differ.

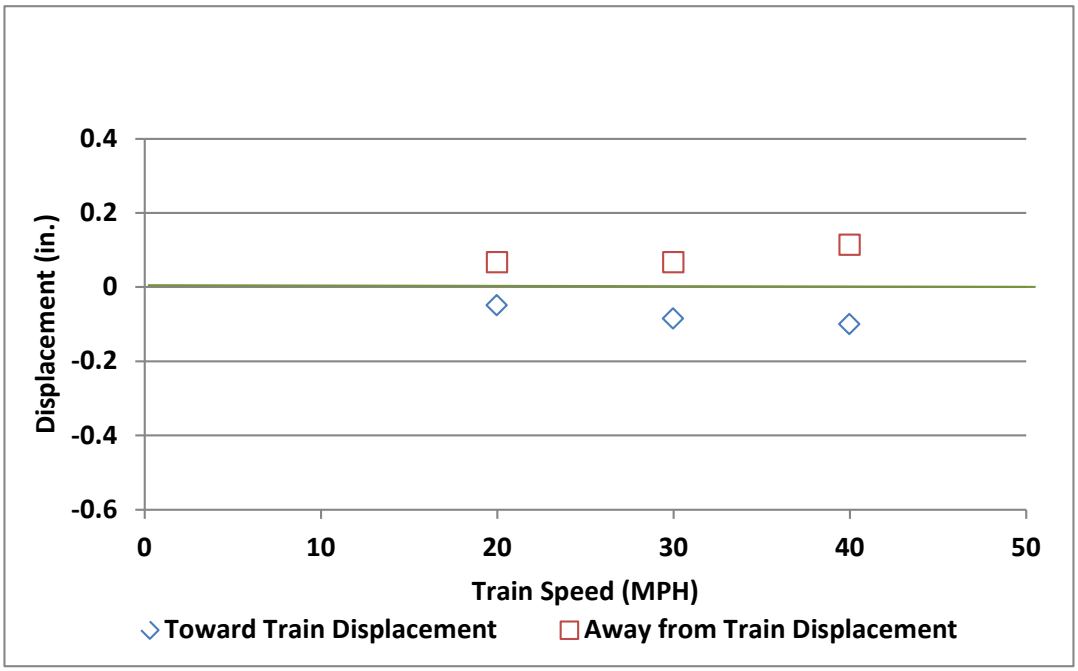

Figure 82. Each speed dataset represents the maximum longitudinal displacement measured in each direction under the entire train at the given speed

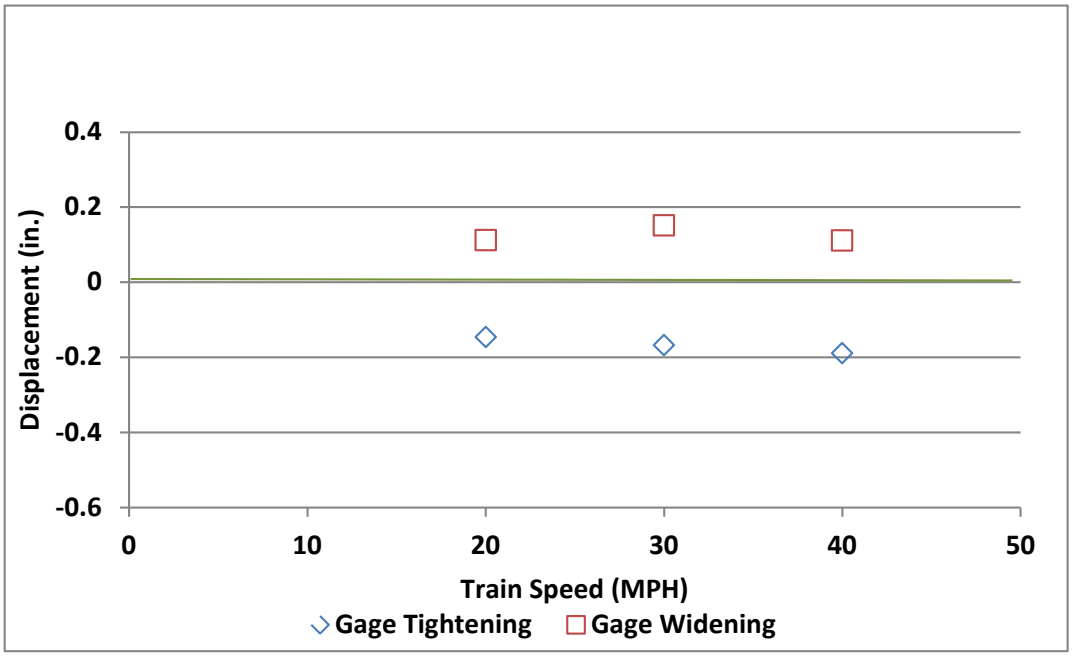

Figure 83. Each speed dataset represents the maximum lateral displacement measured in each direction under the entire train at the given speed

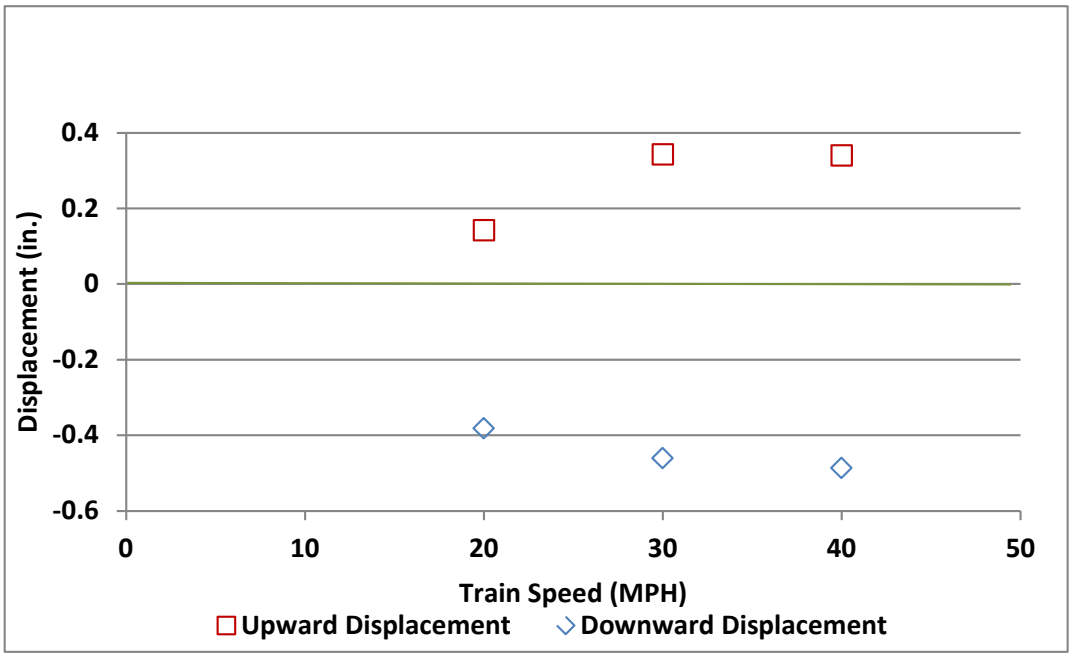

Figure 84. Each speed dataset represents the maximum vertical displacement measured in each direction under the entire train at the given speed

Figures 85 through 91 present the summary of maximum displacements measured during Test Cases 2a through Test Case 12 at 40 mph. Given the similarity in displacement measured in the CW and CCW directions of train travel, each curve indicates the average displacement in CW and CCW directions.

Figures 85 and 86 show the longitudinal displacement that was measured at the outside and inside castings of the southwest frog. The largest displacement away from the train (0.29 in) and toward the train (0.24 in) occurred on the inside corner casting.

The largest variation in the displacements measured during all the test cases are as follows: (1) outside corner, away from the train 0.09 in; toward the train 0.15 in and (2) inside corner, away from the train 0.20 in; toward the train 0.14 in.

Slightly higher longitudinal displacement was measured at the inside and the outside castings during Test Cases 8, 10, and 11. A layered tile configuration was tested in Test Case 8, with the pad material sandwiched between two layers of steel flangeway spacer tile. Test Cases 10 and 11 tested the solid rubber flangeway spacer tile. It may be that the raising the resilient layer higher in the superstructure allowed the increased movement.

Test Case 12 tested without pads and the castings were bearing directly on steel plate; the increased friction between the steel components may have contributed to the lower longitudinal displacement that was measured.

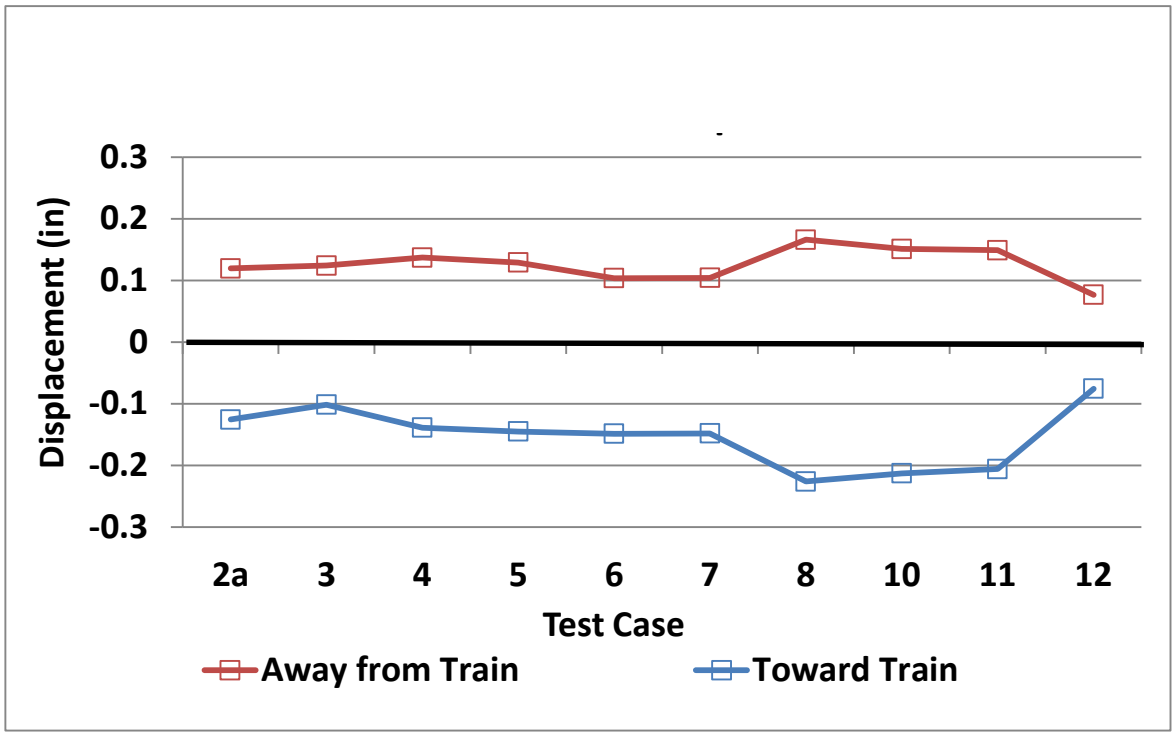

Figure 85. Longitudinal displacement of the outside corner toward and away from the train at 40 mph

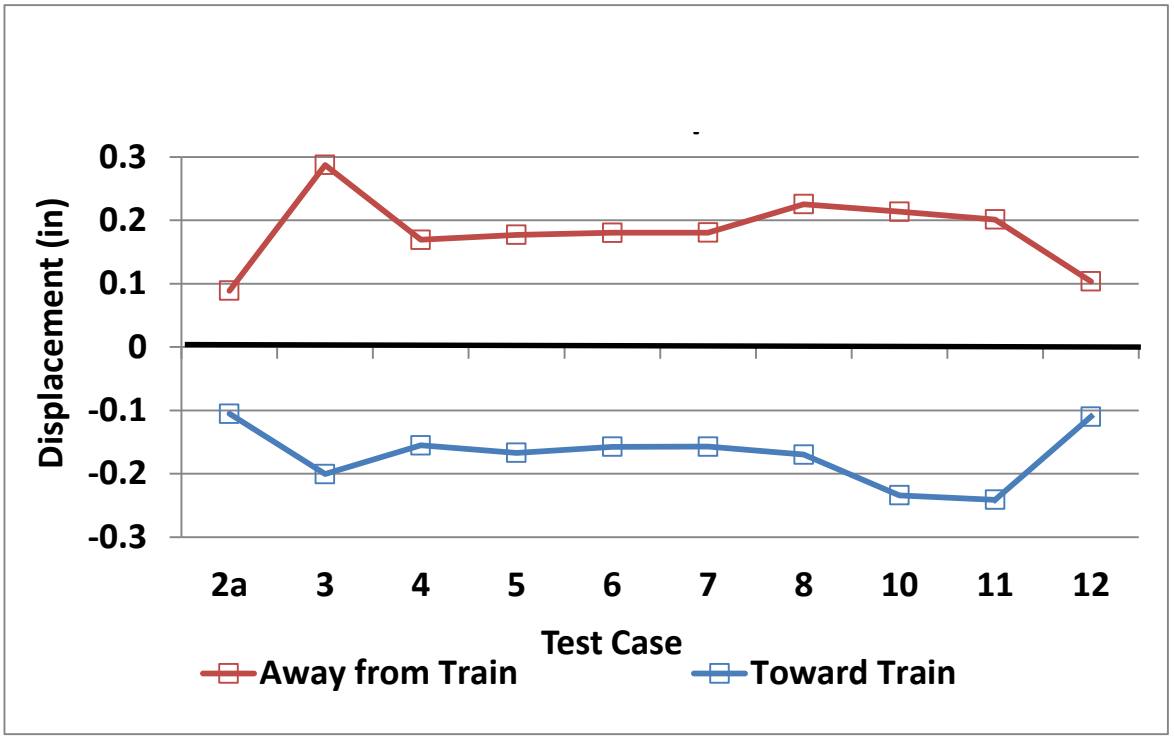

Figure 86. Longitudinal displacement of the inside corner toward and away from the train at 40 mph

Figures 87 and 88 show the lateral displacement (gage widening and gage tightening) measured at the outside and inside castings. The largest displacement in both, gage widening (0.24 in) and gage tightening (0.22 in) directions occurred on the outside corner casting.

The largest variation in the displacements measured during all the test cases are as follows:

- Outside corner, gage widening 0.13 in; gage tightening 0.07 in
- Inside corner, gage widening 0.13 in; gage tightening 0.13 in

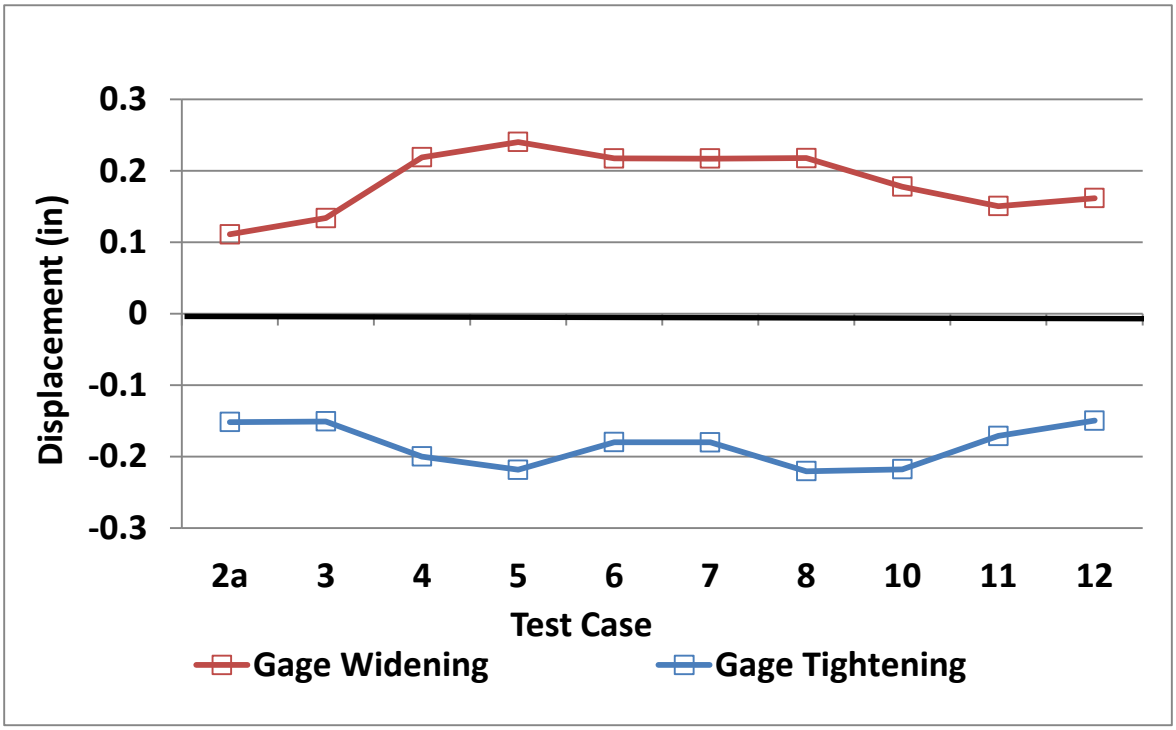

Figure 87. Lateral displacement of the outside corner in gage widening and gage tightening direction at 40 mph

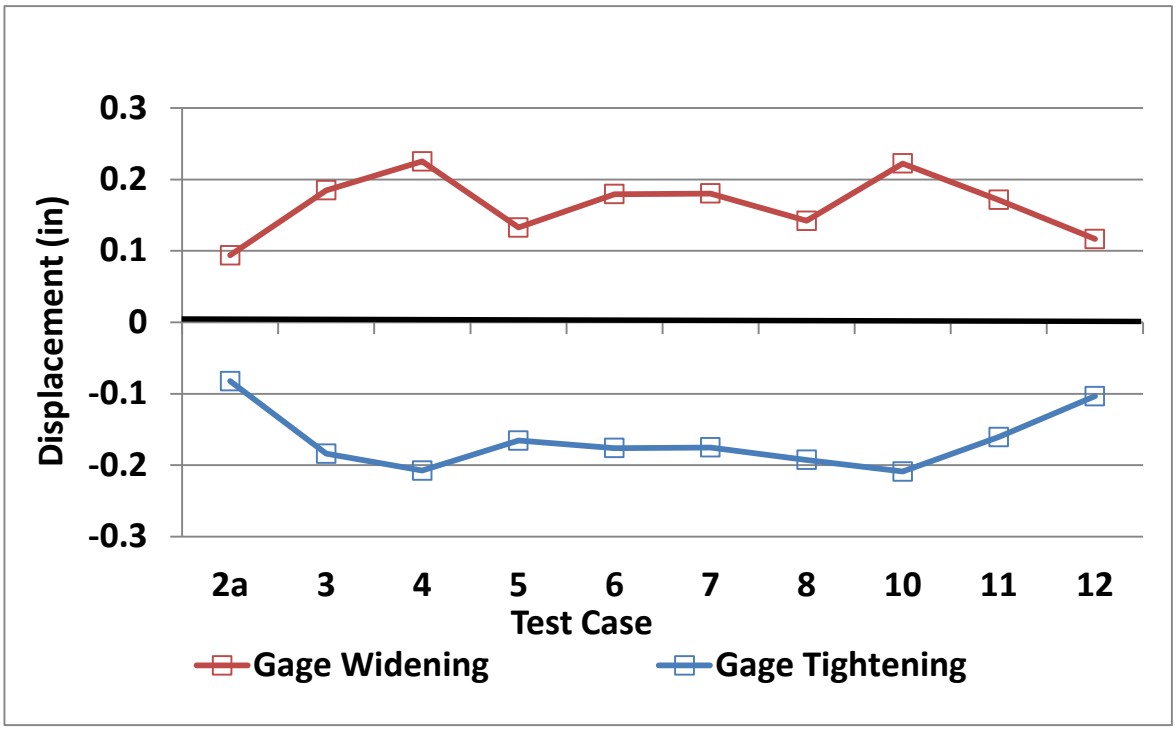

Figure 88. Lateral displacement of the inside corner in gage widening and gage tightening direction at 40 mph

Figures 89 and 90 show the vertical displacement (upward and downward) that was measured at the outside and inside castings. The largest displacement in both upward (0.95 in) and downward (1.16 in) directions occurred on the inside corner casting.

The largest variation in the displacements measured during all the test cases are as follows:

- Outside corner, upward 0.28 in; downward 0.50 in
- Inside corner, gage upward 0.64 in; downward 0.63 in

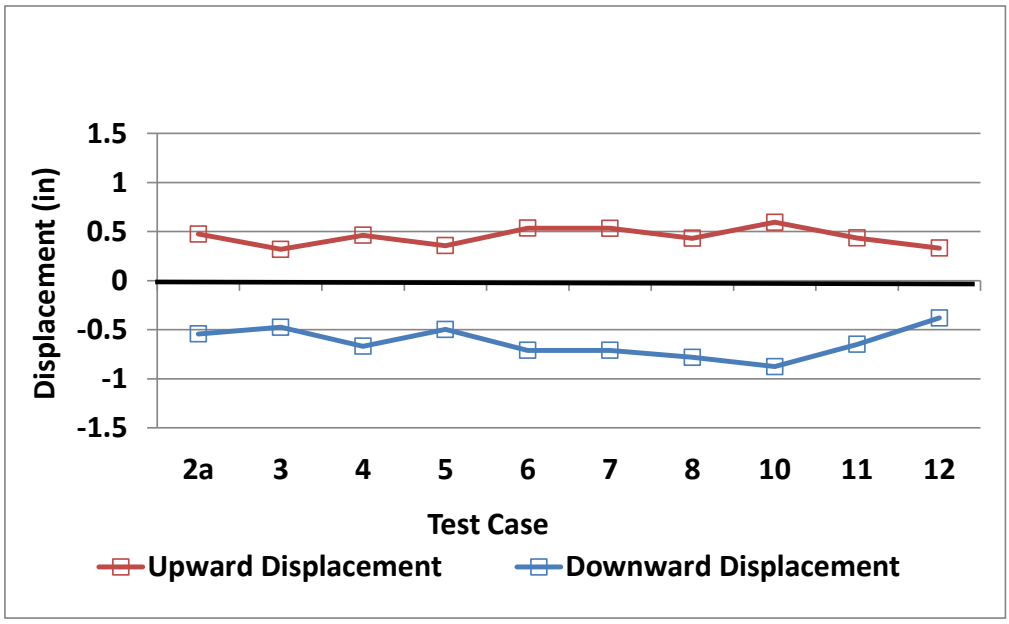

Figure 89. Vertical displacement of the outside corner in upward and downward direction at 40 mph

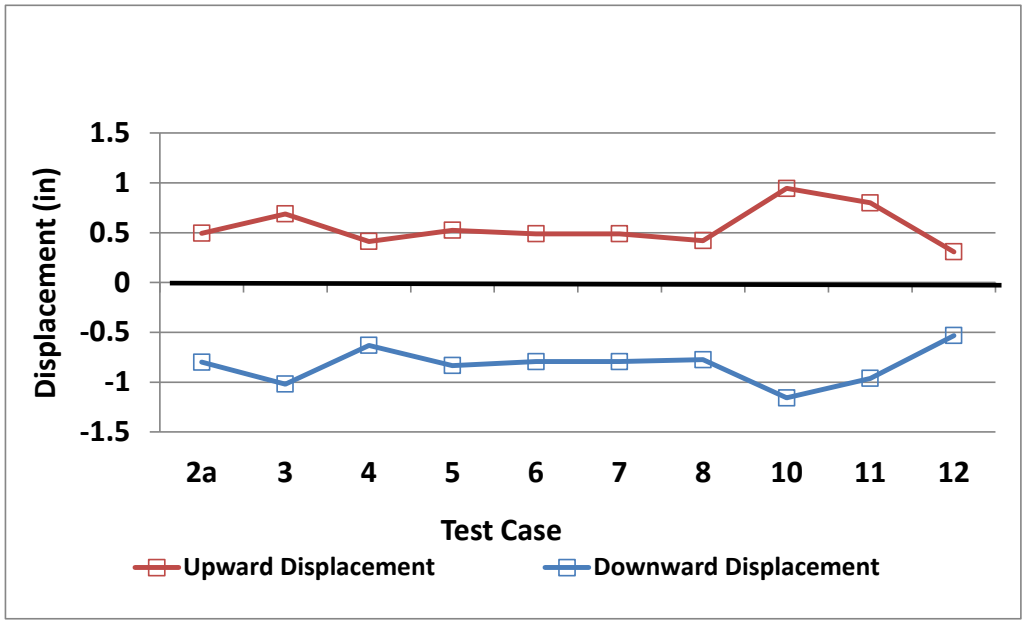

Figure 90. Vertical displacement of the inside corner in upward and downward direction at 40 mph

Figure 91 shows the vertical displacement measured at the tie under the southwest corner. It indicates the upward and downward movement of the crossing diamond's wood-tie platform through the ballast section. The largest displacement in the downward direction was 0.4 in; in the upward direction it was 0.25 in.

The largest variation in the displacements measured at the tie under the southwest frog during all the test cases are as follows:

- Upward 0.18 in
- Downward 0.19 in

The data indicates a reduction in the downward vertical displacement with the progression of the test cases, which suggests a combination of settlement and ballast compaction.

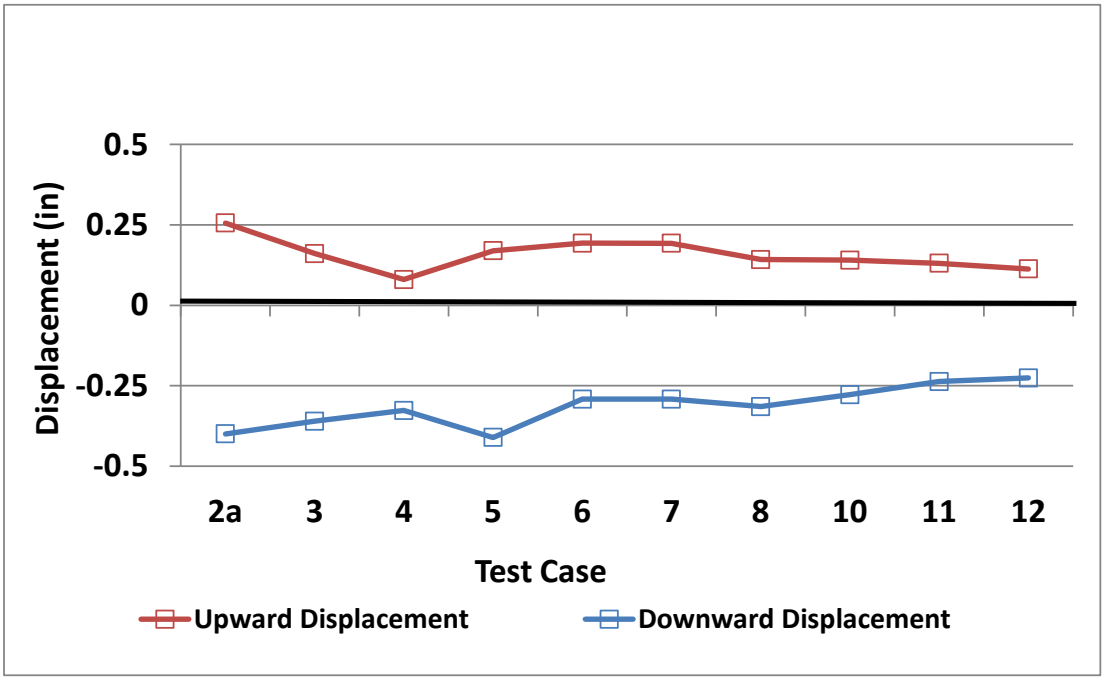

Figure 91. Vertical displacement of the crossing diamond's wood-tie platform through the ballast section

3.9 Pad Material Durability

The full-coverage rubber pad between the platework and the castings/rails that came with the prototype crossing diamond deteriorated under the severe environment of the HAL train during the first 102 laps. The pad failed to resist the effects of heat energy and abrasion (as shown in Figures 92 and 93). It should be noted that the FAST operating environment is more severe than revenue service in two respects. The first is that the average car load is 315,000 pounds and average train speed is 40 mph. Second, the closed loop operation has a train passing over the test location every 4 minutes. Thus, the crossing diamond is being loaded about 40 percent of the time for 8 hours at a time. This does not allow much time for damping elements, such as rail seat pads, to dissipate heat.

Figure 92. The full-coverage rubber pad failed to resist the heat generated by the passing train (102 laps). The material melted and oozed upward between the casting corners and the flangeway spacer tile (see a sample placed on the casting).

Figure 93. The full-coverage rubber pad failed to resist heat and abrasion between components. Removed after 102 laps of the HAL train

The Nortrak pad was in service for 35 MGT to evaluate its durability. To date, the Getzner Type B pad has been in service for 27 MGT and continues to accumulate tonnage. On the basis of this limited tonnage period of service and qualitative evaluation, the team predicts that the Nortrak pad and the Getzner Type B pad placed between the platework and the castings/rails will provide good long-term performance. Figure 94 shows the condition of the Nortrak pad after 35 MGT in service.

Figure 94. Nortrak pad material in good condition after 35 MGT

Although the Getzner Type B pad performed well under the castings and rails, the presence of cutting along the interface of the pad and the edge of the steel flangeway spacer tile was noted, as shown in Figure 95. When the full-coverage pad was modified to accommodate Test Case 10 and the solid rubber spacer tile, the footprint of the spacer tile was cut out of the full-coverage pad, as shown previously in Figure 21. After Test Case 12 (with no pads) was completed, it was time to test the durability of the Getzner Type B pad. To do this, the cutout footprint of the spacer tile was inserted under the steel tile as shown in Figure 96 (tile is removed for the photo).

The photo indicates that the material under the castings/rails continues to perform well after 27 MGT. It also appears that cutting out the footprint, which made the material directly under the steel tile a separate piece, provided the expansion some space under load to relieve the edge effect and led in better performance at this location as well.

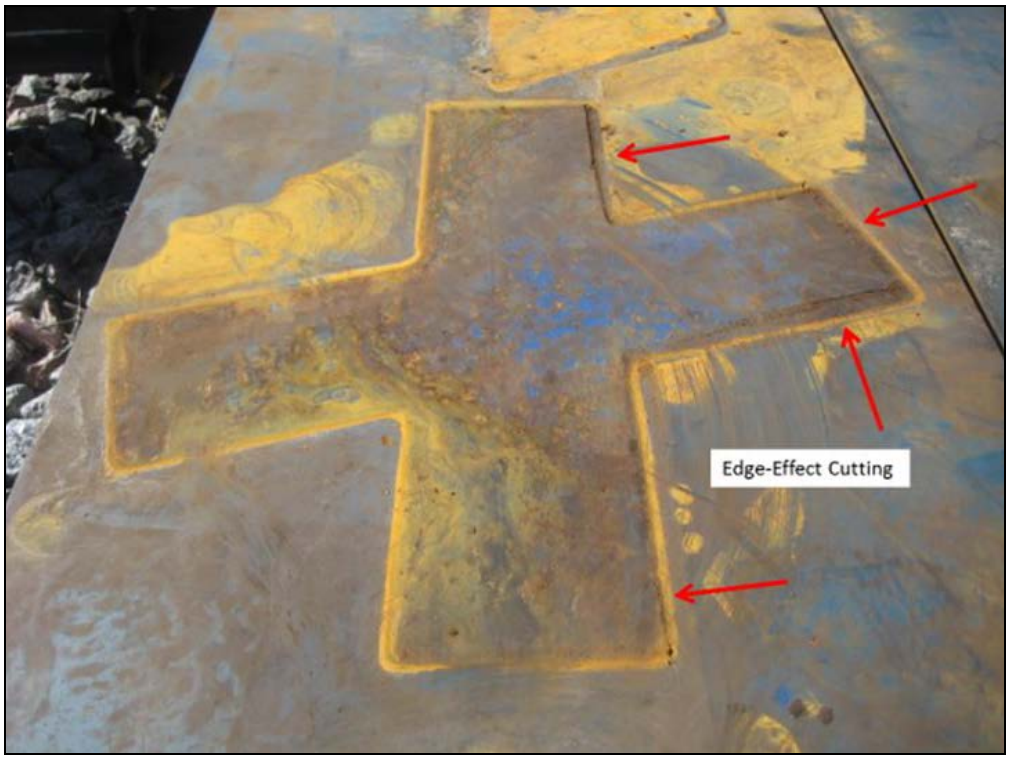

Figure 95. Getzner Type B pad showing evidence of edge effect cutting from the steel flangeway spacer tile

Figure 96. Getzner Type B full-coverage pad with separate under-tile piece performing well after 27 MGT

4. Maintenance

4.1 Maximum-Flexibility Configuration

The team defined the maximum-flexibility configuration period as the early part of the test, when the prototype crossing diamond was fitted with split (2-part) flangeway spacers (as described earlier in this report). During this test period, numerous maintenance challenges were met and resolved as described in the following sub-sections.

4.1.1 Differential Elevation of Components

The center "square" of the crossing diamond serves as guardrails. After some initial traffic, this section ratcheted upward about 1 in above the running rail (Figure 97). As a result of this displacement, likely severe and cyclic under traffic, frequent maintenance was required to address fastener component failures (Figure 98).

The elevated guardrails placed the half of the split spacer fastened to the guards in the path of the wheel flange (Figure 99); this required grinding on that spacer for clearance.

In addition, welded tabs intended to keep the castings in contact with the platework broke often and required rewelding.

Figure 97. Differential elevation between the guardrail (left) and the running rail (right), about 1 in

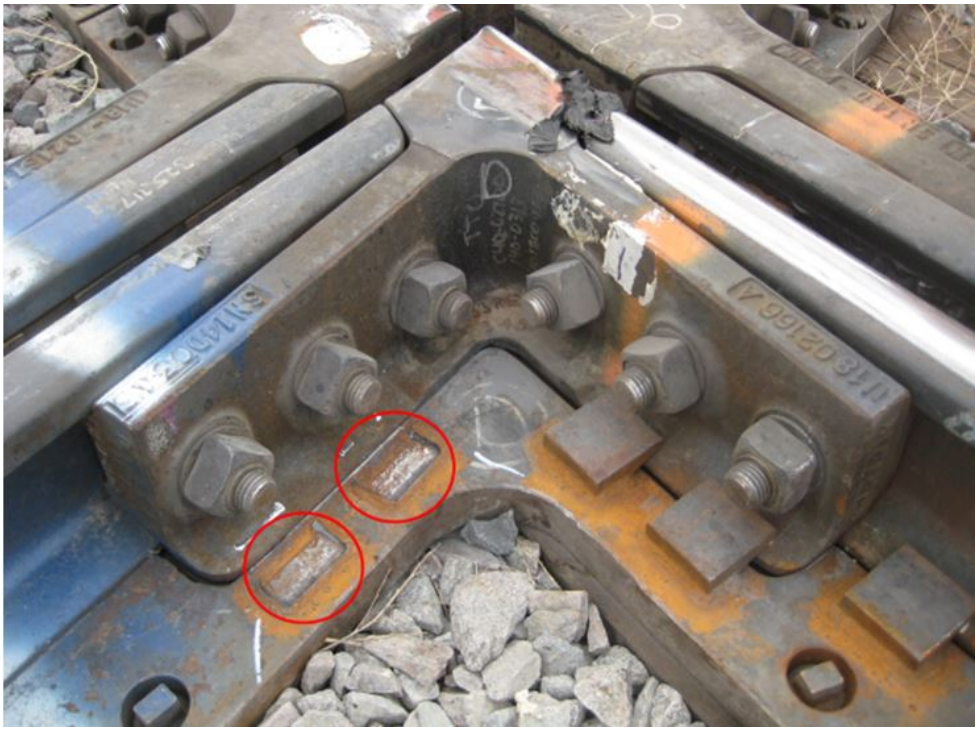

Figure 98. Welded tabs intended to keep the castings from jumping out of the milled platework required frequent replacement

Figure 99. Wheel flange marks on the split spacer fastened to the rising guardrail

To address these problems, the guardrail square was secured to the platework. Figure 100 shows vertical keepers that were designed and fabricated at TTCI's machine shop, then installed.

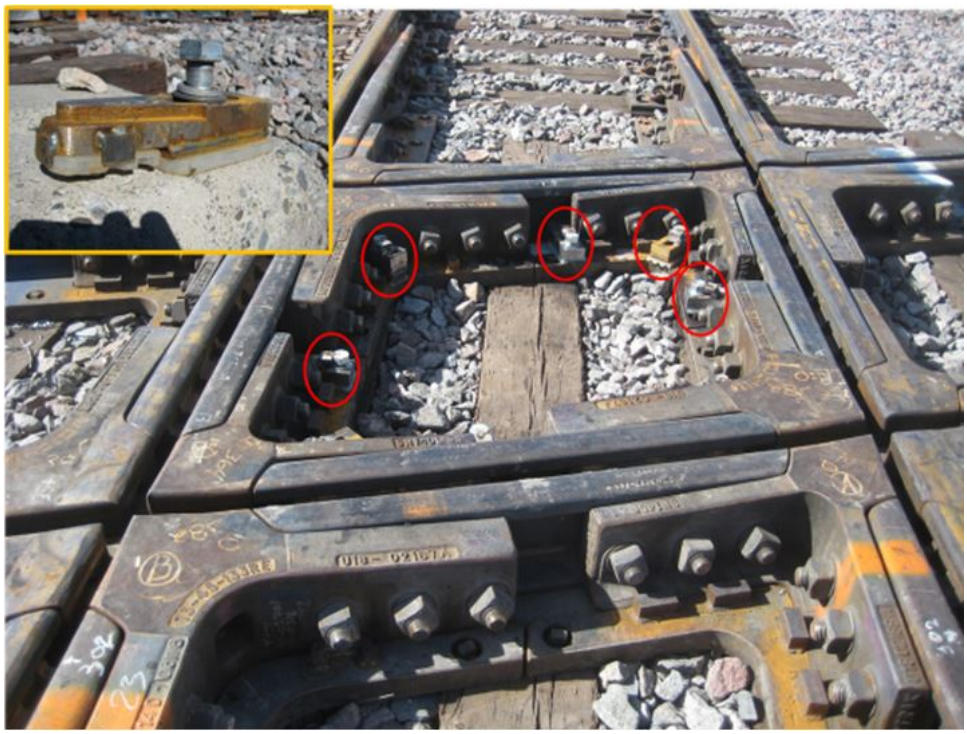

Figure 100. Vertical keepers designed to secure the guardrail square to the platework

The vertical keepers helped reduce the amount of welding maintenance and kept the flangeway clear. However, the severe dynamic environment led to the keeper bolts breaking. Ultimately, these maintenance issues were resolved as the split flangeway spacers were replaced with solid spacers and through bolts.

4.2 General Maintenance and Component Failure

- Typical maintenance on the crossing diamond included grinding to remove metal flow and shelling from the casting corners, as shown in Figure 101.
- The castings on the outside rail shelled more than those on the inside rail. In order to prevent further damage and to continue the test, these casting were swapped with the unused ones on the inside rail.
- Many broken bolts were replaced.
- Replaced a broken leg rail that had been in service 59 MGT (a replacement was machined in house) shown in Figure 102.
- The top of the flangeway spacer tiles did not require maintenance; however, wear is evident where the casting corners bear, as shown in Figure 103.
- Figure 104 shows a leg rail chipped at the interface with the casting at the southwest frog; it was slotted periodically.
- Figure 105 shows the top half of a layered flangeway spacer tile that broke.

Figure 101. Casting corners were ground as required to remove metal flow

Figure 102. The leg rail on the northwest frog broke after 59 MGT

Figure 103. Wear on the top of a flangeway spacer tile where the casting corners bear

Figure 104. Chipped leg rail at the southwest frog was slotted

Figure 105. The top half of a layered flangeway spacer tile broke and was replaced

5. Summary and Conclusions

This project evaluated the potential benefits of various configurations of high angle frogs and frog foundations on wheel-rail vertical forces and frog performance. Testing occurred under 315,000-pound cars with nominal 39-ton axle loads at the HTL of FAST at the TTC in Pueblo, CO.

The testing plan was based on both Phase I and Phase II of the project. These tests determined that track stiffness, track damping and frog flexibility (i.e., the capability for differential vertical movement between opposite sides of the frog across the flangeway) affect wheel-rail vertical forces. [1, 2] A prototype crossing diamond was built using a design that had the potential to increase frog flexibility. The commercially available SRR design was modified to add rail seat pads of various configurations above the frog platework. Additionally, options for joining the four castings that make up each frog were developed. These options allowed assessment of frog flexibility on wheel-rail forces and frog performance. A total of 14 frog configurations were evaluated over about 70 MGT of 315,000-pound car traffic.

Other results from the project included:

- Rail seat pads contribute significantly to wheel-rail force reduction. Reductions of 20 to 30 percent were measured for maximum and 99th percentile vertical dynamic wheel loads.
    - A range of rail seat pads were tested. A relatively soft pad intended to produce optimal stiffness, on the basis of theoretical results, disintegrated under the first 100 trains.
    - Two supplier recommended pads were tested with good success. The softer of the two pads tested produced lower track stiffness and lower dynamic vertical loads.
- When more flexibility was added to the SRR design, it provided little dynamic performance improvement when rail seat pads were in place.
    - The flexible frog design, with no direct connections between the four castings that make up a frog, did not significantly affect dynamic vertical loads.
        - The additional degrees of freedom did contribute to maintenance issues that involved the inner guard position and related component breakage.
        - From previous phases of the project, a jointed frog (one with the ability for the two sides of the flangeway to move vertically with respect to one another) had lower dynamic vertical loads than a traditional solid (one piece) frog.

This project's results can guide frog designers through the potential ranges of track stiffness and frog flexibility and allow them to improve high angle frog performance, which may spur them to develop additional concepts and improve frog performance.

The tests concluded that a flexible frog is useful in lowering dynamic forces. However, the addition of a simple mechanical joint, as is done in three-rail crossing diamonds, is likely near optimal in terms of flexibility. Additional flexibility, such as split flangeway spacers in the SRR design adds little to dynamic performance. But it does increase related component maintenance and alignment degradation of the frog.

Rail seat pads were effective at lowering dynamic vertical loads. In the FAST test situation, the pads were able to reduce vertical dynamic wheel loads at 40 mph to a level similar to that at 20 mph without pads.

The long-term durability and dynamic performance of the prototype and its design features should be determined.

References

1. Shu, X., D. Davis, and M. Akhtar. (February 2013). "Next-Generation Foundations for Special Trackwork – Phase I." DOT/FRA/ORD-13/10 Department of Transportation, Federal Railroad Administration, Office of Research & Development, Washington, D.C.
2. Shu, X., D. Davis, and R. Jimenez. (submitted to FRA May 2015). "Next-Generation Foundations for Special Trackwork – Phase II." Department of Transportation, Federal Railroad Administration, Office of Research & Development, Washington, D.C.
3. Remington, J.A., K.L. Schultz, and R.R. Hein. (May 5, 1998). Rail crossing assembly SRR patent. http://www.google.com/patents/US5746400
4. Akhtar, M. and D. Davis. (June 2008). "An analytical Procedure for Predicting Crack Initiation in Crossing Diamond Frog Materials," *Technology Digest* TD-08-026, Association of American Railroads, Transportation Technology Center, Inc., Pueblo, CO.
5. Davis, D. and M. Akhtar. (November 2007). "Crossing Diamond Life Cycle Analysis: Tools for Development of a Speed Policy for Crossing Diamonds," *Technology Digest* TD-07-040, Association of American Railroads, Transportation Technology Center, Inc., Pueblo, CO.

Appendix.
Data Tables

Table A-1. Maximum wheel forces (kips)

Train Speed	Test Case	Inside CW Vertical	Inside CW Lateral	Outside CW Vertical	Outside CW Lateral	Inside CCW Vertical	Inside CCW Lateral	Outside CCW Vertical	Outside CCW Lateral
20 MPH	2a	58.30765	16.56609	55.6819	12.72307	67.28296	17.56014	71.06001	11.88081
	2b	58.54829	21.89784	56.12664	16.92944	52.59134	22.43396	58.99313	23.03799
	3	60.23618	16.87372	56.70399	13.31895	54.87532	16.92887	63.52736	17.30734
	4	68.55578	20.30316	62.96644	12.90452	56.38996	14.18816	61.20896	12.16887
	5	58.650	21.58851	57.36796	17.14396	56.57178	23.21095	59.92157	17.39156
	6	64.21098	19.67862	63.87466	12.56198	53.89674	22.56064	60.59989	15.29535
	7	67.33163	10.01006	55.36116	14.75548	54.96982	13.60416	63.44722	11.10478
	8	66.87194	10.55319	62.35861	14.31888	64.56073	15.1336	63.31349	15.26022
	9	61.307	9.170978	55.47423	11.86904	56.56403	15.54349	62.13097	17.1445
	10	53.53757	11.69743	56.75847	12.13859	66.42899	18.87356	66.44785	12.97365
	11	60.578	23.75611	54.3395	15.07874	57.01086	16.88362	64.27728	32.18885
	12	80.93246	16.33017	82.72308	19.06478	82.88483	17.12398	80.75829	32.99241
30 MPH	2a	71.81565	13.49747	62.3625	17.21805	72.91287	23.56264	80.10486	13.5332
	2b	66.18815	24.71977	65.81513	32.06913	71.01745	34.80655	64.10516	30.65545
	3	61.52647	19.97252	69.24002	16.36888	63.9459	24.72745	63.36398	18.77181
	4	64.13525	26.80688	60.43945	17.78627	65.50105	22.81192	63.84672	15.35465
	5	61.50148	29.95557	62.25733	19.49361	62.74191	35.12791	63.10913	18.7089
	6	59.59366	24.81095	57.93341	15.05207	64.09376	27.34746	61.23611	16.21399
	7	66.39302	11.54635	66.8794	18.65045	63.81692	20.61835	57.52144	11.75712
	8	61.1389	12.91471	66.04996	17.19014	67.4244	21.49834	66.12869	14.88339
	9	57.18808	10.29612	64.6656	17.60437	63.23613	19.34082	62.48495	16.37694
	10	53.74565	12.87694	70.14036	16.70664	71.04627	21.82536	77.50552	23.60727
	11	59.42475	31.21214	68.03309	19.86981	73.48337	25.4111	60.20384	41.48518
	12	80.10002	18.63152	81.12951	26.42443	82.68372	23.56497	74.53362	31.92554
40 MPH	2a	93.8403	20.11209	69.07514	21.43683	93.3843	23.99858	93.83234	18.90479
	2b	88.05023	37.19943	71.7503	36.17762	76.6719	51.55764	77.97557	38.44541
	3	81.52715	31.77783	64.8631	15.96956	72.93796	31.55659	73.11584	26.57943
	4	82.83032	31.51509	70.56518	23.42868	80.42112	29.44915	76.83185	16.09237
	5	76.19041	37.14457	73.70065	19.82608	81.500	49.83483	76.12568	25.4451
	6	77.40388	35.17103	71.09368	24.09958	77.03789	40.84919	72.37522	25.12402
	7	78.70607	19.45119	71.89935	19.49281	81.52267	24.8569	73.29565	16.35909
	8	82.8218	17.07345	74.50661	17.60936	88.53764	25.29249	81.98615	22.56519
	9	74.12595	16.60511	67.27818	17.84396	80.84921	24.48697	70.53967	24.39026
	10	73.58418	16.37573	64.64495	14.47923	71.72977	21.50687	82.36246	30.60898
	11	73.11256	37.39442	78.84168	20.1175	77.83012	30.01875	68.24078	47.69168
	12	94.53797	22.0554	96.97359	27.54097	97.12707	35.88546	76.69934	35.09872

Table A-2. 99th percentile wheel forces (kips)

Train	Test	Inside	CW	Outside	CW	Inside	CCW	Outside	CCW
Speed	Case	Vertical	Lateral	Vertical	Lateral	Vertical	Lateral	Vertical	Lateral
20 MPH	2a	60.57201	10.24743	52.86512	9.463597	56.11288	10.17412	63.12633	10.42807
	2b	55.07283	14.56867	48.82146	12.46324	48.54039	16.18443	52.24422	18.49578
	3	54.5591	11.67367	46.98457	10.4535	47.88875	9.458226	55.606	10.49991
	4	56.7738	12.48573	50.9647	8.674343	51.90722	9.772508	56.07801	9.447818
	5	53.568	12.84103	49.05705	11.40912	50.95885	16.18434	53.84825	10.36238
	6	52.21882	13.18018	49.86465	9.905795	50.87685	14.59666	60.59989	15.29535
	7	52.34565	7.030645	50.58569	9.7014	49.29684	8.591353	53.04364	7.138639
	8	54.3109	7.673175	51.04689	8.548587	52.77105	10.29679	56.96216	7.927705
	9	54.32228	7.319479	49.92811	7.689363	49.6189	10.67059	56.75468	9.220966
	10	52.19056	9.411987	46.92493	9.428486	45.73935	11.15668	59.35945	8.922673
	11	55.32161	19.78196	50.40714	11.27972	50.3786	13.73574	55.57148	27.4904
	12	56.64859	13.30796	56.83625	13.80372	60.58019	13.57512	63.17682	15.77199
30 MPH	2a	56.10297	10.33882	49.92972	11.16551	72.91287	23.56264	80.10486	13.5332
	2b	59.00256	16.22104	54.56244	24.27925	59.54446	28.95048	55.36742	23.19768
	3	56.20276	12.10346	56.0127	12.39378	55.95522	13.55395	54.22121	13.50549
	4	58.95005	14.88129	56.99316	12.11625	59.14167	12.1529	57.49949	10.45051
	5	54.58102	17.10271	56.47023	14.51555	58.86156	22.92411	52.63618	12.72997
	6	52.70217	13.66848	52.94962	11.62811	56.43327	18.39989	54.41104	12.78315
	7	55.10154	8.205856	59.0166	10.92898	59.21727	13.39367	52.34375	7.960898
	8	55.88829	8.222762	55.63055	10.95542	59.16025	14.60533	57.76717	9.705775
	9	51.07171	7.333831	58.48619	12.90615	60.11968	15.00807	54.23706	9.270605
	10	50.63969	9.267307	61.66404	11.93861	60.45118	16.21357	59.40472	10.1747
	11	56.60023	28.82859	63.80117	16.70644	66.14101	19.77039	56.99304	35.76621
	12	67.94273	16.18208	70.29634	18.79522	83.4068	25.34	68.59706	20.23491
40 MPH	2a	83.56152	16.74643	62.84498	14.57637	84.59559	19.10927	87.15602	17.09836
	2b	69.01274	22.15157	62.35746	29.01107	68.10764	33.11356	64.34555	30.95435
	3	71.02391	21.9277	57.56689	13.27263	66.54088	14.74623	60.73527	17.71467
	4	71.37478	18.612	64.1754	13.49598	71.25122	17.39375	62.77902	13.85066
	5	63.58538	18.01229	62.49664	13.97713	68.992	27.74627	63.5739	15.97244
	6	68.20906	20.41258	61.27119	12.56921	66.54012	23.14098	63.40675	14.01945
	7	71.29563	12.53729	61.83821	10.99889	67.2818	16.53785	58.82498	11.26143
	8	72.14788	15.30973	65.35034	12.85962	74.1306	19.64605	65.76548	14.22165
	9	69.65418	14.3942	62.49609	12.47651	71.71208	19.60638	63.0113	17.02868
	10	63.7109	13.64495	59.64628	11.69623	67.93977	17.35003	66.37059	15.59819
	11	69.83667	30.85725	58.7602	14.43335	69.4604	21.71132	62.70746	43.10949
	12	81.79985	19.57929	76.08478	18.70792	82.93661	26.84249	69.51661	20.57742

Abbreviations and Acronyms

AMS	austenitic manganese steel
BHN	Brinell hardness number
CCW	counterclockwise
CW	clockwise
FAST	Facility for Accelerated Service Testing
GRL	gross rail load
HAL	heavy axle load
HTL	High Tonnage Loop
IWS	instrumented wheelsets
Nortrak	voestalpine Nortrak
SRR	Straight Rail Reversible
TPU	thermoplastic polyurethane
TTC	Transportation Technology Center (the site)
TTCI	Transportation Technology Center, Inc. (the company)